

AD-A151 571

AN EXPLORATORY INVESTIGATION OF SHARP FIN-INDUCED SHOCK

1/2

WAVE / TURBULENT. (U) AIR FORCE INST OF TECH

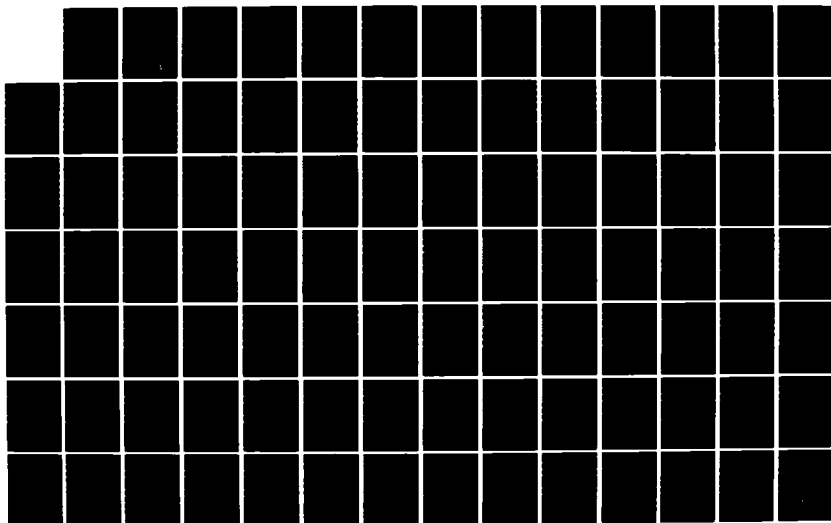
WRIGHT-PATTESSON AFB OH S P GOODWIN NOV 84

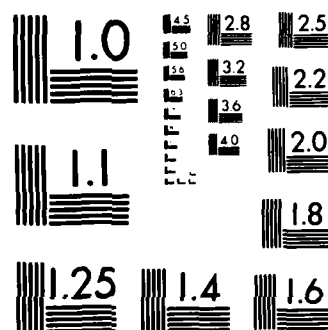
UNCLASSIFIED

AFIT/CI/NR-85-27T

F/G 28/4

NL





MICROCOPY RESOLUTION TEST CHART  
NATIONAL BUREAU OF STANDARDS-1963 A

UNCLASS

SECURITY CLASSIFICATION OF THIS PAGE (When Data Entered)

①

REPORT DOCUMENTATION PAGE		READ INSTRUCTIONS BEFORE COMPLETING FORM
1. REPORT NUMBER AFIT/CI/NR 85-27T	2. GOVT ACCESSION NO.	3. RECIPIENT'S CATALOG NUMBER
4. TITLE (and Subtitle) An Exploratory Investigation Of Sharp FIN - Induced Shock Wave / Turbulent Boundary Layer Interactions At High Shock Strengths		5. TYPE OF REPORT & PERIOD COVERED THESIS/DISSERTATION
7. AUTHOR(s) Scott P. Goodwin		6. PERFORMING ORG. REPORT NUMBER
9. PERFORMING ORGANIZATION NAME AND ADDRESS AFIT STUDENT AT: Princeton University		8. CONTRACT OR GRANT NUMBER(s)
11. CONTROLLING OFFICE NAME AND ADDRESS AFIT/NR WPAFB OH 45433		10. PROGRAM ELEMENT, PROJECT, TASK AREA & WORK UNIT NUMBERS
MONITORING AGENCY NAME & ADDRESS (if different from Controlling Office)		12. REPORT DATE Nov 1984
		13. NUMBER OF PAGES 139
		15. SECURITY CLASS. (of this report) UNCLASS
		15a. DECLASSIFICATION/DOWNGRADING SCHEDULE
DISTRIBUTION STATEMENT (of this Report) PROVED FOR PUBLIC RELEASE; DISTRIBUTION UNLIMITED		
DISTRIBUTION STATEMENT (of the abstract entered in Block 20, if different from Report)		
18. SUPPLEMENTARY NOTES APPROVED FOR PUBLIC RELEASE: IAW AFR 190-1 LYNN E. WOLAVER 28 Feb 85 Dean for Research and Professional Development AFIT, Wright-Patterson AFB OH		
19. KEY WORDS (Continue on reverse side if necessary and identify by block number)		
20. ABSTRACT (Continue on reverse side if necessary and identify by block number) ATTACHED		

AD-A151 571

DTIC FILE COPY

P  
DTIC  
ELECT  
MAR 25 1985  
S D

DD FORM 1 JAN 73 1473

EDITION OF 1 NOV 65 IS OBSOLETE

UNCLASS

85

03

11

053

SECURITY CLASSIFICATION OF THIS PAGE (When Data Entered)

AN EXPLORATORY INVESTIGATION OF SHARP FIN-INDUCED SHOCK  
WAVE/TURBULENT BOUNDARY LAYER INTERACTIONS AT HIGH SHOCK  
STRENGTHS

Scott P. Goodwin, 2LT, USAF

1984, 139 pages.

Master of Science in Engineering, Princeton University

ABSTRACT

An experimental investigation of sharp fin-induced shock/boundary layer interactions has been carried out at a Mach number of 2.95, unit Reynolds numbers ranging from 1 to 4 million per inch, boundary layer thicknesses of 0.14 and 0.50 inches, and fin angles of attack between 12 and 22 degrees. Surface pressure and surface flow visualization data were collected.

The results showed that high shock strength interactions were qualitatively similar to those at low shock strengths. When compared to two-dimensional test results, the present three-dimensional data were seen to have a similar dependence on Reynolds number but a different sort of dependence on shock strength. The data were also seen to possess conical similarity. As was the case at lower shock strengths, the interactions could be scaled using unit Reynolds number, boundary layer thickness, and normal Mach number. The appearance of the feature termed "secondary separation" was noted to depend on boundary layer thickness. Competing feature and turbulence scales were hypothesized to produce this dependence. Finally, comparisons of the experimental surface data with results produced using various computational schemes demonstrated that computational codes require more work before they can be used to successfully predict the structure of three-dimensional interactions.

Key sources include L.S. Dolling and S.M. Bogdonoff (AIAA Paper 81-0336), G.S. Settles and R.L. Kimmel (AIAA Paper 84-1557), F.K. Lu (Princeton MSE Thesis 1584-T), and A.A. Zheltovodov (Zhurnal Prikladnoi Mekhaniki i Tekhnicheskoi Fiziki, May-June 1982, pp 116-123). Private communications with D. Knight (Rutgers University) and C.C. Horstman (NASA Ames) provided the computational data.

Accession For	
NTIS GRA&I	<input checked="checked" type="checkbox"/>
DTIC TAB	<input type="checkbox"/>
Unannounced	<input type="checkbox"/>
Justification	
By	
Distribution/	
Availability Codes	
Dist	Avail and/or Special
A-1	



AFIT/NR  
Wright-Patterson AFB OH 45433

AUTHOR: GOODWIN, SCOTT P.

1. Did this research contribute to a current Air Force project?

( ) a. YES

( ) b. NO

( ) a. YES

( ) b. NO

( ) a. MAN-YEARS

( ) b. \$

( ) a. HIGHLY

( ) b. SIGNIFICANT

( ) c. SLIGHTLY

( ) d. OF NO  
SIGNIFICANCE

5. AFIT welcomes any further comments you may have on the above questions, or any additional details concerning the current application, future potential, or other value of this research. Please use the bottom part of this questionnaire for your statement(s).

NAME \_\_\_\_\_

**GRADE**

POSITION

## ORGANIZATION

LOCATION

STATEMENT(s):

77

AN EXPLORATORY INVESTIGATION OF SHARP FIN - INDUCED  
SHOCK WAVE / TURBULENT BOUNDARY LAYER INTERACTIONS  
AT HIGH SHOCK STRENGTHS

by

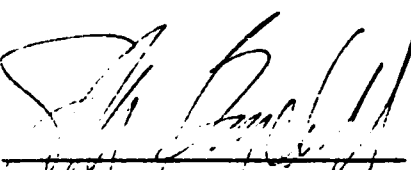
Scott P. Goodwin


Princeton University  
School of Engineering and Applied Science  
Department of Mechanical and Aerospace Engineering

Submitted in partial fulfillment of the requirements  
for the degree of Master of Science in Engineering  
from Princeton University, 1984

prepared by

  
Scott P. Goodwin

  
Professor S.M. Bogdonoff  
Thesis Advisor

  
Dr. A.J. Smits  
Thesis Reader

November, 1984

AN EXPLORATORY INVESTIGATION OF SHARP FIN-INDUCED SHOCK  
WAVE/TURBULENT BOUNDARY LAYER INTERACTIONS AT HIGH SHOCK  
STRENGTHS

Scott P. Goodwin, 2LT, USAF

1984, 139 pages.

Master of Science in Engineering, Princeton University

ABSTRACT

An experimental investigation of sharp fin-induced shock/boundary layer interactions has been carried out at a Mach number of 2.95, unit Reynolds numbers ranging from 1 to 4 million per inch, boundary layer thicknesses of 0.14 and 0.50 inches, and fin angles of attack between 12 and 22 degrees. Surface pressure and surface flow visualization data were collected.

The results showed that high shock strength interactions were qualitatively similar to those at low shock strengths. When compared to two-dimensional test results, the present three-dimensional data were seen to have a similar dependence on Reynolds number but a different sort of dependence on shock strength. The data were also seen to possess conical similarity. As was the case at lower shock strengths, the interactions could be scaled using unit Reynolds number, boundary layer thickness, and normal Mach number. The appearance of the feature termed "secondary separation" was noted to depend on boundary layer thickness. Competing feature and turbulence scales were hypothesized to produce this dependence. Finally, comparisons of the experimental surface data with results produced using various computational schemes demonstrated that computational codes require more work before they can be used to successfully predict the structure of three-dimensional interactions.

Key sources include D.S. Dolling and S.M. Bogdonoff (AIAA Paper 81-0336), G.S. Settles and R.L. Kimmel (AIAA Paper 84-1557), F.K. Lu (Princeton MSE Thesis 1584-T), and A.A. Zheltovodov (Zhurnal Prikladnoi Mekhaniki i Tekhnicheskoi Fiziki, May-June 1982, pp. 116-123). Private communications with D. Knight (Rutgers University) and C.C. Horstman (NASA Ames) provided the computational data.

## ABSTRACT

An experimental investigation of sharp fin-induced shock wave/turbulent boundary layer interactions at high angles of attack has been carried out at a freestream Mach number of 2.95. The tests were conducted over a range of angles of attack from 12 to 22 degrees. The unit Reynolds number was varied between 1 and 4 million per inch. Additionally, tests were made using two fully developed, equilibrium turbulent boundary layers of thicknesses 0.14 and 0.50 inches. The test model was mounted on and normal to either the tunnel floor or a horizontal flat plate. Both surfaces were at near adiabatic conditions. Surface flow visualization and surface pressure data were collected.

The above test ranges were selected to fulfill the objectives of more fully exploring the surface feature called "secondary separation," extending the concepts of conical similarity and upstream influence scaling into the high angle of attack regime, and provide the initial data for checks of computations of these flows.

The results indicated that the surface data of the high shock strength interactions were qualitatively similar to that at low shock strengths. The effect of shock strength on the surface pressure distribution was noted to be different from what has been seen in two-dimensional interactions. On the other hand, the effect of Reynolds number on the surface features was similar to that observed in two-dimensional experiments. Conical similarity of the surface data was present. The interactions were seen to scale using the



normal Mach number, unit Reynolds number, and boundary layer thickness in the same manner as was found at lower shock strengths. The appearance of the feature termed secondary separation was concluded to depend on shock strength and boundary layer thickness but not on Mach number or unit Reynolds number. Finally, comparisons of the experimental surface data with that obtained by two independent computations showed fair agreement. However, disagreements between the experiments and the computations indicated that the codes require more work before they can be used to confidently predict three-dimensional shock/boundary layer interactions.

## ACKNOWLEDGEMENTS

I would like to extend my thanks and appreciation to the many people who helped to make this thesis a reality. First, the guidance of my advisor, Professor S.M. Bogdonoff, was greatly appreciated. I am also indebted to the following for their insight, numerous valuable discussions, and comments: Drs. A.J. Smits, D.K.M. Tan, G.S. Settles, D.S. Dolling, D. Knight, and C.C. Horstman. I am grateful to Mr. R.L. Kimmel and Mr. T.T. Tran for their comments as well as discussions. I would be remiss if I did not recognize the cooperation and expertise of the technical staff: Bill Stokes, Bob Bogart, Dick Gilbert, Gary Katona, and Sharon Matarese. Finally, I would like to thank my wife, Ann, for her continuing support and understanding during the compilation of this thesis.

This research was sponsored by the Air Force Office of Scientific Research under contracts F49620-81-K-0018 and F49620-84-C-0086 monitored by Dr. James Wilson.

This thesis carries 1687-T in the records of the Department of Mechanical and Aerospace Engineering.

## TABLE OF CONTENTS

<u>Section</u>	<u>Page</u>
ABSTRACT .....	ii
ACKNOWLEDGEMENTS .....	iv
TABLE OF CONTENTS .....	v
LIST OF FIGURES .....	vii
LIST OF SYMBOLS .....	xi
 CHAPTER I: INTRODUCTION AND BACKGROUND	
1.1 Introduction .....	1
1.2 Background .....	2
1.3 Objectives .....	18
 CHAPTER II: TEST PROGRAM	
2.1 Test Conditions .....	20
2.2 Data Acquisition .....	22
 CHAPTER III: EQUIPMENT AND TECHNIQUES	
3.1 Wind Tunnel .....	24
3.2 Test Section .....	24
3.3 Shock Generators .....	25
3.4 Experimental Techniques .....	29
3.4.1 Surface Flow Visualization .....	29
3.4.1.1 Kerosene-Lampblack Technique .....	29
3.4.1.2 Local Kerosene-Lampblack Technique .....	30
3.4.1.3 Moving Kerosene-Lampblack Technique .....	31
3.4.1.4 Alcohol Washdown Technique .....	31
3.4.2 Temperature Measurements .....	32
3.4.3 Pressure Measurements .....	33
3.4.3.1 Stagnation Pressure Measurements .....	33
3.4.3.2 Surface Pressure Measurements .....	33
3.4.3.3 Pitot Pressure Measurements .....	33
3.4.4 Computer System .....	34
 CHAPTER IV: RESULTS AND DISCUSSION	
4.1 Coordinate Systems .....	35
4.2 Surface Flow Visualization Results .....	36
4.2.1 Alcohol Washdown Technique Results .....	37
4.2.2 Comparisons to Previous Work .....	38
4.2.3 Analysis of the High Angle Data .....	39
4.2.4 Local Kerosene-Lampblack Results .....	44
4.2.5 Conical Similarity .....	45
4.3 Upstream Influence Scaling Results .....	46
4.4 Surface Pressure Results .....	49

4.4.1	Comparisons with Previous Data .....	49
4.4.2	General Description .....	50
4.4.3	Analysis of the High Angle Pressure Data .....	51
4.4.4	Conical Similarity in the Pressure Distributions ..	55
4.5	Pressure Distribution-Flow Visualization Comparisons ..	56
4.5.1	Upstream Influence .....	57
4.5.2	Line of Separation .....	57
4.5.3	Secondary Separation .....	59
4.6	Discussion of Secondary Separation .....	59
4.7	Discussion of Attachment .....	62
4.8	Comparisons with Computations .....	64
4.8.1	Computation of Knight .....	64
4.8.1.1	Surface Feature Comparison .....	64
4.8.1.2	Surface Pressure Distribution Comparison ..	65
4.8.2	Computation of Horstman .....	65
4.8.2.1	Surface Feature Comparison .....	65
4.8.2.2	Surface Pressure Distribution Comparison ..	65
4.9	Fluctuating Surface Pressure Measurements .....	66

#### CHAPTER V: CONCLUSIONS AND RECOMMENDATIONS

5.1	Summary of Findings .....	67
5.2	Recommendations for Further Study .....	70

REFERENCES .....	73
------------------	----

TABLE I: TEST MATRIX

FIGURES

## LIST OF FIGURES

<u>Figure</u>	<u>Title</u>
1.	Two-dimensional Shock/Turbulent Boundary Layer Interaction
2.	Sharp Fin Configuration
3.	Surface Feature Definitions of Lu (12)
4.	Blunt Fin Configuration
5.	Swept Compression Corner Configuration
6.	Continuity Argument of Peake and Tobak (33)
7.	Viscous Critical Point Analysis of Hornung and Perry (35); (a) Two-dimensional Separation, (b) Three-dimensional "Separation"
8.	Photograph of 8"x8" Wind Tunnel
9.	Photograph of Variable Angle Shock Generator
10.	Photograph of Shock Generator Installed in Tunnel
11.	Photograph of External Drive Mechanism
12.	Plan View of Shock Generator Assembly
13.	Coordinate Systems
14.	Definition of Surface Feature Line Angles
15.	Alcohol Washdown/Kerosene-Lampblack Comparison

16. Comparison of Surface Feature Angles with Previous Data
17. Photograph of Typical Kerosene-Lampblack Trace,  $\alpha=16$  deg., Thin Boundary Layer
18. Effect of Test Variables on Upstream Influence Line Angle; (a) Unit Reynolds Number Effect, (b) Boundary Layer Thickness Effect
19. Effect of Test Variables on Separation Line Angle; (a) Unit Reynolds Number Effect, (b) Boundary Layer Thickness Effect
20. Effect of Unit Reynolds Number on Secondary Separation Line Angle
21. Effect of Reynolds Number on Upstream Influence Angle for Curves of Constant Boundary Layer Thickness
22. Effect of Reynolds Number on Upstream Influence Angle for Curves of Constant Unit Reynolds Number
23. Photograph of Local Kerosene-Lampblack Trace, Upstream Application,  $\alpha=15$  deg., Thin Boundary Layer
24. Photograph of Local Kerosene-Lampblack Trace, Downstream Application,  $\alpha=15$  deg., Thin Boundary Layer
25. Photograph of Local Kerosene-Lampblack Trace,  $\alpha=15$  deg., Thin Boundary Layer
26. Plot of Conical Similarity Interaction Response Functions
27. Effect of Shock Strength on Upstream Influence in  $L_u$  versus  $L_s$  Coordinates
28. Effect of Boundary Layer Thickness on Upstream Influence in  $L_u$  versus  $L_s$  Coordinates
29. Effect of Unit Reynolds Number on Upstream Influence in

$L_u$  versus  $L_s$  Coordinates

- 30. Effect of Shock Strength on Upstream Influence in  $L_{un}$  versus  $L_s$  Coordinates
- 31. Effect of Boundary Layer Thickness on Upstream Influence in  $L_{un}$  versus  $L_s$  Coordinates
- 32. Effect of Unit Reynolds Number on Upstream Influence in  $L_{un}$  versus  $L_s$  Coordinates
- 33. Collapse of Upstream Influence Data Using Scheme of Dolling and Bogdonoff (23); (a) Key, (b) Data
- 34. Comparison of Surface Pressure Data with Oskam, et. al. (7)
- 35. Comparison of Surface Pressure Data with Duplicated Data of  $L_u$  (12)
- 36. Typical Surface Pressure Distribution
- 37. Effect of Shock Strength on the Surface Pressure Distribution
- 38. Effect of Unit Reynolds Number on the Surface Pressure Distribution
- 39. Effect of Boundary Layer Thickness on the Surface Pressure Distribution
- 40. Typical Collapse of the Surface Pressure Data
- 41. Typical Pressure Distribution/Kerosene-Lampblack Comparison Plot
- 42. Topographic Pressure Plot

- 43. Effect of the Test Variables on Separation Pressure Ratio; (a) Unit Reynolds Number Effect, (b) Boundary Layer Thickness Effect
- 44. Photograph of  $\alpha = 20$  deg., Thick Boundary Layer Kerosene-Lampblack Trace
- 45. Computed Surface Shear Vectors of Knight (44)
- 46. Comparison of Surface Pressure Distribution with Computed Data of Knight (44)
- 47. Computed Surface Streamlines of Horstman (45)
- 48. Comparison of Surface Pressure Distribution with Computed Data of Horstman (45)



## LIST OF SYMBOLS

<u>Symbol</u>	<u>Definition</u>
$L_{incept}, L_i$	Length measured along inviscid shock trace on the test surface from the model leading edge to the point where conical surface features are developed (see Figure 13).
$L_s$	Length measured along inviscid shock on test surface from the model leading edge (see Figure 13).
$L_u$	Upstream influence length measured from inviscid shock trace in freestream direction (see Figure 13).
$L_{u_1}, L_{u_2}$	Streamwise upstream influence length at specific spanwise locations (see Figure 13).
$L_{un}$	Upstream influence length measured from inviscid shock trace in direction normal to the shock (see Figure 13).
$M_\infty, M$	Freestream Mach number.
$M_n$	Component of the freestream Mach number normal to the inviscid shock.
$p$	Local static pressure.
$P_0$	Stagnation pressure of the incoming flow.
$P_\infty$	Static pressure of the incoming flow.
$P_2/P_1$	Pressure ratio across the inviscid shock.

$\left[ P/P_{\infty} \right]_{\text{sep}}$	Pressure ratio at the line of surface streamline convergence.
$Re_u$	Unit Reynolds number.
$Re_{\delta}$	Reynolds number based on the boundary layer thickness at the fin leading edge position.
$x$	Streamwise coordinate measured from the fin leading edge (see Figure 13).
$x_s$	Streamwise coordinate measured from the inviscid shock trace (see Figure 13).
$\Delta x$	Streamwise distance from the fin leading edge to the virtual origin.
$z$	Spanwise coordinate measured from the fin leading edge (see Figure 13).
$z_1, z_2$	Specific spanwise positions.
$\Delta z$	Spanwise distance from the fin leading edge to the virtual origin.
$\alpha$	Fin angle of attack measured from the freestream direction.
$\beta_o$	Inviscid shock angle (see Figures 3 and 14).
$\beta_A$	Attachment angle (see Figures 3 and 14).
$\beta_{u1}$	Upstream influence angle (see Figures 3 and 14).
$\beta_{s1}$	Separation angle (see Figures 3 and 14).
$\beta_{s2}$	Secondary separation angle (see Figures 3 and 14).

$\delta$	Boundary layer thickness at the fin leading edge position.
$\delta^*$	Boundary layer displacement thickness.
$\theta$	Polar coordinate angle.
$\mu$	Freestream Mach angle.

## CHAPTER I

### INTRODUCTION AND BACKGROUND

#### 1.1 INTRODUCTION

From the first manned flight to break the sound barrier in 1947 to the present day, supersonic speeds have become increasingly commonplace. Naturally, interest in and concern about flow phenomena unique to this regime have grown as well. One of the principal flows receiving attention is the interaction between a shock wave and a boundary layer, especially the interaction of a shock wave with the more often encountered and less understood turbulent boundary layer. Interactions of this type occur routinely and a few examples include the interactions occurring at wing - fuselage junctions and control surfaces of supersonic aircraft, in supersonic engine inlets, on boundary layer splitter plates, and on the blades of various turbomachinery.

The majority of investigations, both experimental and computational, have concentrated on shock wave - turbulent boundary layer interactions as the turbulent boundary layer is more often encountered in practice. Many researchers have sought to simplify the problem by examining a two - dimensional interaction, such as the flowfield induced by supersonic flow over a compression corner (Fig. 1). The elimination of one dimension allows for increased spatial resolution, overcoming a typical difficulty for computational schemes. Although a great deal has been learned about this

interaction, the effect of the third dimension on the problem must be considered if an understanding of the flows of the examples cited above is to be gained. The introduction of an extra spatial degree of freedom has presented great difficulty in the use of computational techniques. Thus, until recently, the bulk of investigations of these three - dimensional interactions has necessarily been experimental. Such research, however, should not only be dedicated to increasing our understanding, but also to helping to develop and verify computational codes which can reduce the need for costly experiments.

One of the simplest geometries producing a three - dimensional shock wave - turbulent boundary layer interaction consists of a sharp edged plate mounted normal to some flat surface and set at some angle to the incident flow. This configuration is commonly referred to as a sharp fin and is depicted in Figure 2. This simple configuration is desirable since it produces a planar shock wave allowing us to highlight the general features of three - dimensional flows without introducing additional effects produced by more complex geometries. While the study of geometry effects are important, the sharp fin represents the simplest geometrical case for the three - dimensional interaction.

## 1.2 BACKGROUND

The sharp fin configuration and related geometries have been investigated over a wide range of conditions in the course of experimental and computational studies. A common feature of many of these studies is the deduction of the flow field structure from surface data alone, a process which can easily give mistaken impressions about the flow field.

One of the earliest detailed studies of the interaction between a sharp fin - induced shock wave and a turbulent boundary layer was due to Stanbrook (1). The experiments, conducted over a Mach number range from 1.6 to 2.0, revealed a spanwise growth of the interaction, indicating a flow which was three - dimensional in nature. The interaction was seen to have a large upstream influence, that is to say, the interaction started at a point which was significantly upstream of the inviscid shock wave location. Stanbrook noted that when the fin was deflected between 7.5 and 8 degrees into the incoming flow, creating a pressure ratio across the shock of about 1.5, the maximum angle of deflection of the surface streaks in the oil flow visualization data was equal to the inviscid shock wave angle. This condition was defined to indicate "separation". This "separation" was seen to occur at lower pressure ratios than observed in studies of two - dimensional interactions and it appeared to coincide with a line of convergence of the oil streaks as the fin deflection angle was increased. Stanbrook hypothesized that the boundary layer separated at this line of convergence and rolled up in a vortex to form a separated region.

McCabe (2) followed Stanbrook's work with a similar study at Mach numbers of about 2 and 3 and boundary layer thicknesses of 0.14 and 0.23 inches. Some of the results were compromised by the fact that the fin was placed on the centerline of a 4 inch wide wind tunnel and wall effects were most likely present. "Separation" was noted at fin angles of 8.5 degrees in the Mach 2 case and 5.5 degrees for Mach 3 when Stanbrook's criterion was applied. The results also indicated a pressure ratio of 1.5 at separation. McCabe suggested that, since the low energy streamlines of the boundary layer near the wall were deflected the most by the pressure gradient and successively

higher energy streamlines were deflected by decreasing amounts, the phenomenon affecting separation was the "twisting" of the incoming boundary layer to form a weak vortex. It was also observed that the complete pressure rise took place over a large distance, some  $50 \delta^*$ . Finally, a tendency towards a second convergence, or "secondary separation", of the surface streamlines was observed in the region near the inviscid shock location for fin deflection angles of between 15 and 20 degrees.

Green (3) reviewed the state of shock wave - turbulent boundary layer interaction research up to 1970 and made several important remarks. First, separation can occur in three - dimensional flows without the velocity component of the flow which is parallel to the freestream reversing direction. Second, the characteristic feature of separation is that limiting or surface streamlines converge asymptotically to a line of separation where the separation surface leaves the test surface. Third, a conical flow, in which the scale of the interaction grows linearly with distance along the shock, can be expected to occur when a swept shock wave interacts with an initial, uniform two - dimensional boundary layer. Finally, the scale of the interaction should depend on the overall pressure rise, the nature of the disturbance invoking the pressure rise, the freestream Mach and Reynolds numbers, and some measure of the incoming boundary layer thickness.

Law (4) examined the interaction of a fin - generated shock wave with a turbulent boundary layer at a Mach number of 6. Fin angles ranging from 4 to 20 degrees were tested at unit Reynolds numbers of 0.83 and 2.50 million per inch. Oil flow patterns and surface pressure distributions were taken. The oil flow results were seen to be insensitive to unit Reynolds number changes

but indicated that, as fin angle increased, the distance between the shock wave and the line of convergence increased while the distance between the fin surface and the shock was nearly constant. The surface features were observed to be conical up to an angle of attack of 16 degrees. At higher angles, tip disturbances from the 3 inch high fin probably contaminated the results. Additionally, a line of secondary convergence was visible in the oil flow sketches for angles of attack between 10 and 20 degrees. Law stated that this secondary flow as well as "dips" in the pressure distributions indicated the presence of a possible secondary vortex.

A study by Peake (5) attempted to control the "separation" by using air injection. The tests were conducted at a Mach number of 2.4 and a unit Reynolds number of 1 million per inch. Peake noted experimentally that, for three - dimensional separation, the shear stress and skin friction at the line of separation need not be zero and that the separating and attaching streamlines need not be one and the same. A major conclusion of the study was that the development of the flow, with increasing fin deflection angle, was gradual, progressive, steady, and quasi-conical with the flow showing a line of separation as the boundary layer rolled up to form a free shear layer in the form of a flattened vortex within the depth of the original boundary layer.

Detailed surveys of the flow fields at angles of attack of 4 and 10 degrees were performed by Oskam (6) at Mach 3. The surface flows were found to be conical and the 10 degree case exhibited convergence of the surface streamlines. However, the surveys showed no sudden movement of fluid away from the surface. This was thought to disprove the notion of a free shear



layer leaving the surface as was proposed earlier. As no evidence of either a free shear layer or a vortex was found, a flow model was proposed which was dominated by extensive wave interactions and localized secondary flows.

Later work by Oskam, Bogdonoff, and Vas (7) presented further analysis of the data set above. Again, their conclusion was that the boundary layer was not separated in the case where the angle of attack was 10 degrees. Therefore, it was stated that the criterion used by both Stanbrook and McCabe, the surface flow being parallel to the shock wave, was not a sufficient condition for determining flow separation in three dimensions.

The same investigators presented yet another analysis (8) but this time for the corner region. High local heat transfer rates were noted in this area which would indicate the presence of an attachment process. However, the survey data did not show this to be the case. Instead, on the surface, a region of flow was directed inwards while the secondary flow in the corner was moving away from the fin. This produced, locally, a phenomenon which appeared to be an attachment but which the investigators concluded was not.

A final discussion by Oskam, Vas, and Bogdonoff (9) not only continued the analysis of the original data set but also presented an in - depth examination of the feature of separation. The conclusions based on a theoretical analysis used were that three - dimensional separation could occur without the classic two - dimensional indicators of reverse flow and zero skin friction but that a three - dimensional separation had no distinctive character of its own. They showed that three - dimensional separation could, in one extreme, look like a two - dimensional separation and, in the other extreme, appear to be unperturbed, parallel, attached flow.

In contrast to the preceding wave dominated model of Oskam, et. al., Kubota and Stollery (10) proposed a "double layer viscous" model based on a set of experiments at Mach 2.3. They proposed that the flow on the surface of the fin turned downward to flow out along the floor, forming an "induced layer" which penetrated further outboard as the fin angle was increased. Eventually, this induced layer was large enough to force the floor boundary layer to lift off the surface, dragging the induced layer up and over to form a weak vortical layer.

McClure (11) followed the surveys of Oskam (6) with an additional set of surveys at an angle of attack of 10 degrees. The tests were done with two boundary layer thicknesses, 0.18 and 0.51 inches, to attempt to scale the flow fields. Little success was obtained scaling by a length scale, the boundary layer thickness, alone. The results improved when the flow fields were scaled using the normal Mach number and the unit Reynolds number in addition to the boundary layer thickness. The results also agreed with those of Oskam (6) in that the interaction appeared to be dominated by a series of compression waves.

The surface features of these interactions were examined extensively by Lu (12) who provided an excellent pictorial definition of the features under consideration. Figure 3 shows a representative sketch. The locus of points where the incoming streamlines were first deflected from their original trajectories was defined as upstream influence line. Downstream of the upstream influence line, a line of streamline convergence can be clearly seen. This is the line of separation already mentioned several times. Near the fin a system of feather - like diverging lines form what was termed attachment.

Finally, between the lines of separation and attachment was a second line of convergence thought to be a line of "secondary separation".

The analysis of Lu (12) showed that the upstream influence data for fins with swept as well as unswept leading edges could be correlated when scaled using unit Reynolds and normal Mach numbers and boundary layer thickness. The conclusion was that upstream influence was strongly dependent on the shock wave and its shape near the surface rather than on the geometry causing the shock. Finally, Lu (12) introduced acetone vapor into the flow through surface pressure orifices in an to visualize the off - surface flow behavior. The results seemed to indicate that the upstream boundary layer lifted off the surface to rise over a secondary flow region moving vigorously in the spanwise direction.

Zubin and Ostapenko (13) examined the sharp fin induced interaction over a range of fin angles previously unexplored. Angles varying from from 5 to 22.5 degrees were tested at a Mach number of 2.95 and a unit Reynolds number of 0.63 million per inch. They placed rows of surface pressure orifices in arcs about the leading edge. The pressure data obtained in this fashion demonstrated an important point concerning conical flows; the static pressure was constant along rays emanating from the origin of the conical flow. At fin angles in excess of 12.5 degrees a line of secondary separation was observed which disappeared at a fin angle of 22.5 degrees. Changes in local Reynolds number were postulated to be the mechanism governing the feature.

Zhel'tovodov (14) in doing similar work noted three characteristic regimes of these interactions as angle of attack was increased. The first was flow without boundary layer separation followed by interactions with separation and

a third regime was delineated by the appearance of secondary separation.

In later work, Zheltovodov (15) extended this classification to include three more regimes as secondary separation was observed to weaken, disappear, and reappear as angle of attack was increased. Again, Reynolds number changes in the "return" flow of the "separated" region were given as the explanation. In addition to the state of the boundary layer in the "return" flow, the intensity of the internal shock wave which develops in the "return" flow was cited as a possible factor influencing the feature of secondary separation. It should be noted that the reports of Zheltovodov (14),(15) included no information regarding the state of the incoming boundary layer or its thickness other than to state that the incoming layer was tripped and that the boundary layer within the interaction underwent transition from a laminar to a turbulent condition.

The sharp fin interaction is not the only one which has been investigated. The interactions induced by other geometries, the blunt leading edge fin of Figure 4 and the swept compression corner of Figure 5 for example, have also been examined experimentally.

Dolling and Bogdonoff (16) studied a related geometry, a fin with a blunt leading edge (Figure 4). At a Mach number of 3, the experiments showed that three regions could be seen in the surface flows. First, a highly unsteady inner region was visible close to the fin. Next, a boundary or transition region was noted outboard of the inner region. Finally, an outer region was found which was similar to the interaction produced using a sharp fin.

Another geometry producing a three - dimensional flow field that has

received considerable attention is the swept compression corner (Figure 5). Settles, Perkins, and Bogdonoff (17) examined this configuration in a preliminary investigation at Mach 3. The scale of the secondary crossflow was seen to increase as the compression corner was swept back further and further. The surface features exhibited a tendency towards cylindrical symmetry. In other words, they tended to run parallel to the inviscid shock wave. The investigators also made the point that the surface features alone could give the mistaken impression that the entire flow was highly skewed from the streamwise direction.

Many researchers have attempted to place the ever growing body of experimental data into a structured framework by generalizing the flow structure, developing prediction techniques, searching for the governing parameters through scaling studies, or correlating the data on some observed flow feature. Korkegi (18) commented on the flow structure. Because the surface shear does not go to zero at a line of three - dimensional separation, even though its component normal to the line does, Korkegi argued that the terms separation and attachment could be used in a broader sense in three dimensions than in two. Separation was viewed as a line along which the flow lifts off as a continuous surface. A pressure ratio of about 1.5 was seen to be required to form the familiar line of convergence. An elevated heat transfer rate close to the fin - floor junction was hypothesized to be due to an attachment phenomenon in that region. The separated region was visualized as being a vortex which "scavenged" fluid from the outer flow. The return flow of this vortex, that is, the lateral outflow along the surface, could then separate as well, causing the feature of secondary separation which was associated with a "dip" in the surface pressure distributions. Korkegi (18)

saw this structure as also being a vortex similar to the separation vortex, except that it "scavenged" flow from the primary vortex rather than the external flow.

Korkegi (19) also attempted to develop a correlation for incipient separation in fin - generated interactions. The data presented indicated that a normal Mach number of about 1.22 was required for incipient separation in interactions with skewed shock waves. Korkegi (19) hypothesized that a lesser pressure ratio was required to produce a separation in three dimensions than in two because the direction of the streamlines need not be completely reversed.

Hayes (20) examined a variety of data for Mach numbers of between 3 and 6 with unit Reynolds numbers ranging from 0.13 to 2.33 million per inch, boundary layer thicknesses of between 0.13 and 6.0 inches, and fin angles up to 20 degrees in trying to develop a set of prediction techniques. In the analysis, surface pressure distributions were divided into outer and inner regions. The outer region extended from upstream influence to the inviscid shock wave location. If the pressures were high enough in this region, separation occurred. A plateau was seen to develop in the pressure distribution which Hayes (20) concluded was a result of boundary layer separation. In other words, a "dead air" region was present which experienced only mild pressure gradients. The inner region, from the shock to the fin, was thought to be dominated by an imbedded vortex which produced a sharp pressure peak close to the fin.

Other investigators have attempted to gain insight into shock wave - boundary layer interactions by using scaling techniques to reveal the dominant

physical parameters. Settles and Bogdonoff (21) started with the five factors which Green (3) proposed as determining the interaction scale. Dimensional analysis was applied to produce nondimensional groups of the relevant parameters. The results were then applied to upstream influence data from swept compression corner experiments at Mach 3 to show that data for a variety of conditions could be successfully correlated.

Dolling and Bogdonoff (22) used the preceding results, with some slight modifications based on experimental observations, to examine Mach 3 sharp fin interactions. Data for a number of angles of attack, unit Reynolds numbers, and boundary layer thicknesses were successfully correlated by:

$$\frac{L_{un} Re_u^{1/3}}{M_n \delta^{2/3}} = f \left[ \frac{L_s Re_u^{1/3}}{\delta^{2/3}} \right] \quad (1)$$

In further discussion, Dolling and Bogdonoff (23) reiterated that the interaction scale increased with increasing boundary layer thickness and with decreasing unit Reynolds number. However, the method was stated to have some limitation as the effect of freestream Mach number had not been explored.

Following the success of Dolling and Bogdonoff, McClure and Dolling (24) attempted to scale the flow field using a similar method. The flow field produced by a 10 degree fin at Mach 3, which had conical surface features, was surveyed using two different boundary layer thicknesses. The data was scaled and the two cases compared. A favorable collapse of the data was found but the collapse was not as good as was obtained for the surface features.

Dolling (25) investigated the Mach number effect mentioned above by comparing upstream influence data obtained at Mach 2 with the Mach 3 results.

The comparison indicated that some modification of the scaling principle of Equation (1) may be necessary. In particular, the exponents for the boundary layer thickness and unit Reynolds number may need to be expressed as functions of freestream Mach number.

Another approach to structuring all of the three dimensional data has focused on the observed symmetries of the interactions, both cylindrical and conical. Teng and Settles (26) examined the upstream influence data of swept compression corners at Mach 3 and a unit Reynolds number of 1.6 million per inch and found that both cylindrical and conical symmetry were present. The transition between the two was postulated to be due to the detachment of the inviscid shock wave from the corner line of the test model.

Lu and Settles (27) investigated conical similarity in swept and unswept fin - induced interactions. Conical similarity was demonstrated through the analysis of surface flow visualization results as well as through surface pressure distributions. At a given angle of attack, when the streamwise coordinate of the pressure distribution was normalized by the spanwise distance to the conical origin, the pressure data for several spanwise locations collapsed on a single curve indicating that the static pressure was constant along rays from that same origin. This observation strongly supports the concept of conical similarity.

Settles and Kimmel (28) extended the notion of conical similarity by generalizing it to include interactions produced by disparate shock generators. Assuming that semi - infinite shock generators, which imposed no length dimensions on the flow, were used and that the inviscid shock location was the proper reference point, interaction response functions based on



various surface feature angles were plotted to demonstrate that the surface patterns were approximately identical for different shock generators if the upstream influence and shock angles were similar. This similarity broke down as the generator - floor junction was approached and geometry effects began to be felt. The similarity of the upstream portions of the interactions produced by different shock generators did, however, gave rise to the notion of a three - dimensional "free - interaction" concept.

To this point, all of the investigations discussed have concentrated on mean measurements of one type or another. There were no measurements of fluctuations of any sort in the three - dimensional interactions examined in the aforementioned experiments. Dolling and Bogdonoff (29) began to address this lack of high frequency data by measuring surface pressure fluctuations in a blunt fin - induced interaction. High frequency pressure transducers were used to collect the data at a Mach number of 3 and a unit Reynolds number of 1.60 million per inch. Surface pressure fluctuations two orders of magnitude greater than those in the incoming turbulent boundary layer were observed.

Recently Tan, Tran and Bogdonoff (30) made similar measurements under nearly identical conditions for a sharp fin with a deflection angle of 10 degrees. The shock structure was found to be quite steady and quite different from the shock fluctuations observed in a two dimensional case of similar shock strength. In the interaction, the transverse scale was noted to be larger than the longitudinal and the broad - band space correlations were found to be aligned with the surface isobars. A double layer model with two groups of structures moving in different directions at different speeds was offered as a possible explanation.

Three dimensional interactions have not been considered from only an experimental standpoint. Several investigators have taken a more theoretical approach. In particular, the flows have been analyzed using topology to theorize the structure from surface data. One of the first to do so was Maskell (31) who described the two basic forms of separation, free vortex layers and bubbles, which can be combined to form a variety of flow patterns. The common characteristic identified was that separation occurs where distinct limiting streamlines in the solid surface converge.

Goldberg (32) also theorized that separation was characterized by the turning of incoming streamlines to form a thin separation line. It was stated that since the separation line does not thicken, continuity requires that some fluid lift off the surface.

Peake and Tobak (33) also considered separation from a topological standpoint, stating that a necessary condition for separation was the convergence of the oil streak lines. They sought to demonstrate that it was also a sufficient condition by applying continuity in the same manner as Goldberg. Figure 6 illustrates the argument well. The streamlines must leave the surface because the width of a stream tube between them decreases as the lines converge, indicating that the height must increase as shown. Even in compressible flow, the fluid cannot be compressed to an infinite density. Therefore, the height of the stream tube must increase and the streamlines must leave the surface. However, the surveys of Oskam (6) show Figure 6 to be an inaccurate representation. Profiles of yaw angle suggest that the two shaded downstream boxes would be more correctly drawn with their tops skewed to the left as the dashed lines in Figure 6 indicate.

Hunt, et. al. (34) showed the shear stress line onto which all shear stress lines converge asymptotically to be the line where the separated surface meets the solid surface. This occurrence is a separation if the divergence of the surface shear stress vector is negative and an attachment if it is greater than zero. They also observed that any kinematically possible flow must fit the topological rules used in this and the preceding analyses.

Hornung and Perry (35) recognized that the definition of two - dimensional separation, reverse flow and zero skin friction, was inadequate for three dimensions. Their analysis showed that two - dimensional separatrices, special streamlines which divide the flow into distinct regions, had three - dimensional equivalent streamsurfaces which could "bifurcate". In the terminology of Hornung and Perry (35), a separation line becomes an open negative bifurcation line while an attachment was defined as a positive bifurcation. Note that throughout the discussion attachment has been used instead of the term reattachment. The former is the more correct term as all of these topological analyses have concluded that the separating streamline is not necessarily the attaching streamline. The unambiguous terminology of Hornung and Perry (35) will be used interchangeably with the more traditional names of the features throughout the remainder of this paper.

Hornung and Perry (35) proceeded to perform a viscous critical point (a point where the wall shear stress is zero) analysis in imposing a uniform shear flow in the third dimension on a flow exhibiting a classic two dimensional separation. Both the two - dimensional and three - dimensional flows are shown in Figure 7. The plot in the X-Y plane of the three - dimensional case shows streamlines converging to form a negative bifurcation.

The investigators noted that this three - dimensional case did not exhibit the traditional signs of two - dimensional separation; no streamline left the surface, no reverse flow was present, and the wall shear was finite everywhere. However, material was transported away from the wall at exactly the same rate in both cases leading to the conclusion that the three - dimensional flow was "just as separated" as the two - dimensional one.

The final method of examining three - dimensional interactions has been through computations. Horstman and Hung (36) computed the two cases which Oskam (6) surveyed. A time - averaged solution of the Navier - Stokes equations was used in conjunction with an eddy viscosity turbulence model. They obtained good agreement for the 4 degree case and fair agreement at 10 degrees. Plots of the velocity vectors seemed to indicate the presence of a recirculation region. However, because the appearance of the vortex was dependent on the viewing direction and because the computational domain was not large enough to show one full revolution, the results were said to be inconclusive. Despite this conclusion, tracing of individual particles showed them to be lifting from the surface at the line of convergence more than they would lift in an attached, undisturbed boundary layer.

Knight (37) also computed the same two flow cases using a different scheme and obtained good agreement with the experiment and the computation above. Knight also saw significant lifting of the fluid in the vicinity of the line of surface streamline coalescence.

In addition, Horstman (38) computed a variety of swept compression corner cases. The computation verified the conical - cylindrical boundary found by Teng and Settles (26) and indicated there was some validity to the shock

detachment hypothesis. The location of the upstream influence line was also calculated satisfactorily. However, the computation failed to predict the pressure distributions for cases with "large" separations. The conclusion was that the conical - cylindrical boundary and upstream influence were computed well because they appear to be primarily inviscid phenomena and do not depend, in a significant manner, upon the turbulence model.

### 1.3 OBJECTIVES

As can be seen, the preceding studies have been limited in terms of the systematic variation of the incoming flow conditions at high shock strengths where significant changes in the surface features of the flow have been reported. In light of the preceding statement, the general objective of this study was to improve our understanding of three - dimensional flows, and specifically, to systematically investigate a range of sharp fin - generated interactions which have recieved a limited examination to date. As previously discussed, the simplest geometry, the sharp fin, was chosen to avoid introducing geometry effects into a program designed to vary and examine the effect of the incoming conditions.

In particular, the incoming flow parameters of Reynolds number and boundary layer thickness were altered over a range of high angles of attack to fulfill the following specific objectives:

- 1) Examine more fully the fin deflection angle range where the feature termed "secondary separartion" was seen to appear and disappear, as well as to investigate the effects of the incoming flow conditions on other surface features at high shock strengths,

- 2) Extend upstream influence scaling principles for fins into the high angle of attack regime,
- 3) Extend conical similarity concepts into the high angle of attack regime,
- 4) Explore three - dimensional interactions with shock strengths seen previously only in two - dimensional cases to highlight points worthy of future, more detailed examination and,
- 5) Produce the initial data for checks of computations of strong shock induced three - dimensional interactions.

## CHAPTER II

### TEST PROGRAM

#### 2.1 TEST CONDITIONS

To satisfy the objectives previously outlined, the incoming boundary layer thickness, unit Reynolds number, and fin deflection angle were all varied to give a test matrix consisting of twenty-eight distinct combinations of those three variables (see Table 1). The nominal freestream Mach number in all cases was 2.95.

The test model was run in two different boundary layers, each having a different thickness. First, the model was placed on the floor of the wind tunnel at a streamwise distance of 38.3 inches from the two-dimensional nozzle throat. This position approximately corresponds to the location used by Oskam (6), McClure (11), and Lu (12). The placement of the model differs from several previous investigators; Stanbrook (1), McCabe (2), and Peake (5) to name a few, who mounted their shock generators perpendicular to the sidewall of the two - dimensional nozzles of their test facilities. These tests were therefore conducted in a non - uniform boundary layer since the pressure gradients in the nozzle force the sidewall boundary layers to collect along the centerline. Placing the fin, or shock generator, on the floor or ceiling eliminates this problem. For the floor boundary layer, at the fin leading edge position, the boundary layer thickness was approximately 0.50 inches depending on the value of the unit Reynolds number. This results checks with

that found by Tran (39) and Settles (40).

The model was also tested in a second, thinner boundary layer by placing it on a flat plate with a sharp leading edge. The fin leading edge was located 10.3 inches downstream of the plate leading edge, again in a position similar to Oskam (6), McClure (11), and Lu (12). At this position on the plate, the boundary layer thickness was about 0.14 inches, depending on the value of the unit Reynolds number, as the surveys of Tran (39) indicated. On both the plate and floor, the fin leading edge was located at least one inch from the sidewall, depending on the angle of attack, to avoid any possible interference with the sidewall boundary layer.

Both layers, at all unit Reynolds numbers tested, were two-dimensional, equilibrium, naturally turbulent layers on surfaces at near - adiabatic conditions. They were extensively surveyed by both Settles (40) and Oskam (6) and were found to fit the universal wall - wake profile discussed by Sun and Childs (41).

Four different unit Reynolds numbers over a range from 1 to 4 million per inch were tested to check the Reynolds number scaling of the upstream influence data and to examine the effect of unit Reynolds number on the surface features of the interactions. This range represents more than a decade spread in Reynolds number based on boundary layer thickness. This variation was accomplished by altering the tunnel stagnation pressure, from 65 to 250 psia. The minimum unit Reynolds number was chosen based on tunnel operating constraints while the selection of the maximum was dictated by transducer limitations.



Finally, fin deflection angle,  $\alpha$ , was varied to examine the range of angle of attack where secondary separation appears and disappears. Zheltovodov (15) reported that the feature of secondary separation, at Mach 3, first appeared at an angle of attack of 12 degrees and that it vanished at an angle of 20 to 22 degrees. Therefore, this was the range of angles selected. It was also originally hoped to test any angles greater than 22 degrees but this was found to be not possible with the current wind tunnel arrangement. At angles of 12 and 15 degrees comparisons with the data of Oskam (6) and Lu (12), respectively, were possible. These checks were necessary to insure that the data at the lower angles of the test range were correct before extending the tests into the higher shock strengths. A range of angles from 12 to 22 degrees corresponds to a normal Mach number range of 1.46 to 1.92, and an inviscid pressure ratio across the shock of 2.31 to 4.13. The specific angles tested, as well as the boundary layer thicknesses and unit Reynolds numbers they were examined at, are given in Table 1.

## 2.2 DATA ACQUISITION

All of the data collected during the course of this study were mean measurements as this work represents an exploratory investigation into shock - boundary layer interactions at high shock strengths undertaken partially with the hope of identifying points worthy of more detailed future examination.

Two types of data were obtained. The first type was surface flow visualization data while the second was surface pressure distribution data. Admittedly, the deduction of flow field structures from surface data is a difficult and even questionable process. However, this study was performed to obtain a general picture of the interactions in the high angle of attack

regime and to pinpoint features which should receive more detailed examination. In this sense, the collection of surface data alone is quite appropriate as long as caution is exercised in making deductions concerning the flow field.

## CHAPTER III

### EQUIPMENT AND TECHNIQUES

#### 3.1 WIND TUNNEL

The experiments were conducted in the 8-inch-by-8-inch cross section high Reynolds number supersonic blowdown tunnel (Figure 8) located at the Princeton University Gas Dynamics Laboratory. A more detailed description of the facility can be found in the report by Vas and Bogdonoff (42). Briefly, pressurized air was supplied by four Worthington four stage air compressors. The air was dried to reduce condensation problems. A system of tanks with a total capacity of 2000 cubic feet was used to store the air at ambient temperature and pressures of up to 3000 psia. A hydraulically controlled valve released the air into the stilling chamber at stagnation pressures ranging from 60 to 500 psia. The settling chamber temperature varied by a few degrees Kelvin during a tunnel run since there were no heaters in the chamber to maintain a constant temperature. The air expanded, from the stilling chamber, through a convergent - divergent nozzle to a nominal Mach number of 2.95 in the working section downstream of the nozzle. This working section was comprised of three interchangeable 35.5 inch long test sections. The air was then exhausted to atmosphere through a diffuser section.

#### 3.2 TEST SECTION

The test section used for this study was installed in the position just downstream of the nozzle section. It was first used by Oskam and is more

fully described in Reference 6. The section was fitted, on top and bottom, with two 12 inch diameter openings centered 2.5 inches off the tunnel centerline. Glass windows or instrumentation, installed in circular plates, could be inserted into these openings. A horizontally mounted flat plate with a sharp leading edge could be fitted two inches above the tunnel floor. The model was placed either on the tunnel floor or the flat plate. This allowed for testing at two different incoming boundary layer thicknesses at the same value of unit Reynolds number. Both the plate and floor were instrumented with a large number of 0.032 inch diameter surface pressure taps in rows aligned with the undisturbed freestream direction.

### 3.3 SHOCK GENERATORS

It is difficult to achieve high angles of attack due to tunnel blockage problems. Previous investigators at Princeton, such as Oskam (6), McClure (11), and Lu (12), used either a fixed angle fin or a rather large 8 inch by 10 inch variable angle fin which were both limited to an angle of attack of about 15 degrees. Above this value the tunnel starting shock could not be passed through the test section. The model acted as a second throat of too small an area, creating a stalled condition in the tunnel. A variable angle fin could overcome this problem by setting the angle at a low value, passing the starting shock to create a supersonic channel throughout the test section, and then setting the desired angle. Constriction was not a problem since the critical area for Mach 3 flow was smaller than that for the normal starting shock wave. The same idea was used by Oskam (6). However, the fin of this study was much smaller than Oskam's. Therefore it did not create as much freestream blockage and, since it did not span the tunnel height, it did not

interact with the ceiling boundary layer. Consequently, the current fin could produce higher angles than were possible with Oskam's large fins.

The model assembly, made of brass, is pictured in Figure 9. The fin was pinned roughly 1.25 inches aft of the leading edge into a mounting plate which was bolted onto the sidewall through an aerodynamically shaped spacer. The channel formed by the mounting plate and the sidewall was slightly divergent since it was found that with a straight channel, a blockage was formed which spilled around the leading edge of the fin. An aerodynamic "fairing" was pinned to the trailing edge of the 5 inch high, 6 inch long sharp fin. The other end of this fairing was trapped and allowed to slide in a pair of rails machined in the trailing edge of the mounting plate, forming a triangular assembly when viewed from the top, as can be seen in Figure 10. The drive mechanism was a series of linkages pinned into the hinge formed by the junction of the fin and the fairing. The linkages were then connected to a 1 inch diameter screw which could be turned from outside (Figure 11), thereby allowing the angle to be adjusted. A plan view of the entire mechanism, which could be installed for use on both the flat plate and the tunnel floor, is shown in Figure 12. The model was capable of being positioned at any angle between 12 and 30 degrees. The fin position was determined by reading the dial gauge visible in Figure 11. The gauge, accurate to 0.001 inches, was linked to the handle by a bell crank.

Because the pivot point for the fin did not coincide with the leading edge of the fin, the edge swung through a small arc as the fin angle was changed. This movement produced a variation in the streamwise position of the leading edge of 0.01 inches and a spanwise variation of 0.23 inches over the test

range of 12 to 22 degrees angle of attack. The change in incoming boundary layer thickness caused by the streamwise shift of 0.01 inches was not measurable and the uniformity of the incoming turbulent layer insured that the small spanwise differences in the leading edge position for different angles of attack would not influence the test.

The model was calibrated by preparing a calibration table. The table was made by setting the fin angle using a universal bevel protractor accurate to a tenth of a degree and noting the dial gauge reading. The calibration was linear and was checked at least every other day during testing. The error in the fin angle was estimated to be less than 0.25 degrees.

An initial investigation was conducted using two 5 inch high sharp fins of lengths of 5 and 7 inches mounted on the 9 degree adapter arm described by Lu (12). The adapter was then attached to a sting mount normally used for testing freestream models. This preliminary investigation, at angles of attack ranging from 15 to 18.5 degrees, verified that the interaction was independent of the length of the fin and that the fin length was semi - infinite.

The present model can be considered to be semi - infinite with respect to both length and height. The preliminary tests, using the sting mounted fins, showed no differences in the data for lengths of 5 and 7 inches. The data also agreed well with that of Lu (12) who used 10 inch long fins. As stated, the chord length of the present model was 6 inches. It was felt that this was sufficient to insure that the model was semi - infinite in length.

The model was also semi - infinite in terms of height. McClure (11)

surveyed the interaction of a 10 degree, 4 inch high fin and then reduced the height to 3.5 inches for a second survey. Comparisons of the two data sets showed no appreciable differences. Additionally, prior to this study, a set of calculations was performed for the propagation of a disturbance from the upper tip of the fin leading edge along a Mach cone which spread into the interaction region. For the worst case, it was found that the disturbance did not come within two incoming floor boundary layer thicknesses of the test surface until it was downstream of the trailing edge of the fin. Here, an expansion would have already disrupted the flow. For the thinner boundary layer on the flat plate, these calculations showed that the disturbance would not come within six incoming boundary layer thicknesses of the surface until downstream of the trailing edge of the fin. Therefore, the conclusion was made that the fin height was semi - infinite.

Finally, the effect of tunnel span was checked to see if it were wide enough to permit the conical flow of the interaction, if it were indeed conical, to develop. Lu (12) cited a criterion for the inception length,  $L_i$ , which is the length along the inviscid shock trace, measured from the leading edge, beyond which conical flow has been established. When this length was scaled using boundary layer thickness and unit Reynolds number in the manner of Dolling and Bogdonoff (23), a value of 1000 resulted. The worst case, giving the longest inception length, is a thick boundary layer with a low value of unit Reynolds number. When the shock wave is at its greatest angle to the freestream, the amount of conically developed flow in the spanwise direction, within the test section, will be at a minimum. Thus, the worst case occurred at the highest angle of attack, 22 degrees, with the thickest boundary layer, 0.51 inches, and the corresponding unit Reynolds

number, 1.08 million per inch, tested. This worst case calculation, allowing one inch in the spanwise direction for each of the sidewall boundary layers, indicated that the inception length, as measured from the fin leading edge along the inviscid shock trace, was just over 4 inches, leaving a little more than 3 inches of uncontaminated conical flow along the shock direction. This was deemed sufficient for the measurements desired. The data confirmed the results of this calculation.

A number of additional checks were also made during the study. First, care was taken that the fin was positioned normal to the surface. Second, checks were made to insure that there were no gaps between the nylon base of the fin and the test surface, assuring that there was no leakage under the fin. Third, data was taken with and without the fairing piece installed to make sure that it had no influence upon the test. Finally, a small mirror was glued to the fin and a laser was reflected off that mirror, using the laser beam as an optical lever. The reflected beam formed a spot on the tunnel floor which could be readily observed during tunnel operation. Movement of the spot would have indicated that the fin was vibrating. This simple check showed that the model was stationary.

### 3.4 EXPERIMENTAL TECHNIQUES

#### 3.4.1 Surface Flow Visualization

During the course of this study, four different types of flow visualization were used. They included the kerosene - lampblack, local kerosene - lampblack, moving kerosene - lampblack, and alcohol washdown techniques.

##### 3.4.1.1 Kerosene - Lampblack Technique



The initial surface flow visualization technique used was that first reported by Settles (40), and later by Settles and Teng (43). Kerosene and finely ground lampblack powder were mixed to form a thin paste which was then applied on the test surface in bands usually upstream of the fin and along the fin - test surface junction. When the tunnel was started, the mixture spread over the surface showing the surface shear lines, or limiting streamlines. The kerosene evaporated, leaving lampblack deposits in the form of fine streaks, which, if completely dry, did not smear upon tunnel shutdown. The surface pattern was then removed using large pieces of transparent tape. The tape was mounted on clean white paper producing a clear, full scale, undistorted, permanent record of the "footprint" of the interaction. Various features could then be located and measured either in an angular sense using a protractor or in a linear sense with a scale. Angular measurements were accurate to within 0.5 degrees and linear measurements to 0.01 inches.

#### 3.4.1.2 Local Kerosene - Lampblack Technique

This technique was actually a variation of the method just described. The difference was that the mixture was applied only in discrete locations on the test surface. The advantage of this method was found to be that it could be used to give a better indication of where different portions of the flow either originate or terminate, at least on the surface. For example, if the paste was applied only upstream of the interaction, the resulting "trace" could be used to determine whether or not the line of "separation" was a line of exclusion, in other words, if that line indicated a boundary between the flow upstream of it and that downstream of it. The remainder of the technique was exactly the same as above.

#### 3.4.1.3 Moving Kerosene - Lampblack Technique

This method represents yet another variation on the basic kerosene - lampblack technique. The techniques discussed in sections 3.4.1.1 and 3.4.1.2 were used only when the fin angle was fixed. At several angles where data were desired, the tunnel could not be started with the fin fixed at such a severe angle. As discussed earlier, this was the reason for variable geometry. To obtain kerosene - lampblack traces at these angles, the mixture was applied as above with the model positioned at the maximum possible angle at which the tunnel would start. The control valve was then opened to start the run. Once the starting shock had passed the model, the desired angle was quickly set before the mixture dried. Tunnel start was determined by monitoring a static pressure orifice. When the starting shock passed over the tap, the static pressure decreased significantly from its initial atmospheric value. At this point the tunnel was assumed to be started and the model angle could be increased without inducing a tunnel stall. It was possible to set any angle desired within the 20 to 30 seconds required for the paste to completely dry. It should be noted that a thinner mixture, in other words, a greater than normal ratio of kerosene to lampblack, insured that the paste did not dry before the model angle was set. The procedure then continued as before.

#### 3.4.1.4 Alcohol Washdown Technique

The primary disadvantage of the technique described above is that, despite the thinner mixture, the kerosene was evaporating and depositing lampblack on the surface while the fin was moving. This may have introduced ambiguities into the traces akin to photographic double exposures. Therefore, the traces

taken using the moving kerosene - lampblack method had to be verified using another means which was independent of the movement of the fin.

In the method used do to this, ethyl alcohol was substituted for kerosene as the liquid "carrier" portion of the paste. This mixture was then applied to the test surface. The alcohol had a much higher vaporization pressure than the kerosene and, thus, would evaporate quickly to atmosphere with no flow over it to reduce the static pressure. The paste would be completely dry in 60 seconds or less and would not be disturbed by the flow when the tunnel was started. After tunnel start - up, the fin angle was set and a small amount of alcohol was then sucked through a few selected surface pressure taps in the same manner Lu (12) used to "inject" acetone into the boundary layer for vapor screen visualization, allowing the pressure differential across the pressure tap to draw the fluid into the tunnel. The alcohol dissolved the dried lampblack and allowed it to flow producing a pattern which could be removed in the manner outlined above. The alcohol and kerosene produced traces could then be compared for verification. Note that it was useful to do a moving kerosene lampblack test prior to performing the alcohol washdown tests to give a general idea of the local surface flow directions so that paste application and alcohol introduction sites could be selected.

#### 3.4.2 Temperature Measurements

Stilling chamber temperature was measured with a chromel - alumel thermocouple referenced to an ice bath. The thermocouple amplifier was calibrated daily over a range of 233 to 293 degrees Kelvin against a millivolt source to an accuracy of better than 1 degree Kelvin.

### 3.4.3 Pressure Measurements

#### 3.4.3.1 Stagnation Pressure Measurements

Settling chamber pressure was monitored using a Pace 500 psi transducer referenced to atmosphere. It was calibrated daily against a Heise pressure gauge accurate to 0.2 percent of its fullscale deflection of 500 psia. The transducer was calibrated over a range of 50 to 300 psia with less than 1 percent error as measured by the standard deviation from a least squares fit of the calibration data.

#### 3.4.3.2 Surface Pressure Measurements

Surface static pressures were measured using four Druck 50 psi transducers installed in four separate computer controlled 48 port model 48J4 Scanivalves. All were referenced to vacuum. Calibrations were performed daily against a Wallace and Tiernan pressure gauge accurate to 0.1 percent of a 35 psia full scale reading. The transducers were calibrated over a range of 2 to 35 psia with an error of less than 1 percent as measured by the standard deviation from a least squares fit. While taking measurements, a 200 millisecond delay taken between successive readings was adequate to allow the pressure between the scanivalve port and the transducer face to equilibrate.

#### 3.4.3.3 Pitot Pressure Measurements

Several boundary layer pitot profiles were taken to obtain values of the boundary layer thickness needed for scaling purposes and to check the state of the incoming layer. The measurements were made using a cobra probe as a pitot probe. Briefly, a cobra probe consists of three small pitot tubes soldered

side by side. The two outside tubes are used as nulling ports to align the center tube with the local flow direction in a highly skewed flow field. A more detailed discussion of the cobra probe can be found in either (6) or (11). The two nulling ports were used only to insure that the probe was aligned with the freestream. The center pitot port dimensions were 0.020 inches by 0.010 inches. The vertical position of the probe was measured using a linear potentiometer with a three inch travel calibrated against a dial gauge accurate to 0.001 inches.

The transducer used to measure the pitot pressure was a Pace 200 psi transducer referenced to vacuum. It was also calibrated against the Heise pressure gauge to less than 1 percent error as measured by the standard deviation from a least squares fit.

#### 3.4.4 Computer System

Daily calibrations and data acquisition for the surface pressure and boundary layer profile measurements were performed using a Hewlett-Packard HP1000 minicomputer. Control commands for the Scani-valves and for the stepping motor of the probe drive were issued by a Hewlett-Packard 2240 Measurement and Control Processor. A Preston Scientific GMAD 4 analog-to-digital converter read in the data with a resolution of better than 1 millivolt over an input range of  $\pm 10$  volts. Once again, calibration of all the instrumentation for the surface pressure and boundary layer profile measurements was carried out daily prior to the start of testing.

## CHAPTER IV

### RESULTS AND DISCUSSION

#### 4.1 COORDINATE SYSTEMS

The coordinate systems used in the following discussion are depicted in Figure 13. Surface pressures were recorded during the experiment in a cartesian coordinate system with the origin fixed at the fin leading edge and the  $Y = 0$  plane on the test surface. The  $X$  - axis paralleled the incoming freestream with the positive sense being in the downstream direction. The positive  $Z$  - axis was oriented in the spanwise direction away from the fin's surface and normal to the stream. For analysis, all of the coordinates were transformed into a non-orthogonal system having the  $X$  values referenced to the inviscid shock wave trace in the  $Y = 0$  plane. Points downstream of the shock location were taken as having positive values for  $X_s$ . The  $Z$  coordinate values remained unchanged. The transformation between the two systems was given by, where  $\beta_0$  is the inviscid shock wave angle:

$$X_s = X - Z \cot \beta_0 \quad (2)$$

This shock - based coordinate system facilitates comparison of data at different shock strengths since the movement of the inviscid shock wave with increasing angle of attack is inherently accounted for. The inviscid shock was used as a reference point following the suggestions of (21) through (25). These studies concluded the shock was the proper point of reference for interactions of this type.

Figure 13 also illustrates an intrinsic coordinate system advanced by Dolling and Bogdonoff (23) for the purpose of scaling upstream influence data. Upstream influence lengths were measured at a distance from the leading edge along the inviscid shock trace,  $L_s$ , in one of two ways. The first was to measure the distance from the shock trace to the line of upstream influence in the freestream direction, giving the parameter  $L_u$ . The second length,  $L_{un}$ , was defined as the normal distance to upstream influence as measured from the inviscid shock trace. The X and Z coordinates of a point of upstream influence could be transformed into the streamwise system of Dolling and Bogdonoff (23) using the following equations (see, for example, Lu (12)):

$$L_u = -X + Z \cot \beta_0 \quad (3)$$

$$L_s = Z / \sin \beta_0 \quad (4)$$

Values of the coordinates in the system normal to the shock could be obtained with the following transformations (again, see Lu (12)):

$$L_{un} = -X \sin \beta_0 + Z \cos \beta_0 \quad (5)$$

$$L_s = X \cos \beta_0 + Z \sin \beta_0 \quad (6)$$

#### 4.2 SURFACE FLOW VISUALIZATION RESULTS

The following sections discuss the surface flow visualization results. First, the results obtained using the moving kerosene - lampblack technique will be compared to the alcohol washdown data to verify the former. Second, the data at angles of attack of 12 and 15 degrees will be compared with that of Oskam (6) and Lu (12) to further confirm the correctness of the data.

Having demonstrated the validity of the data, the surface flow visualization results will be examined in detail in the third section. This will be followed by a discussion of the local kerosene - lampblack results and some remarks regarding conical similarity. The majority of the analysis of the surface features will rely on the measurements of the surface feature line angles defined in Figure 14.

#### 4.2.1 Alcohol Washdown Technique Results

The traces obtained using the alcohol washdown technique were compared to those gathered with the moving kerosene lampblack procedure to verify that the second method was not yielding ambiguous results. The plot of Figure 15 shows that the angles obtained using the two methods agreed to within the experimental error of 0.5 degrees. This comparison allows the moving kerosene lampblack traces to be used as the principal technique. The "convergence" of the upstream influence and separation line angles evident in Figure 15 will be discussed later.

The reason for preferring the kerosene based data over that obtained with the ethyl alcohol carrier was that the latter technique displayed a few difficulties. First, the limited number of pressure taps which could be used as "injection" sites greatly restricted the surface area which could be covered. For example, the row of taps closest to the fin could not be used to highlight details close to the fin - floor junction because the flow direction along the surfaces there was away from the junction. This produced a resolution problem, which could be overcome with more pressure taps.

The second difficulty encountered was that the alcohol drawn into the



tunnel tended to wash away the lampblack deposits rather than dissolving them and allowing the lampblack to flow. Despite this, enough lampblack streaks remained to allow measurements to be made. A possible solution to this problem is to introduce lesser quantities of alcohol into the flow through the use of a more precise injection mechanism.

Finally, the streaks produced by the washdown technique had an irritating habit of "sticking" to the test surface more than the kerosene produced streaks. Occasionally, clear, sharp streaks on the surface would not lift off with the adhesive tape. However, the deposits which could be removed were adequate for measurement purposes. Perhaps a better carrier fluid could be found for future applications.

These disadvantages indicate that the technique was inadequate for producing the primary data base. The finer detail and greater resolution achievable with the kerosene technique make the data produced using it more desirable as long as there are no ambiguities present. It was obvious that if the alcohol washdown technique is to replace the kerosene lampblack method for variable geometry applications, some improvements must be made. However, the procedure, as it stands, works well as a tool for verification.

#### 4.2.2 Comparisons to Previous Work

Qualitative comparisons of the present data with the surface flow visualization results obtained by Oskam (6) at an angle of attack of 12 degrees and by Lu (12) at 15 degrees indicated general agreement. Measurements of the angles made between the lines of upstream influence, "separation", and "secondary separation" and the freestream direction agreed

with those found by Oskam (6) and Lu (12) within the experimental error of  $\pm 0.5$  degrees. The positive bifurcation, or attachment line, was not plotted because there were some discrepancies, which will be discussed later, between the current data and that of Lu (12).

The agreement of the data with previous work can be clearly seen in Figure 16. The plot shows the angles of each of the three features above plotted against the angle of the inviscid shock trace for the thin boundary layer and a unit Reynolds number of 1.60 million per inch. The measurements of Oskam (6), Lu (12), and the present study are shown. The good agreement of the data at the lower angles of attack, as well as the smooth continuation of the trends, assured that the model was semi - infinite and lent confidence to the data. This agreement also indicated that the surface features at high shock strengths were qualitatively similar to those generated by shock waves of sharp fins at low angles of attack.

Additionally, since both Oskam (6) and Lu (12) judged their data to be conical in nature, this comparison gave the first indication that conical symmetry was present at high angles of attack as well.

#### 4.2.3 Analysis of the High Angle Data

The principal method of analysis of the surface flow visualization data consisted of examining the kerosene - lampblack traces for the features previously defined, marking the lines of those features found, and taking various measurements of the lines such as the angles they made with the freestream direction (Figure 14) and their actual physical position with respect to the inviscid shock location. A representative trace is shown in

Figure 17.

One of the first measurements taken once the feature lines had been drawn on a trace was the coordinates of the virtual origin,  $\Delta X$  and  $\Delta Z$ , which were necessary for later analysis. This point was found by extending the feature lines, including the inviscid shock trace, beyond the leading edge as shown in Figure 13. The lines intersected within a small region which, to a first approximation, could be called a point, defined to be the conical, or virtual, origin. All of the traces analyzed showed that the features seemed to originate from that single point. The only exception was the upstream influence line which consistently intersected the other surface feature lines at locations further upstream and further from the leading edge in the negative  $Z$  direction than the virtual origin. In terms of determining a unique virtual origin, this study was able to achieve better resolution than earlier studies at lower angles of attack. In these previous tests, smaller feature line angles and "slower" convergence of the limiting streamlines led to increased scatter in the location of the virtual origin. At higher angles of attack, these difficulties did not occur, allowing the location of the conical origin to be determined with greater certainty, and showing that there appeared to be a unique conical origin. The existence of such a point further supports the conical symmetry of the interaction.

The location of the virtual origin tended to move towards the leading edge of the fin in both the spanwise and streamwise directions as the angle of attack increased. This trend was also evident in the data of Lu (12).

The variation of the surface features with increasing angle of attack (increasing shock strength) was also of great interest. Initially, the

feature angles were plotted against shock angle. However, as angle of attack and shock angle increase, the feature angles could increase simply through rotational movement of the interaction. Thus, the initial plots showed only that the angles were increasing. Such a plot did not reveal if the angular "size" of the interaction were remaining constant and the flow field was merely "pivoting" with the inviscid shock about the virtual origin. To avoid this, feature angles measured were with respect to the shock angle before plotting against shock angle.

Figures 18, 19, and 20 show the plots of the upstream influence, negative bifurcation, and "secondary separation" angles less the appropriate value of shock angle versus shock angle for various unit Reynolds numbers and boundary layer thickness combinations. The plots show that, regardless of Reynolds number and  $\delta$ , all of the feature angles increased with increasing shock strength. This was not too surprising. The upstream extent of the interaction has been shown to depend directly on the pressure rise across the shock, particularly through the various scaling studies of (21) through (25). Therefore, the upstream extent of the interaction and the feature angles, as a measure of that extent, should increase as well. The angular spreading of the interaction, with increasing shock strength, also accounts for the observed changes in the virtual origin location. No comments regarding the downstream extent of the interaction can be made based on this data set.

The three figures under discussion also show the dependence of the surface feature angles on boundary layer thickness. The investigations of (21) through (25) suggested that the only scale for the extent of the interaction is some measure of the boundary layer thickness. The current data support

this finding as the upstream influence angles were seen to be 2 to 4 degrees greater for the thicker floor boundary layer. Similarly, the angle of the line of "separation" increased by a degree or two as the boundary layer thickness was changed from 0.14 to 0.50 inches. A possible explanation is that, in increasing  $Re_\delta$ , the skin friction coefficient was decreased. With a smaller skin friction coefficient, the streamlines near the wall are less able to negotiate adverse pressure gradients and will be deflected sooner. This would produce higher feature angles in the thick boundary layer cases. The effect of boundary layer thickness on the angle of the "secondary separation" line could not be observed as the feature was not visible for the floor boundary layer tests. This fact, as well as other observations of this feature, will be discussed in more detail later.

The plots of the feature angles also showed a slightly decreasing trend, outside of the experimental error, for all of the feature angles as unit Reynolds number increased. This trend was observed by Lu (12) as well. Consider the upstream influence line. The incoming boundary layer thickness can be expected to decrease as the unit Reynolds number increases. It was shown above that the angular size of the interaction is proportional to boundary layer thickness. Thus, as unit Reynolds number is increased, the angular size of the interaction would be expected to decrease. Consequently, the surface features should be more swept.

This same argument can be applied to the negative bifurcation line equally well. If this line of "separation" is shown to be a line of exclusion dividing the flow into two regions upstream and downstream of it, as will be done later, it can be thought of as defining the upstream extent of the

interaction. Once the region in which the remaining features can develop is defined by the separation line, the features downstream of it must occur in a clearly defined zone. Since the negative bifurcation line is more swept for increased unit Reynolds number, it seems likely that the other features would also be more swept.

In further examining the effect of Reynolds number on the surface features, the upstream influence angle was plotted against  $Re_\delta$ . Figure 21 shows the data at angles of attack of 14 and 18 degrees with the points connected according to the test surface they were obtained on, floor or plate. Figure 22 shows the same data but for curves of constant tunnel stagnation pressure (i.e., constant unit Reynolds number). The trends visible in both figures are the same as those reported by Settles (40) for two - dimensional upstream influence data. The conclusion of Settles was that  $Re_\delta$  may not have been the appropriate parameter to correlate the data with. Unit Reynolds number was thought to be the more significant parameter for the two - dimensional data. The same appears to be true in three dimensions. As was the case in (40), no explanation is known for this unit Reynolds number effect.

Finally, a few remarks concerning repeatability are necessary. The values of the surface feature angles could be verified as several traces were taken at each angle of attack, including those using the alcohol washdown technique. The measurements were found to be within  $\pm 0.5$  degrees of each other. Other checks were also possible in the case of upstream influence since four different methods could be used to either directly measure or calculate the angle. The kerosene - lampblack or alcohol - lampblack traces provided direct measurements while the angle could also be calculated from the

coordinates used for the upstream influence scaling checks and from the pressure distributions. All four methods were found to agree, for a given angle of attack, within  $\pm 0.5$  degrees of a mean value. No method was consistently high or low with respect to the mean.

#### 4.2.4 Local Kerosene - Lampblack Results

The technique of section 3.4.1.2 was applied to help determine the origin and extent of certain portions of the surface flow. When the kerosene - lampblack mixture was applied upstream of the interaction, none of it crossed from the upstream to the downstream side of the negative bifurcation line. This would indicate that this line was a "line of exclusion" which divides the surface flow into two regions. This result supports the concepts of three-dimensional separation discussed earlier. Lu (12) also observed the line of separation to be a line of exclusion.

Conversely, if the paste was spread on the test surface along the junction of the fin and the floor from the leading to the trailing edge, the region downstream of the separation line filled in with none of the lampblack being deposited on the upstream side of the line. The fact that this line can be shown to be a line of exclusion lends credence to the argument of the preceding section regarding the effect of unit Reynolds number. Since the bifurcation line is a line of exclusion, once it has been established, the angular extent of the interaction is determined and the other features should lie within the region downstream of the separation line.

Additionally, for the case of the thin boundary layer, if the paste was spread along the fin-floor junction at a distance of roughly 1.0 to 1.5 inches

from the leading edge along the corner line, the line of "secondary separation" could also be shown to be a line of exclusion. The above results are presented in Figures 23 through 25 for an angle of attack of 15 degrees.

#### 4.2.5 Conical Similarity

The data obtained from the kerosene - lampblack traces were also examined for evidence of conical symmetry. There is no reason to expect a conical flow to develop in the far field ( $Z = \infty$ ) of a sharp fin - induced interaction because none of the boundary conditions imposed on the flow are conical. However, investigators such as Lu and Settles (27) have observed conical surface features for these types of interactions within the confines of their tunnel test section. Similar features may be expected to occur at higher shock strengths. Feature angles, particularly upstream influence, were plotted using interaction response functions in the manner of Settles and Kimmel (28). When the angular difference between the upstream influence angle and the shock angle were plotted against the difference between the shock angle and the freestream Mach angle, Settles and Kimmel (28) reported, for fins, a line described by:

$$\beta_{ui} = 1.59\beta_o - 10.0 \quad (7)$$

A least squares fit of the data of Oskam (6), Lu (12), and the current study gave the following result:

$$\beta_{ui} = 1.63\beta_o - 11.0 \quad (8)$$

The data of Oskam and Lu were used to obtain a larger range over which to fit the line. A plot of the two curves (Figure 26) shows that the two are in general agreement as both would fit inside a  $\pm 0.75$  degree error band.



Hence, conical similarity for fins at angles of attack up to 22 degrees appears to have been demonstrated for the conditions tested. The fact that conical symmetry was present is consistent with the findings of earlier work.

#### 4.3 UPSTREAM INFLUENCE SCALING RESULTS

The analysis used in this portion of the study follows that used by Dolling and Bogdonoff (23). The location of the points of upstream influence, that is, the points where the incoming limiting streamlines were first deflected from their initial trajectories, were located on the kerosene - lampblack traces and measured at a number of spanwise locations using the cartesian reference frame of Figure 13. The coordinates were then transformed into the intrinsic system also shown in Figure 13 using equations (3) through (6).

When  $L_u$ , the streamwise upstream influence length, was plotted against the distance along the shock,  $L_s$ , the trends reported by Dolling and Bogdonoff (23) continued. Figure 27 shows that the dependence on angle of attack or, more precisely, dependence on normal Mach number was hidden since, for a single combination of unit Reynolds number and boundary layer thickness, all of the data fell on a single curve. This indicated that, although the data was collapsed,  $L_u$  versus  $L_s$  was not the proper reference frame for demonstrating all dependencies of the data. As shown in Figure 28, upstream influence for the thicker boundary layer occurred at a greater streamwise distance from the inviscid shock trace. Upstream influence, in this frame, also moved closer to the shock trace as unit Reynolds number increased. The flattening curves of Figure 29 demonstrate this.

When the normal upstream influence length,  $L_{un}$ , was plotted against  $L_s$ ,

the effect on upstream influence of increasing the normal Mach number, or increasing the pressure rise across the shock was clearly seen. Figure 30 illustrates that the greater the pressure rise associated with the shock, the further upstream it was felt. This choice of coordinates, which is now an orthonormal system, also retains the boundary layer thickness and Reynolds number trends mentioned before as Figures 31 and 32 show.

The final step in the analysis was to scale the data using unit Reynolds number, boundary layer thickness, and normal Mach number in the manner detailed earlier. Note that scaling by normal Mach number is equivalent to changing coordinates from  $L_{un}$  back to  $L_u$  since the streamwise and normal upstream influence lengths, as well as the streamwise and normal Mach numbers, differ by a factor which is the sine of the shock angle as the following equations indicate:

$$L_{un} = L_u \sin \beta_0 \quad (9)$$

$$M_n = M_\infty \sin \beta_0 \quad (10)$$

Therefore, data for different angles of attack should be expected to collapse on a single curve. Figure 33 demonstrates the usefulness of the technique as all of the data, for all of the unit Reynolds number, boundary layer thickness, and angle of attack combinations, collapse on a single curve. This result makes it clear that the scaling principle of Dolling and Bogdonoff (23) is valid for fin angles of attack up to 22 degrees for the conditions tested and is a useful approximation for characterizing these interactions. Additionally, a value for the inception length (scaled by  $\delta$  and  $Re_u$ ) of

approximately 1000 is in agreement with the findings of Lu (12).

An important point to note is that the reference boundary layer thickness was that measured at the fin leading edge position rather than an average or local thickness. This was done because of the scarcity of boundary layer information at several of the Reynolds number - boundary layer thickness combinations tested. It does not appear to have affected the results in a visible manner, mainly because of the degree of sweep of the interaction. For highly swept interactions at low angles of attack, the choice of  $\delta$  is the most critical as the following analysis demonstrates.

The portion of the boundary layer furthest from the fin in the spanwise direction must travel further downstream, growing in thickness all the time, than the incoming the incoming boundary layer at the fin leading edge position before it feels the effect of the pressure rise. That same portion of the boundary layer must travel over a relatively lesser and lesser distance to be affected as the angle of attack increases and the interaction becomes less swept. Therefore it has less opportunity to thicken and there is less and less variation, with increasing fin angle, in incoming boundary layer thickness along the line of upstream influence. Thus, the choice of boundary layer thickness to be used for scaling becomes less critical as fin angle increases. In fact, the least error associated with the use of incoming boundary layer thickness would be expected to occur at the highest angle of attack. Calculations showed that at an angle of attack of 20 degrees, the incoming boundary layer thickness, in the case of the thick boundary layer, increased by 5 percent along the upstream influence line from the leading edge to a point defined by the intersection of that line and the plane of  $Z=5$

inches. The thin boundary layer thickened by 33 percent over a similar region. This can be contrasted with calculations made from the data of Lu (12) at an angle of attack of 5 degrees which showed that, for the same positions as above, the incoming thick boundary layer increased in depth along the more swept upstream influence line by 13 percent and the thin layer by 63 percent. This factor of two reduction in the incoming boundary layer thickness variation along the upstream influence line and the collapse of the data would seem to indicate that either the use of incoming boundary layer thickness was valid or the scaling was very insensitive to the choice of boundary layer thickness.

#### 4.4 SURFACE PRESSURE RESULTS

The following discussion presents the surface pressure results by first comparing the data taken at angles of 12 and 15 degrees to that given in (6) and to data duplicated using the arrangement of (12). Having established the validity of the pressure data at low angles, the results at higher angles are then discussed both in general and in detail. This portion of the analysis concludes with an examination of conical similarity with respect to the surface pressure data. In all of the plots supporting the following discussion, the pressure data is shown normalized by the calculated freestream static pressure.

##### 4.4.1 Comparisons with Previous Data

All of the pressure distributions taken were shown to possess excellent repeatability but independent checks of the data were desired.

The pressure distribution at an angle of attack of 12 degrees was compared with that of Oskam, et. al. (7) in Figure 34. The reasonably close agreement tended to confirm the present data but stronger verification was desired. The 15 degree model of Lu (12) was used in a separate test to validate the 15 degree results obtained using the variable angle model. Surface pressure distributions were taken under as near identical conditions as were possible. The comparison between the duplicated data set and the current pressure data is shown in Figure 35 using normalized coordinates to account for differences in the spanwise measurement locations of the two tests. The excellent agreement appears to validate the present data.

In both of these comparisons the effect of the shortened fin length was evident. Although these comparisons and the earlier tests with the sting mounted fins showed that, upstream of the shock, the interactions for fins of different lengths were identical, there were disagreements downstream of the shock. These discrepancies were brought about by the expansion fan being allowed to affect the interaction further upstream than the fins of either Oskam (6) or Lu (12) allowed it to. Oskam showed that a large distance is needed for that final level to be reached and this effect prevents the full downstream pressure rise from being obtained.

Additionally, all of the pressure distributions taken were shown to possess excellent repeatability.

#### 4.4.2 General Description

The surface pressure distributions were analyzed using the inviscid shock trace as the point of reference as suggested by the investigators of studies

(21) through (25).

In general, the streamwise pressure distributions followed the same qualitative trends seen by earlier researchers. The incoming flow showed a constant pressure level. The point of initial pressure rise corresponds to upstream influence. Alternately, upstream influence can be and has been defined in the past as that point where the tangent to the steepest gradient of the initial pressure rise intersects the undisturbed upstream pressure level. For the large gradients seen in this study, the two definitions gave equivalent results. Following the initial pressure rise, a plateau was reached which, as angle of attack increased, became more of a peak rather than a plateau. However, the term "plateau" will be used throughout this discussion to refer to either an actual plateau or the initial peak in the pressure distributions. The plateau was immediately followed by a "dip". The pressure then continued to rise in the downstream direction beyond the inviscid level until it was affected by the expansion fan located at the trailing edge of the fin. These qualitative features are shown in Figure 36.

#### 4.4.3 Analysis of the High Angle Pressure Data

The pressure distributions were examined to evaluate the effect of each of the three test variables. The first step was to check the trend of the data with increasing angle of attack. As Figure 37 shows, the magnitude of and the gradients along the entire pressure curve, from the point of upstream influence on, increase with increases in shock strength. This differs from two - dimensional data which, once the flow has separated, has the same pressure distribution up to the separation point as the shock strength increases. In the current study, the prominence of the dip also increases

monotonically with shock strength.

An interesting point to note is that it appears that upstream influence occurred in the same position relative to the inviscid shock trace for all angles of attack, a trend which the data of Oskam (6), for angles ranging from 2 to 13 degrees, revealed as well. In fact, Oskam, et. al. (9) claimed that, based on analysis of surface pressure distributions, upstream influence was independent of angle of attack. This aspect of the data may have resulted from the choice of coordinate systems. Recall that when the upstream influence length measured in the streamwise direction,  $L_u$ , was plotted against  $L_s$  (Figure 27), all of the data collapsed on a single curve masking any normal Mach number dependence. The pressure distributions were also taken in a streamwise direction, giving an equivalent situation.

It is known that the normal Mach number is proportional to the pressure rise across the shock. Lu and Settles (27) demonstrated that  $L_{un}$ , at a given Z location, was equal to the product of a constant and the normal Mach number. This shows that  $L_u$  is also proportional to the pressure rise (see also (23)). Thus, we have :

$$L_{un} = c M_n \quad (11)$$

Substituting known relations for  $L_{un}$  and  $M_n$  :

$$L_u \sin \beta_o = c M_\infty \sin \beta_o \quad (12)$$

This shows that, after removing the shock angle terms,  $L_u$  should be expected to be a constant for a given freestream Mach number and Z location. This also implies that, for a given boundary layer thickness and unit Reynolds number, pressure disturbances can "feed" upstream of the shock only a finite

streamwise distance which is proportional to the incoming Mach number.

An interesting application for this observation is that, since  $L_U$  appears to be a constant for a given  $Z$  location, the location of upstream influence and its angle can be predicted knowing only the freestream Mach number, the angle of attack, and the value of  $L_U$  for two separate  $Z$  locations. Geometric considerations produced the following equation for predicting the upstream influence angle:

$$\beta_{ui} = \tan^{-1} \left[ \frac{Z_2 - Z_1}{L_{u_1} - L_{u_2} + (Z_2 - Z_1) \cot \beta_o} \right] \quad (13)$$

Substitution of streamwise upstream influence lengths taken from surface pressure distributions and calculation of several angles gave results which agreed with the experimental values of  $\beta_{ui}$  to within  $\pm 3\%$ .

All observations and analysis regarding upstream influence will be made in a streamwise sense. Any unit Reynolds number or boundary layer thickness trends observed using a streamwise system however will remain valid since these trends were consistently present in the upstream influence scaling analysis regardless of the coordinates used.

Figure 38 demonstrates the effect of unit Reynolds number on the pressure distributions. An increased unit Reynolds number gave slightly elevated pressures along the entire curve, delayed upstream influence, and weakened the initial pressure gradient. Lu (12) observed this as well, and noted that the effect of unit Reynolds number decreased with increasing angle of attack. Thus, the current findings continue to be consistent with previous work.



Pressure distributions for different boundary layer thicknesses but the same angle of attack and unit Reynolds number are shown in Figure 39. This figure further demonstrates an observation made earlier; upstream influence occurred slightly more upstream in the interaction with the thick boundary layer.

Another, more significant disagreement between the two curves occurs downstream of the shock wave location. The two sets of data begin to diverge with the pressures in the thin boundary layer being significantly higher. This divergence grows as angle of attack increases. The data of Oskam (6) showed the beginnings of this trend as well. Oskam (6) stated that all transverse pressure gradients, which will be sensed in a streamwise pressure distribution as well as in a spanwise one, remain until incoming boundary layer thicknesses downstream of the inviscid shock location. As the data shows, if both interactions produce the same ultimate downstream pressure ratio, the thicker boundary layer will produce it over a longer physical streamwise distance. Consequently, the expansion fan from the tail of the fin affects the final pressure ratio sooner for the thick boundary layer. This trend can also be seen in Figure 39 which shows the calculated positions of the first wave of the expansion fan in each case. Additionally, the thick boundary layer interaction should display shallower pressure gradients. Closer examination of Figure 39 shows this to be the case. The pressure gradients are less throughout the interaction, with the exception of the plateau region, for the half inch thick floor boundary layer as compared to the plate boundary layer interaction. These results support the concept that the physical size of the interaction, as well as the severity of the accompanying pressure gradients, is determined by the incoming boundary layer.

A final point to note is that not only does the prominence of the dip increase with increasing angle of attack, it also increased with decreasing boundary layer thickness. Figure 39 shows pressure data for the two boundary layers with the fin at an angle of attack of 18 degrees. Note how much more pronounced the dip is for the thin boundary layer. In fact, the dip was not apparent with the thick boundary layer for angles of attack less than 20 degrees. The thick boundary layer cases, when compared to the thin boundary layer tests, had weaker static pressure gradients which indicated a less rapid and, consequently, "weaker" interaction which may not have produced the dip in the streamwise pressure distributions. A higher level of pressure fluctuations in the floor layer could mask this feature as well. A third possibility which could account for the disagreement is differing turbulence scales, as will be explained later. High frequency surface pressure and hot wire measurements may provide some insight into this question.

#### 4.4.4 Conical Similarity in the Pressure Distributions

If the surface pressures and the flow field off the surface are conical, the proper coordinate system would be spherical with its origin at the virtual origin. However, the experiment was designed to use the available pressure tap arrangements which were aligned with the freestream. The ideal situation would have been to have arranged the taps in arcs similar to the setup of Zubin and Ostapenko (13). This problem of not having the surface pressure data in spherical coordinates was addressed quite simply. If all the streamwise coordinates,  $X$  or  $X_s$ , were divided by the spanwise distance from that row of taps to the conical origin,  $Z + \Delta Z$ , a quasi-angular quantity resulted. The new variable was equal to the inverse tangent of the angle

between the freestream direction and a ray from the conical origin to the point of interest. This was equivalent to a polar coordinate system in the  $Y=0$  plane with the  $\theta = 0$  axis parallel to the freestream direction, or positive X-axis. This scheme was convenient since, if the flow is conical, the static pressure at the surface along a ray from the conical origin is a constant. As the investigators of (26) and (27) have argued, if several streamwise pressure distributions at different Z locations for the same test are plotted using the quantity just described, the data will collapse on a single curve if it was produced by a conical flow.

Using this method, the pressure distributions for each of the 28 combinations of angle of attack, boundary layer thickness, and unit Reynolds number were seen to collapse, indicating conical symmetry was present in all cases. Figure 40 shows a typical collapse of the data. Therefore, the conclusion from this evidence and that of the surface flow visualization was that conical similarity of the surface data was present over all conditions tested for angles of attack up to 22 degrees at a Mach number of 2.95.

#### 4.5 PRESSURE DISTRIBUTION - FLOW VISUALIZATION COMPARISONS

As mentioned, the locations of various surface features were measured from the flow visualization data. The conical surface feature lines were then marked as points on the corresponding collapsed pressure distributions in an attempt to correlate the two characteristics of the interactions. Similarly, the pressure distributions could be used to produce topographic style pressure "maps" which could be overlayed on the kerosene - lampblack traces. These plots showed that the lines of constant pressure were, in fact, conical. This was also shown by the collapse of the pressure distributions discussed in the

preceding section. The two methods of comparing the pressure and surface feature data, shown in Figures 41 and 42, were found to be essentially equivalent. However, the former lent itself better to presentation. Thus, the following discussion concentrates on the findings obtained using that technique. The discussion examines each surface feature in turn.

#### 4.5.1 Upstream Influence

The point of upstream influence could be defined in one of two ways discussed in section 4.4.2.

The line of upstream influence could be located using the definitions above and by measuring its location on the surface flow visualization traces. The two methods agreed in all cases.

The incoming flow conditions also influenced the location of the point of upstream influence. As the boundary layer thickness increased, upstream influence was seen to occur at a point further away from the inviscid shock trace. As unit Reynolds number increased, the feature moved closer to the shock wave location. These trends have already been discussed in detail. The fact that upstream influence appeared to occur at a constant location for all angles of attack at a particular Reynolds number-boundary layer thickness combination was also observed in this analysis.

#### 4.5.2 Line of Separation

The next significant feature the line of negative bifurcation, or separation. The line was present for all of the angles of attack in the test range and for all conditions. Comparisons of the surface pressure and

kerosene - lampblack data showed that, as angle of attack increased, this feature tended to occur further and further upstream of the inviscid shock location. In other words, as the shock pressure rise increased, the "separated" region grew in angular size. As already observed, this feature also tended to move towards the shock location as unit Reynolds number increased and as boundary layer thickness decreased.

The pressure ratio at the bifurcation line depended weakly on the test variables as can be seen in Figure 43. The separation pressure ratio was seen to increase with angle of attack as Law (4) noted over a similar range of fin angles at Mach 6. The pressure ratio in question decreased as boundary layer thickness was changed from 0.14 to 0.50 inches. Finally, as unit Reynolds number was increased, the bifurcation pressure ratio also increased. Typical values of the pressure ratio for separation were between 1.5 and 1.6. Such values are consistent with those reported in (1), (2), (14), (19), and (20). The separation pressure ratio, to a first approximation, could be said to occur at approximately 85 percent of the plateau pressure ratio. Practically, this allows the location of the negative bifurcation line to be estimated from a streamwise pressure distribution alone.

As mentioned, Figure 15 showed that, as angle of attack increased, the angles of upstream influence and separation converged. Recall that, at a particular spanwise location, upstream influence occurs at the same streamwise distance from the shock for all fin angles. Second, the initial gradient increases with angle of attack. Third, separation occurs, along the initial rise, within a very narrow band of pressure ratio. The separation pressure ratio can therefore be approximated as a constant. As angle of attack is

increased, the steepening gradient "moves" the location where the separation pressure occurs towards the fixed point of upstream influence. As the two features move physically closer, an angular convergence results.

#### 4.5.3 Secondary Separation

One of the objectives of this investigation was to examine the feature termed "secondary separation". Examination of the data showed that, whenever it was present, it seemed to coincide with a point at or just past the initial peak in a streamwise pressure distribution. As with the other features, it moved closer to the shock as the unit Reynolds number was increased. This observation agrees with that of Zheltovodov (14) who reported a "tightening" of the "secondary separation zone" as unit Reynolds number increased. The effect of the thickness of the incoming boundary layer could not be determined other than to note that in increasing the thickness from 0.14 to 0.50 inches, the feature was no longer visible. As with separation, the secondary separation pressure ratio increased with both increasing unit Reynolds number and angle of attack.

#### 4.6 DISCUSSION OF SECONDARY SEPARATION

As previously mentioned, there were several observations regarding secondary separation which demanded further attention. Secondary separation was visible at all angles of attack from 12 to 18 degrees, inclusive, at all unit Reynolds numbers tested but only for the thin boundary layer. This range of angles of attack is in agreement with the findings of Zheltovodov (14) who stated that secondary separation first appeared when the product of the freestream Mach number and the angle of attack, measured in radians, equaled

0.6. The feature, according to this, should appear at a fin angle of 11.6 degrees for a Mach number of 2.95. Zheltovodov (15) also observed that the secondary bifurcation line disappeared at an angle of attack of 20 degrees for Mach 3 flow. Zubin and Ostapenko (13) also observed secondary separation but, like Zheltovodov, did not report any measure of the boundary layer thicknesses used in their tests. This lack of information is unfortunate because boundary layer thickness appears to play a major role in determining whether or not the feature is visible on the test surface. Kubota and Stollery (10), in examining angles of attack of to 15 degrees at Mach 2.3, did not observe secondary separation in a boundary layer 0.6 inches thick while McCabe (2) did note the feature at both Mach 2 and 3 for boundary layer thicknesses of 0.14 and 0.23 inches. Lu (12), using the same boundary layers as the present study, observed secondary separation at an angle of attack of 15 degrees for the thin boundary layer but not for the thicker one. The surface flow sketches of Law (4), taken from oil flow photographs, showed that the feature was present at a Mach number of 6, a unit Reynolds number of 10 million per foot, and a boundary layer thickness of 0.12 inches over an angle of attack range of 10 to 20 degrees. These results, as well as those of the present study, indicated that the presence of secondary separation does not depend on the freestream Mach number or the value of the unit Reynolds number. As Zheltovodov (15) noted, an angle of attack, or shock strength, dependence was present. The present investigation revealed that secondary separation also depends on the boundary layer thickness in some manner.

Changes within the boundary layer may explain the observations concerning secondary separation. First, assume that the kerosene - lampblack technique is not displaying physically insignificant features due to sensitivities to

unimportant flow parameters. The increase in boundary layer thickness was accompanied by an increase in the physical scale of the turbulent fluctuations. Assume that secondary separation can be described using some physical scale. The size of the eddies in the thin boundary layer may be less than or of the same order as the "size" of the feature. As the boundary layer thickness increased, the scale of the turbulent eddies may have increased at a faster rate than the scale of secondary separation, resulting in a situation in which the larger turbulent fluctuations dominate and suppress the structure causing the feature of secondary separation to appear in the surface flow visualization. Thus, the boundary layer dependence of secondary separation may be due to competing turbulent and feature scales. This hypothesis could not be confirmed or denied with the present data. Measurements of fluctuating quantities in the interactions are necessary to make those determinations. However, these remarks agree with Zheltovodov's postulate (15) that the state of the boundary layer in the return flow region influences secondary separation.

There may also exist an intimate connection between the "dip" seen in the streamwise pressure distributions discussed in Section 4.4.3 and secondary separation. Korkegi (18) also suggested this connection. Both the dip and secondary separation were quite apparent in the tests using the thin boundary layer while both were either less prominent or not apparent for the half inch thick floor boundary layer. The dips were not apparent for angles of attack less than 20 degrees for pressure distributions taken using the 0.50 inch thick boundary layer. The absence of this dip, for whatever reason, including the change in the boundary layer just discussed, could also indicate the absence of secondary separation. The interaction, in a nonlinear fashion, of



changes (due to increasing shock strength) in both turbulence intensities and turbulence scales with changes in the strength and scale of secondary separation may account for the behavior of the feature as angle of attack is increased. This observation is also consistent with the findings of Zubin and Ostapenko (13) who stated that the growth of counter gradients, or dips, in the return flow region could lead to separation of the boundary layer within the principal separated region. Further measurements are necessary to reach a more definite conclusion.

#### 4.7 DISCUSSION OF ATTACHMENT

As mentioned above, there were discrepancies concerning the line of attachment that appeared when the current data was compared to that of Lu (12). The measured angles of the feature line were consistently 3 to 5 degrees lower than the earlier data. This was particularly vexing since the earlier tests, using the sting mounted fins, agreed with that of Lu (12) and because the pressure distributions were seen to match (see section 4.4.1).

A number of checks were made to locate the source of the disagreement. The first thought was that there was leakage under the fin. The test model was run with and without a bolt through the ceiling which forced a seal between the fin base and the floor. Surface pressure distributions and surface flow visualization traces showed no differences between the two cases.

Second, the effect of the afterbody fairing was checked by collecting data with and without it in place. Again, both data types, the surface pressures and flow visualization, agreed.

Third, fin length was proposed as a possible factor. However, as stated, the earlier tests showed that a fin length of as little as 5 inches produced data which agreed with the results of Lu (12). The current model is 6 inches long.

A final potential source of the discrepancy, which could not be checked, was the moving kerosene - lampblack technique. A rapid evaporation of the carrier fluid in this region, occurring while the fin angle was being set, could account for the discrepancies noted. The feature would be formed at a lower angle of attack and shock strength than believed, producing a line whose angle to the freestream was less than predicted. Due to the problems discussed, the alcohol washdown method could not be used to check this hypothesis.

Examination of other data made the discrepancy even more puzzling. The surface flow visualization sketches of Law (4) at Mach 6 showed the attachment line lying close to the fin as was seen in this study. In fact, a nearly constant difference between the attachment angle and the fin angle of 6.5 degrees was reported. The average difference between the two angles in the present data was 6.2 degrees. This apparent agreement may or may not be meaningful due to the Mach number difference of the two studies. However, this was a point which further confused the situation.

As yet, the discrepancy remains unexplained. Perhaps a check of the effect of the fin length using the present configuration would be useful. However, the existence of this discrepancy does not invalidate any results or conclusions.

## 4.8 COMPARISONS WITH COMPUTATIONS

### 4.8.1 Computation of Knight

Using the method outlined in Reference 37, Knight (44) has calculated the flow field for the case of fin deflection angle equal to 20 degrees, a boundary layer thickness of 0.50 inches, and a unit Reynolds number of 1.60 million per inch. The comparisons of the surface shear stress vectors and surface pressure distributions obtained computationally with the experimental data are shown in Figures 44 through 46.

#### 4.8.1.1 Surface Feature Comparison

Upon qualitative comparison with the kerosene-lampblack traces taken at 20 degrees (Figure 44), the surface shear stress plot (Figure 45) was seen to reproduce the essential features of the surface flow visualization. Upstream influence, separation, and attachment are clearly visible in both the experimental and computational data in approximately the same locations. Secondary separation was visible in neither.

However, measurements of the angles of the lines of convergence showed that the separation line was more highly swept for the computational data, although the difference was less than one streamwise grid spacing at the location furthest from the fin in the spanwise direction. In a comparison of 10 degree fin data with computational results, McClure (11) also noted a slight problem with streamwise grid spacing. The stronger shock wave at 20 degrees should be expected to only magnify the problem through steeper pressure gradients. A finer streamwise grid spacing could resolve this minor discrepancy.

#### 4.8.1.2 Surface Pressure Distribution Comparisons

Figure 46 shows the comparison of the actual and computed pressure distributions for the plane  $Z = 1.46$  inches. The computations generally reproduced the features of the pressure distribution. The upstream influence locations agreed for both data sets. The computed pressure data also agreed with the measured pressures through the plateau region. However, the steep gradients upstream and downstream of the shock location were underpredicted. Additionally, the computations showed no evidence of a dip in the distribution. Once again, these discrepancies were quite possibly due to the streamwise grid spacing not being fine enough.

#### 4.8.2 Computation of Horstman

##### 4.8.2.1 Surface Feature Comparison

Horstman (45) has also computed some high angle flow fields. Figure 47 shows a computed surface streamline pattern for an interaction at  $16^\circ$  degrees in the floor boundary layer. Surface feature angles measured from this plot were 6 to 8 degrees lower than the experimental values, despite the general features being reproduced.

##### 4.8.2.2 Surface Pressure Distribution Comparison

Figure 48 shows a comparison of experimental and computed surface pressure distributions at  $Z = 3.40$  inches. The computation predicted the upstream influence location and plateau level but, like Knight, failed to reproduce the gradients. In this case the streamwise grid spacing was as fine or finer than the experimental resolution and should, therefore, not be at fault. Perhaps,

the turbulence model is to blame for the disagreement in this comparison.

#### 4.9 FLUCTUATING SURFACE PRESSURE MEASUREMENTS

Recently, Tan and Tran (46) used the shock generator of this study to examine the fluctuations of surface pressure at angles of attack of 12, 16, and 20 degrees in the floor boundary layer at a unit Reynolds number of 1.60 million per inch. The measurements were made using Kulite high frequency surface pressure transducers. The data showed an initial rise of the fluctuations from their upstream level to a spike near the upstream influence line. The rms fluctuation level then settled to an approximately constant value between the upstream and spike values. The rms levels of the fluctuations were seen to increase as angle of attack was increased. However, these levels were 50 percent or less of those observed in the two - dimensional cases of (47) and (48) which had equivalent shock strengths. Additionally, some unsteadiness of the shock was seen but, again, of levels less than seen in similar two-dimensional cases. The comparatively low levels present in the three - dimensional measurements indicated that while the shock structure did amplify the fluctuations, the unsteady component of the interaction was not dominant. Thus, the mean measurements of this study, while not providing the complete picture, gave a reasonable insight into the interaction.

## CHAPTER V

### CONCLUSIONS AND RECOMMENDATIONS

#### 5.1 SUMMARY OF FINDINGS

An experimental study of the three dimensional shock wave - turbulent boundary layer interaction induced by a sharp fin has been conducted over a range of angles of attack from 12 to 22 degrees, a unit Reynolds number range of between 1 and 4 million per inch, and at boundary layer thicknesses of 0.14 and 0.50 inches. Both surface pressure data and surface flow visualization results were collected. The following conclusions were made:

- (1) The surface flow features of strong shock - induced interactions, with the exception of secondary separation, are qualitatively similar to those observed at lower angles of attack. The upstream extent of the interaction was seen to simply increase with increasing shock strength.
- (2) Using both surface flow visualization and surface pressure data, sharp fins have been demonstrated to produce conical surface features for angles of attack up to 22 degrees under a variety of conditions.
- (3) The upstream influence scaling scheme of Dolling and Bogdonoff (23) was shown to be valid for sharp fins at angles of up to 22 degrees at a Mach number of 2.95, thus increasing the generality of the principle.
- (4) The present data, as well as that of Oskam (6), showed that the streamwise upstream influence length was proportional to the freestream

Mach number.

(5) The alcohol washdown method of surface flow visualization as described herein has some limitations in application but has been shown to be a useful tool for the verification of flow visualization data obtained by other methods.

Additionally, the following observations were made:

(1) As the angle of attack was increased, the location of the virtual origin moved closer to the fin leading edge, in both the streamwise and spanwise directions.

(2) The upstream extent of the interaction was seen to increase with increasing angle of attack, increasing boundary layer thickness, and decreasing unit Reynolds number. This amounts to another confirmation of the scaling results stated in (3) above.

(3) The lines of separation and secondary separation were shown to be lines of exclusion which divide the surface flow into distinct regions.

(4) The line of separation was found to occur at a pressure ratio of approximately 85 percent of the plateau level. The separation pressure ratio increased with increasing angle of attack, increasing unit Reynolds number, and decreasing boundary layer thickness.

(5) Secondary separation was seen to depend on boundary layer thickness as well as on shock strength. It was also associated with a dip in the streamwise pressure distributions which was also dependent on the

boundary layer thickness.

(6) A discrepancy concerning the angle of the positive bifurcation line data was noted between the results of Lu (12) and the present tests. This discrepancy remains to be explained.

(7) Comparisons of surface flow visualization and surface pressure data with the computations of Knight (45) at an angle of attack of 20 degrees and of Horstman (46) at 16 degrees showed fair agreement. Underprediction of surface feature angles and surface pressure gradients was noted in both cases but for, perhaps, different reasons. The discrepancy in Knight's data may have been due to the streamwise grid spacing while the turbulence model may have accounted for the disagreement between the computation of Horstman and the experiment.

(8) Conclusion (4) above allowed the upstream influence angle to be predicted within  $\pm 3\%$  using an equation developed from purely geometrical considerations.

(9) Strong differences and similarities with two - dimensional interactions were observed. The three - dimensional data were different in that the initial pressure rise changed as shock strength increased while, in two dimensions, that portion of the pressure distribution remained constant once the flow separated. The Reynolds number dependence of both two - and three - dimensional interactions were seen to be markedly similar.



Finally, it was hypothesized that competing turbulent and feature scales could account for changes in secondary separation with both angle of attack and boundary layer thickness.

## 5.2 RECOMMENDATIONS FOR FURTHER STUDY

First, there are two improvements of the current study which could be made, especially in terms of resolution. Those areas where improvements could be made include:

(1) Both the pressure tapped floor and the flat plate were found to be inadequately instrumented for some angles since both were designed with lower fin angles in mind. Improved resolution in the pressure distributions at higher angles and the alcohol injection technique could be provided with a reinstrumented plate and / or floor.

(2) The alcohol washdown technique could be improved by examining different carrier fluids in an attempt to eliminate some of its drawbacks.

Second, a number of recommendations for further study have also been generated by this investigation:

(1) The angle at which the tunnel stalled was governed by the interaction of the shock wave and the sidewall boundary layer. If the magnitude of the shock - induced separation of the sidewall boundary layer, which intruded more and more into the interaction as angle of attack was increased, could be reduced, tunnel stall could be delayed and

higher angles of attack than those currently possible could be achieved. Boundary layer control, through the use of suction or blowing to energize the sidewall boundary layer, could be used to reduce the magnitude of the separation. A vertical splitter plate aligned with the freestream direction could be used to keep the shock from reflecting off and separating the wall viscous layer.

(2) Tests at different Mach numbers are necessary primarily to check the upstream influence scaling principle for these high angles as well as examining the effect of Mach number on secondary separation.

(3) Tests using a long, variable position flat plate would provide more information regarding the role of boundary layer thickness on these interactions, especially on the feature of secondary separation. Inclusion of variable stagnation pressure tests in this work could provide insight into the currently unexplained Reynolds number effect on the interaction. A test of this sort could also give additional checks for the scaling of upstream influence.

(4) The steadiness of features, as measured using both high frequency surface pressure transducers and hot wires, under as many conditions as possible should be investigated.

(5) Flowfield surveys at angles of attack where secondary separation is and is not present (15 and 20 degrees are representative examples) could aid in understanding the feature as well as the entire class of flows in general. They are also necessary to provide checks of computed flow fields at the same angles of attack.

(6) The computations of Knight and Horstman were both performed using the thick boundary layer. Experiment and computation both showed that secondary separation was not present. A computation for an angle of attack of 15 degrees in the thin boundary layer, a case where secondary separation occurs, would be useful in further understanding this phenomenon.

(7) Checks of the effect of fin length using the present variable angle configuration may resolve the observed disagreement of the attachment data.

## REFERENCES

- (1) Stanbrook, A. "An Experimental Study of the Glancing Interaction Between a Shock Wave and a Turbulent Boundary Layer." ARC-CP-No. 555, July 1960.
- (2) McCabe, A. "The Three - Dimensional Interaction of a Shock Wave with a Turbulent Boundary Layer." Aeronautical Quarterly, August 1966.
- (3) Green, J.E. "Interactions Between Shock Waves and Turbulent Boundary Layers." Progress in Aerospace Sciences, 11, D. Kuchemann, ed., 1970, pp. 235-340.
- (4) Law, C.H. "Three - Dimensional Shock Wave - Turbulent Boundary Layer Interactions at Mach 6." ARL-TR-75-0191, June 1975.
- (5) Peake, D.J. "Three - Dimensional Swept Shock/Turbulent Boundary Layer Separations with Control by Air Injection." NRC No. 15579, July 1976.
- (6) Oskam B. "Three - Dimensional Flow Fields Generated by the Interaction of a Swept Shock with a Turbulent Boundary Layer." Gas Dynamics Laboratory Report 1313, Princeton University, December 1976.
- (7) Oskam B., Bogdonoff, S.M., and Vas, I.E. "Study of Three - Dimensional Flow Fields Generated by the Interaction of a Skewed Shock Wave with a Turbulent Boundary Layer." AFFDL-TR-75-21, February 1976.
- (8) Oskam, B., Vas, I.E., and Bogdonoff, S.M. "An Experimental Study of Three - Dimensional Flow Fields in an Axial Corner at Mach 3." AIAA Paper 77-689, 1977.
- (9) Oskam, B., Vas, I.E., and Bogdonoff, S.M. "Mach 3 Oblique Shock Wave - Turbulent Boundary Layer Interactions in Three Dimensions." AIAA Paper 76-336, 1976.
- (10) Kubota, H., and Stollery, J.L. "An Experimental Study of the Interaction Between a Glancing Shock Wave and a Turbulent Boundary

Layer." Journal of Fluid Mechanics, 116, 1982, pp. 431-458.

- (11) McClure, W.B. "An Experimental Study into the Scaling of the Interaction of an Unswept Sharp Fin - Generated Shock/Turbulent Boundary Layer Interaction." MSE Thesis, Princeton University, January 1983.
- (12) Lu, F.K.P. "An Experimental Study of Three - Dimensional Shock Wave/Turbulent Boundary Layer Interactions Generated by Sharp Fins." MSE Thesis, Princeton University, November 1982.
- (13) Zubin, M.A. and Ostapenko, N.A. "Structure of the Flow in the Separation Region Resulting From Interaction of a Normal Shock Wave with a Boundary Layer in a Corner." Izvestiya Akademii Nauk SSSR, Mekhanika Zhidkosti i Gaza, May - June 1979, pp. 51-58.
- (14) Zheltovodov, A.A. "Properties of Two - and Three - Dimensional Separation Flows at Supersonic Velocities." Izvestiya Akademii Nauk SSSR, Mekhanika Zhidkosti i Gaza, May - June 1979, pp. 42-50.
- (15) Zheltovodov, A.A. "Regimes and Properties of Three - Dimensional Separated Flows Initiated by Skewed Compression Shocks." Zhurnal Prikladnoi Mekhaniki i Tekhnicheskoi Fiziki, No. 3, May - June 1982, pp. 116-123.
- (16) Dolling, D.S. and Bogdonoff, S.M. "Blunt Fin - Induced Shock Wave/Turbulent Boundary Layer Interactions." AIAA Paper 82-4284, 1982.
- (17) Settles, G.S., Perkins, J.J., and Bogdonoff, S.M. "Investigation of Three - Dimensional Shock/Boundary Layer Interactions as Swept Compression Corners." AIAA Paper 79-1489, 1979.
- (18) Korkegi, R.H. "On the Structure of Three - Dimensional Shock - Induced Separated Flow Regions." AIAA Journal, 14, No. 5, May 1976, pp. 597-600.
- (19) Korkegi, R.H. "A Simple Correlation for Incipient Turbulent Boundary Layer Separation due to a Skewed Shock Wave." AIAA Journal, 11, No. 11, November 1973, pp. 578-579.
- (20) Hayes, J.R. "Prediction Techniques for the Characteristics of Fin -

Generated Three - Dimensional Shock Wave/Turbulent Boundary Layer Interactions." AFFDL-TR-77-10, May 1977.

- (21) Settles, G.S. and Bogdonoff, S.M. "Scaling of Two - and Three - Dimensional Shock/Turbulent Boundary Layer Interactions at Compression Corners." AIAA Paper 81-0334, 1981.
- (22) Dolling, D.S. and Bogdonoff, S.M. "Upstream Influence Scaling of Sharp Fin - Induced Shock Wave/Turbulent Boundary Layer Interactions." AIAA Paper 81-0336, 1981.
- (23) Dolling, D.S. and Bogdonoff, S.M. "Upstream Influence in Sharp Fin - Induced Shock Wave/Turbulent Boundary Layer Interactions." AIAA Journal, 21, No. 1, January 1983, pp. 143-145.
- (24) McClure, W.B. and Dolling, D.S. "Flowfield Scaling in Sharp Fin - Induced Shock Wave/Turbulent Boundary Layer Interactions." AIAA Paper 83-1754, 1983.
- (25) Dolling, D.S. "Effects of Mach Number on Upstream Influence in Sharp Fin - Induced Shock Wave/Turbulent Boundary Layer Interactions." AIAA Paper 84-0095, 1984.
- (26) Teng, H.Y. and Settles, G.S. "Cylindrical and Conical Upstream Influence Regimes of Three - Dimensional Shock/Turbulent Boundary Layer Interactions." AIAA Paper 82-0987, 1982.
- (27) Lu, F.K.P. and Settles, G.S. "Conical Similarity of Shock/Boundary Layer Interactions Generated by Swept Fins." AIAA Paper 83-1756, 1983.
- (28) Settles, G.S. and Kimmel, R.L. "Similarity Conditions for Conical Shock Wave - Turbulent Boundary Layer Interactions." AIAA Paper 84-1557, 1984.
- (29) Dolling, D.S. and Bogdonoff, S.M. "An Experimental Investigation of the Unsteady Behavior of Blunt Fin - Induced Shock Wave/Turbulent Boundary Layer Interactions." AIAA Paper 81-1287, 1981.
- (30) Tan, D.K.M., Tran, T.T., and Bogdonoff, S.M. "Surface Pressure Fluctuations in a Three - Dimensional Shock Wave/Turbulent Boundary Layer Interaction." Princeton University, Abstract submitted to

the AIAA 23rd Aerospace Sciences Meeting, June 1984.

- (31) Maskell, R.C. "Flow Separation in Three Dimensions." RAE Report No. Aero 2565, November 1955.
- (32) Goldberg, T.J. "Three - Dimensional Separation for Interactions of Shock Waves with Turbulent Boundary Layers." AIAA Journal, 11, No. 11, 1973, pp. 1573-1575.
- (33) Peake, D.J. and Tobak, M. "Topology of Three - Dimensional Separated Flows." NASA Tech. Memo. 81294, April 1981.
- (34) Hunt, J.C.R., Abell, C.J., Peterka, J.A., and Woo, H. "Kinematical Studies of the Flows Around Free or Surface - Mounted Obstacles; Applying Topology to Flow Visualization." Journal of Fluid Mechanics, 86, Pt. 1, 1978, pp. 179-200.
- (35) Hornung, H. and Perry, A.E. "Streamsurface Bifurcation, Vortex Skeletons and Separation." IB 222-82 A 25, June 1982.
- (36) Horstman, C.C. and Hung, C.M. "Computation of Three - Dimensional Turbulent Separated Flows at Supersonic Speed." AIAA Paper 79-0002, January 1979.
- (37) Knight, D.D. "A Hybrid Explicit - Implicit Numerical Algorithm for the Three - Dimensional Navier - Stokes Equations." AIAA Journal, 22, No. 8, August 1984, pp. 1056-1063.
- (38) Horstman, C.C. "A Computational Study of Complex Three - Dimensional Compressible Turbulent Flow Fields." AIAA Paper 84-1556, 1984.
- (39) Tran, T.T. "Calibration of the Mach 2 Nozzle in the 8"x8" Supersonic Wind Tunnel." Internal Memo. No. 50, Gas Dynamics Laboratory, Dept. of Mech. and Aero. Engineering, Princeton University, August 1982.
- (40) Settles, G.S. "An Experimental Study of Compressible Turbulent Boundary Layer Separation at High Reynolds Numbers." PhD Thesis, Princeton University, September 1975.

- (41) Sun, C.C. and Childs, M.F. "A Modified Wall - Wake Velocity Profile for Turbulent Compressible Boundary Layers." AIAA Journal of Aircraft, 10, No. 6, June 1973, pp. 381-383.
- (42) Vas, I.E. and Bogdonoff, S.M. "A Preliminary Report on the Princeton University High Reynolds Number 8"x8" Supersonic Tunnel." Internal Memo. No. 39, Gas Dynamics Laboratory, Dept. of Aero. and Mech. Science, Princeton University, 1971.
- (43) Settles, G.S. and Teng, H.Y. "Flow Visualization of Separated Three - Dimensional Shock Wave/Turbulent Boundary Layer Interactions." AIAA Paper 82-0229, 1982.
- (44) Knight, D.D., private communication, August 1984.
- (45) Horstman, C.C., private communication, October 1984.
- (46) Tan, D.K.M. and Tran, T.T., private communication, August 1984.
- (47) Dolling, D.S. and Murphy, M. "Wall Pressure Fluctuations in a Supersonic Separated Compression Ramp Flow Field." AIAA Paper 82-0986, 1982.
- (48) Dolling, D.S. and Or, C.T. "Unsteadiness of the Shock Wave Structure in Attached and Separated Compression Ramp Flow Fields." AIAA Paper 83-1715, 1983.



TABLE 1  
TEST MATRIX

	THIN BOUNDARY LAYER				THICK BOUNDARY LAYER			
	65	100	175	250	65	100	175	250
$P_o$ (psia)	65	100	175	250	65	100	175	250
$Re_u$ ( $\times 10^{-6}/in.$ )	1.01	1.55	2.71	3.88	1.08	1.60	2.80	3.98
$\delta$ (in.)	0.15	0.14	0.14	0.13	0.51	0.50	0.47	0.45
$Re_\delta$ ( $\times 10^{-5}$ )	1.52	2.17	3.79	5.04	5.51	8.00	13.16	17.91
$\alpha$ (deg.)								
12	•	•	•	•	•	•	•	•
14	•	•	•	•	•	•	•	•
15	•	•	•	•	•	•	•	•
16	•	•	•	•	•	•	•	•
18	•	•	•	•	•	•	•	•
20	•	•	•	•	•	•	•	•
22	•	•	•	•	•	•	•	•

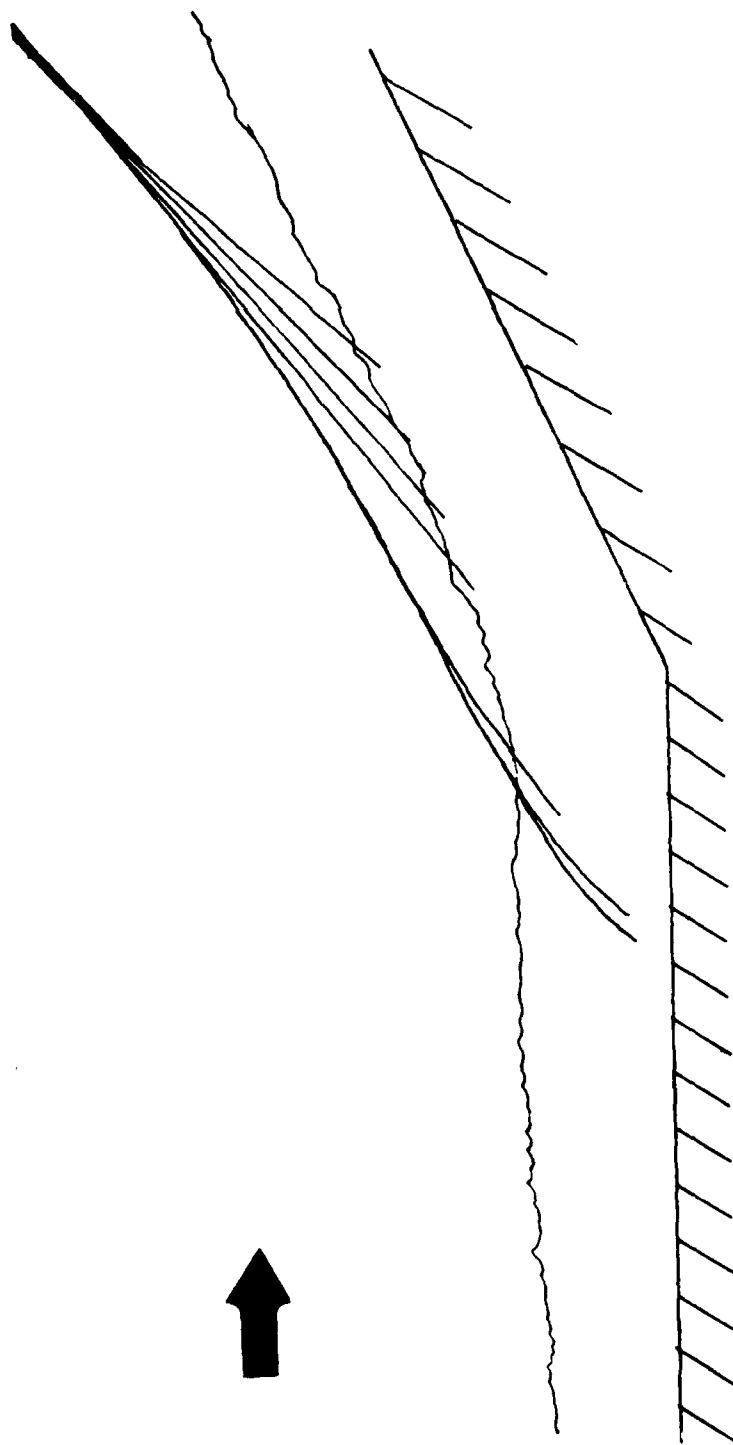


Figure 1. Two-dimensional Shock/Turbulent Boundary Layer Interaction.

AD-A151 571

AN EXPLORATORY INVESTIGATION OF SHARP FIN-INDUCED SHOCK  
WAVE / TURBULENT (U) AIR FORCE INST OF TECH  
WRIGHT-PATTESSON AFB OH S P GOODWIN NOV 84

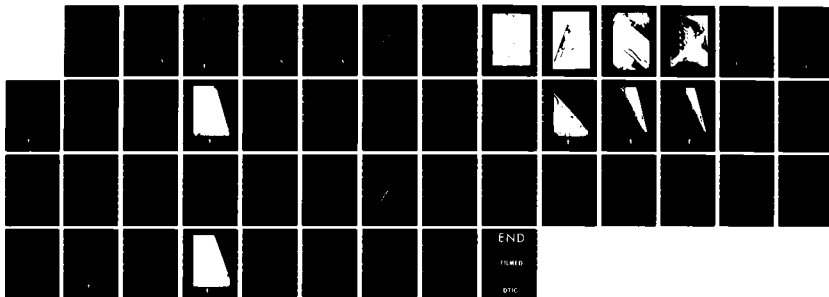
2/2

UNCLASSIFIED

AFIT/CI/NR-85-27T

F/G 28/4

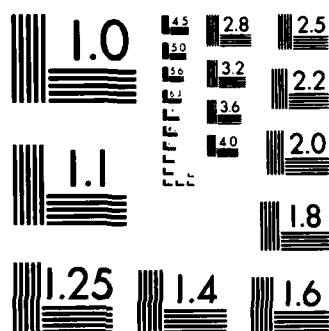
NL



END

FORMED

DTIC



MICROCOPY RESOLUTION TEST CHART  
NATIONAL BUREAU OF STANDARDS-1963 A

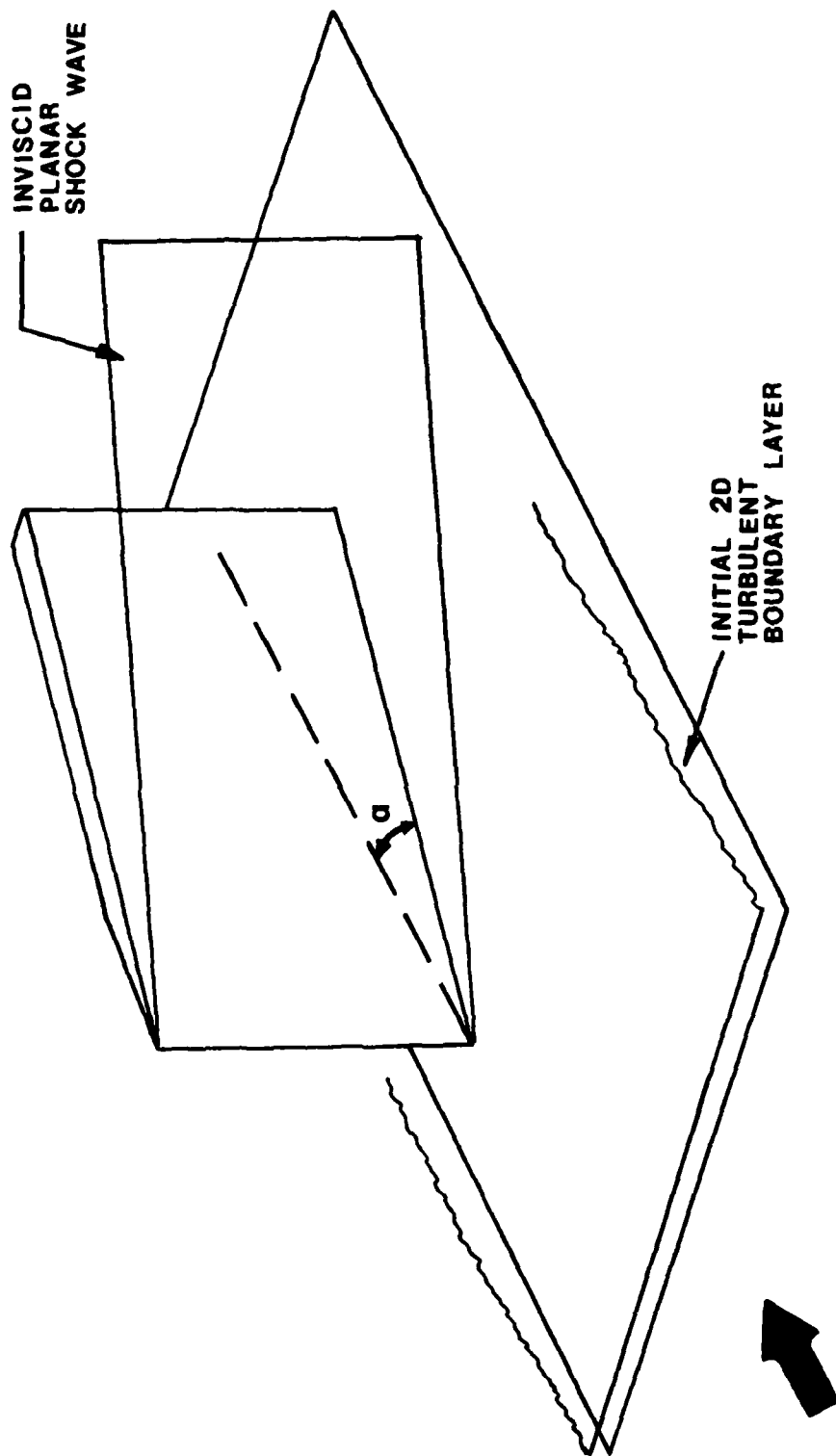


Figure 2. Sharp Fin Configuration.

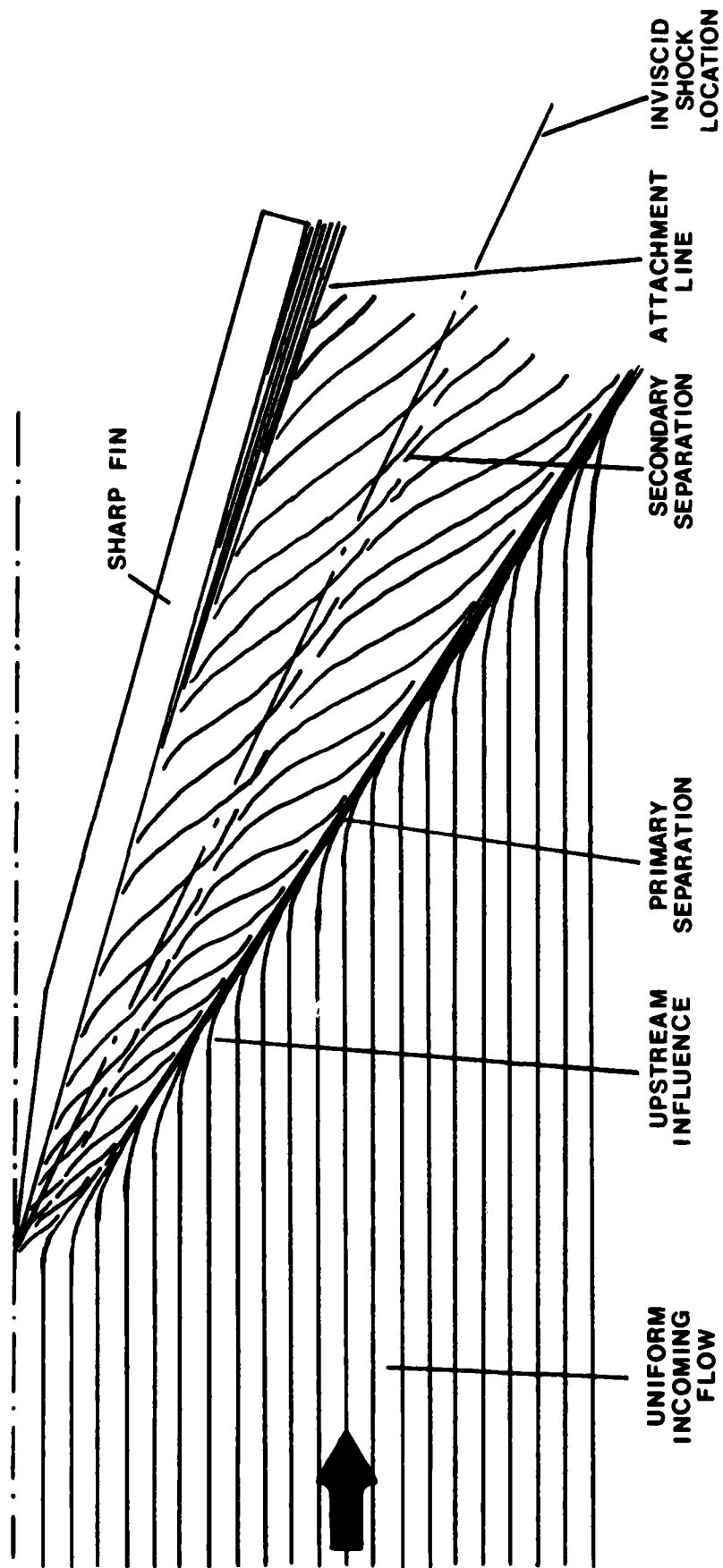


Figure 3. Surface Feature Definitions of Lu (12).

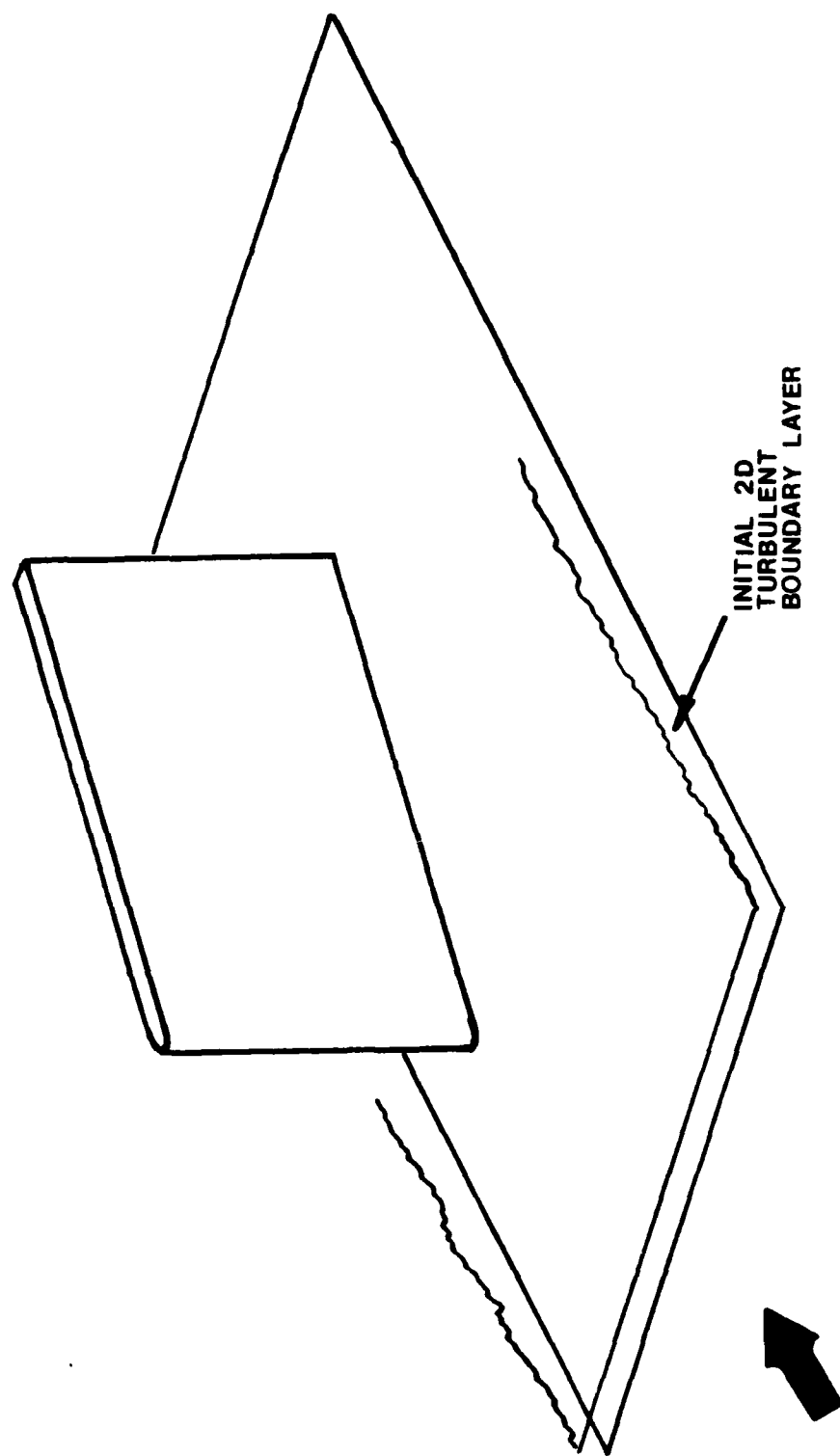


Figure 4. Blunt Fin Configuration.

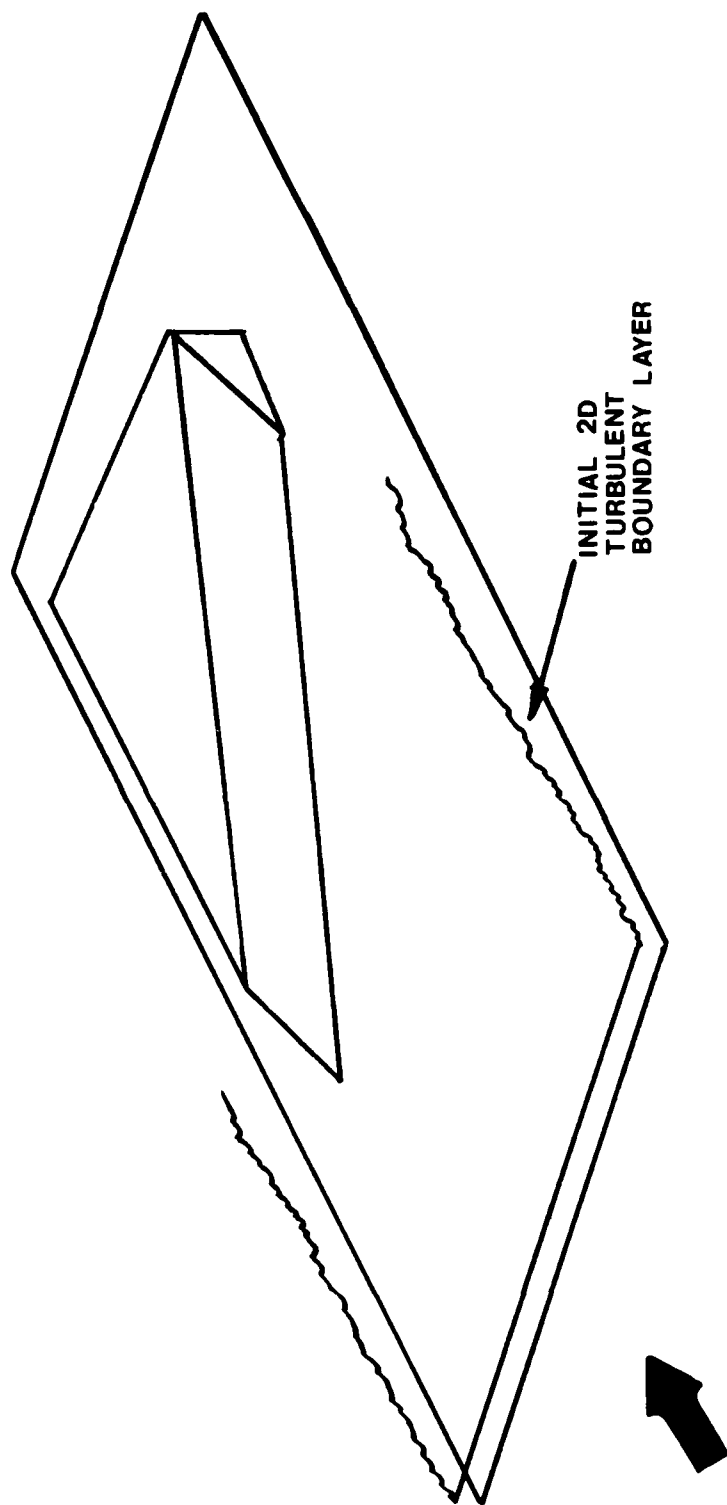


Figure 5. Swept Compression Corner Configuration.



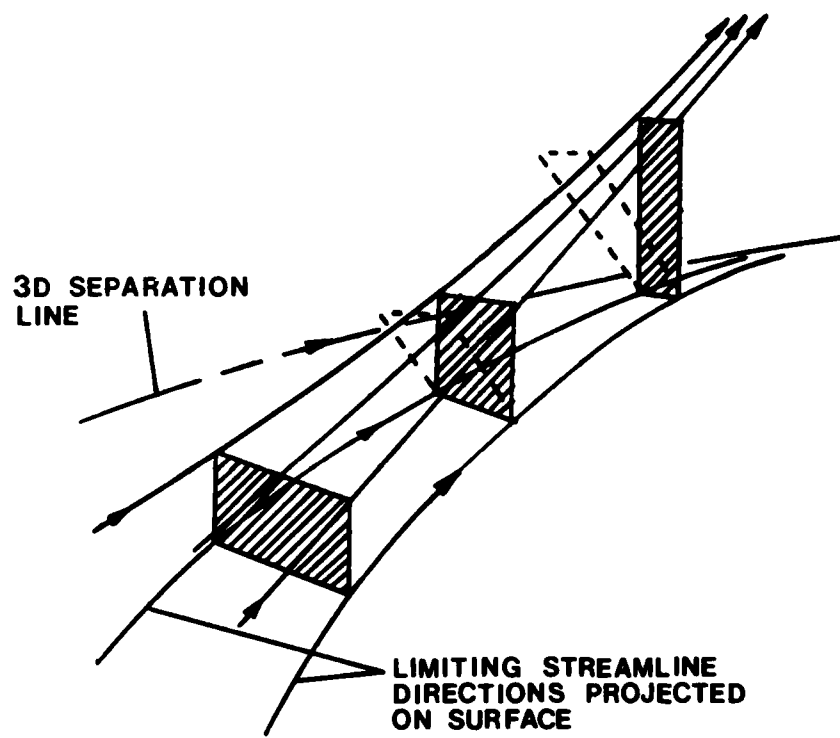
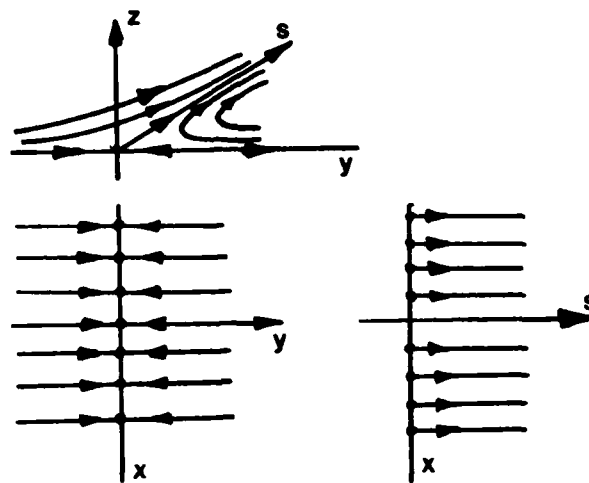
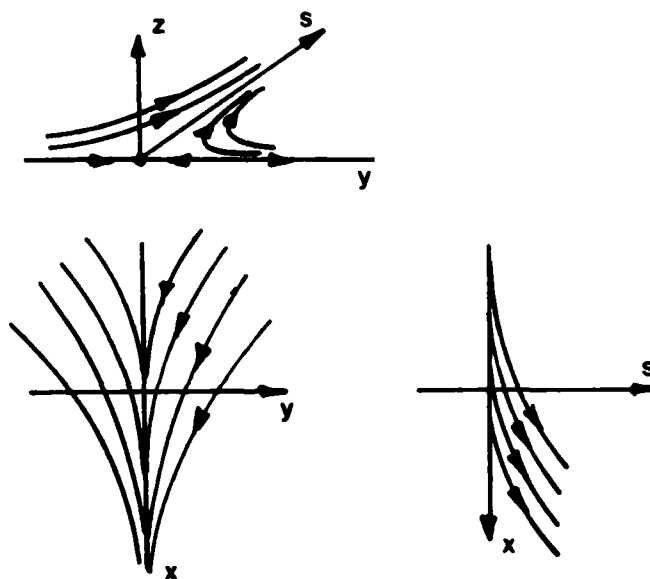


Figure 6. Continuity Argument of Peake and Tobak (33).



(a)



(b)

Figure 7. Viscous Critical Point Analysis of Hornung and Perry (35); (a) Two-dimensional Separation, (b) Three-dimensional "Separation."

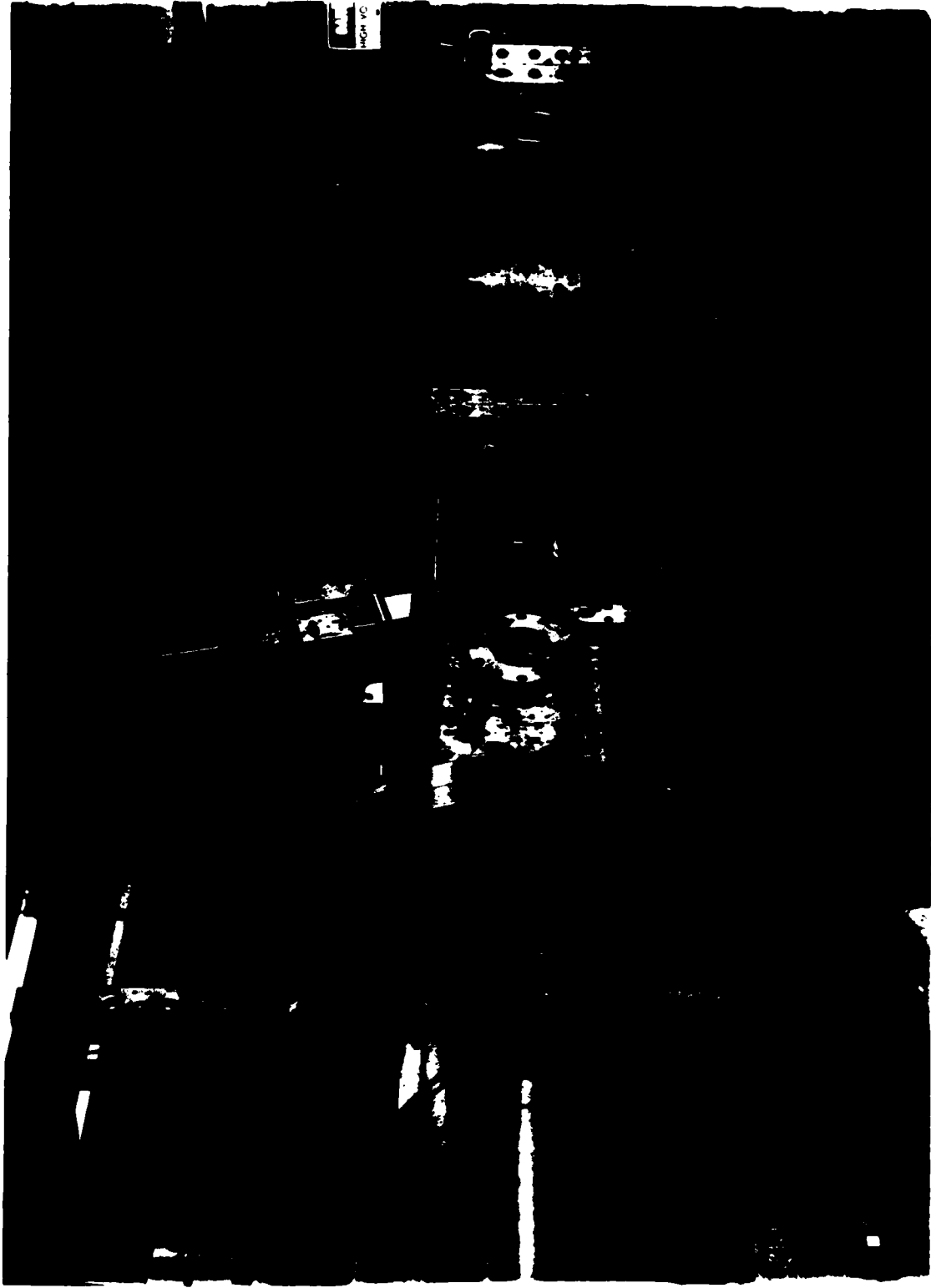


Figure 8. Photograph of 8"x8" Wind Tunnel.

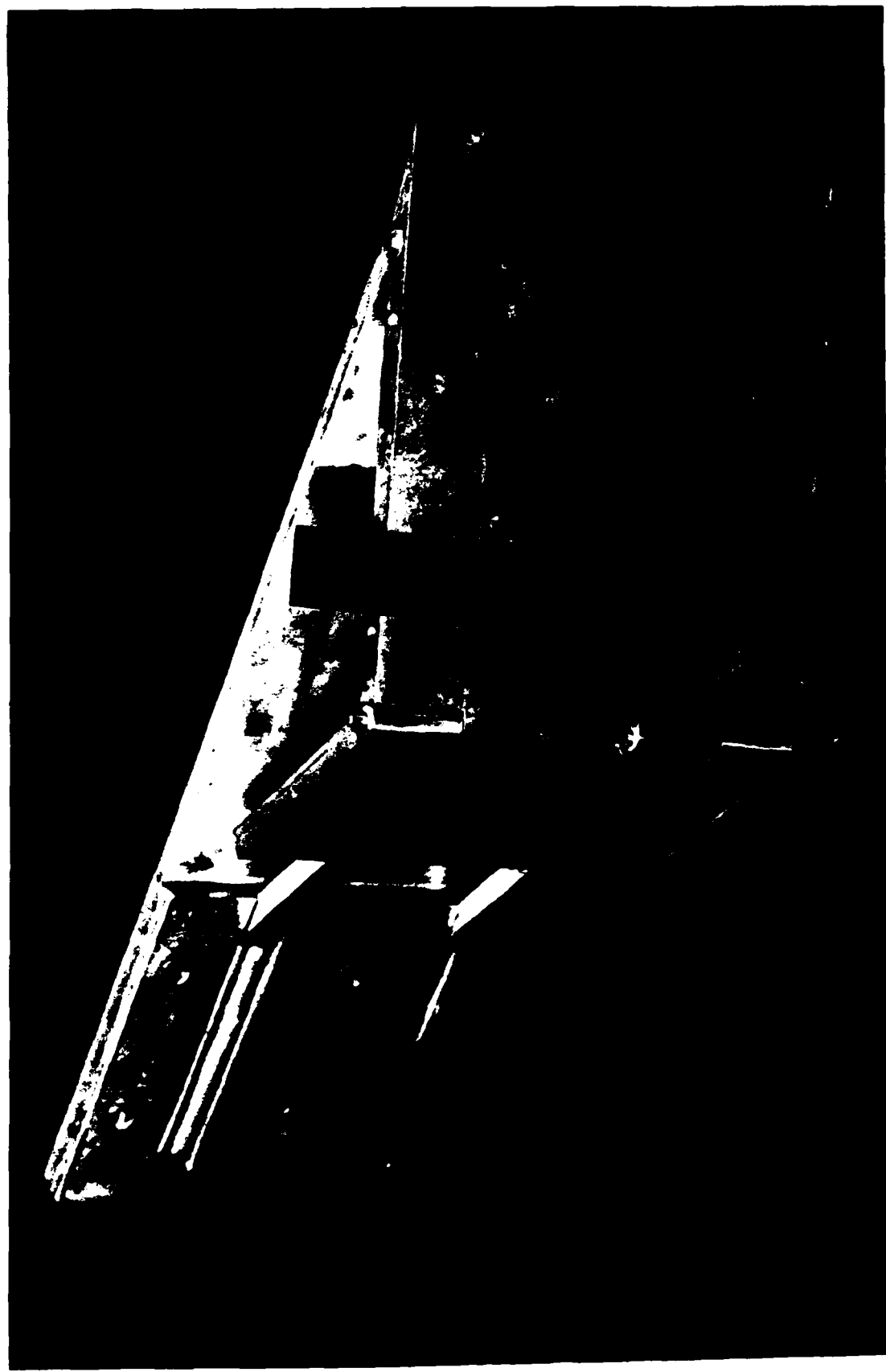


Figure 9. Photograph of Variable Angle Shock Generator.



Figure 10. Photograph of Shock Generator Installed in Tunnel.

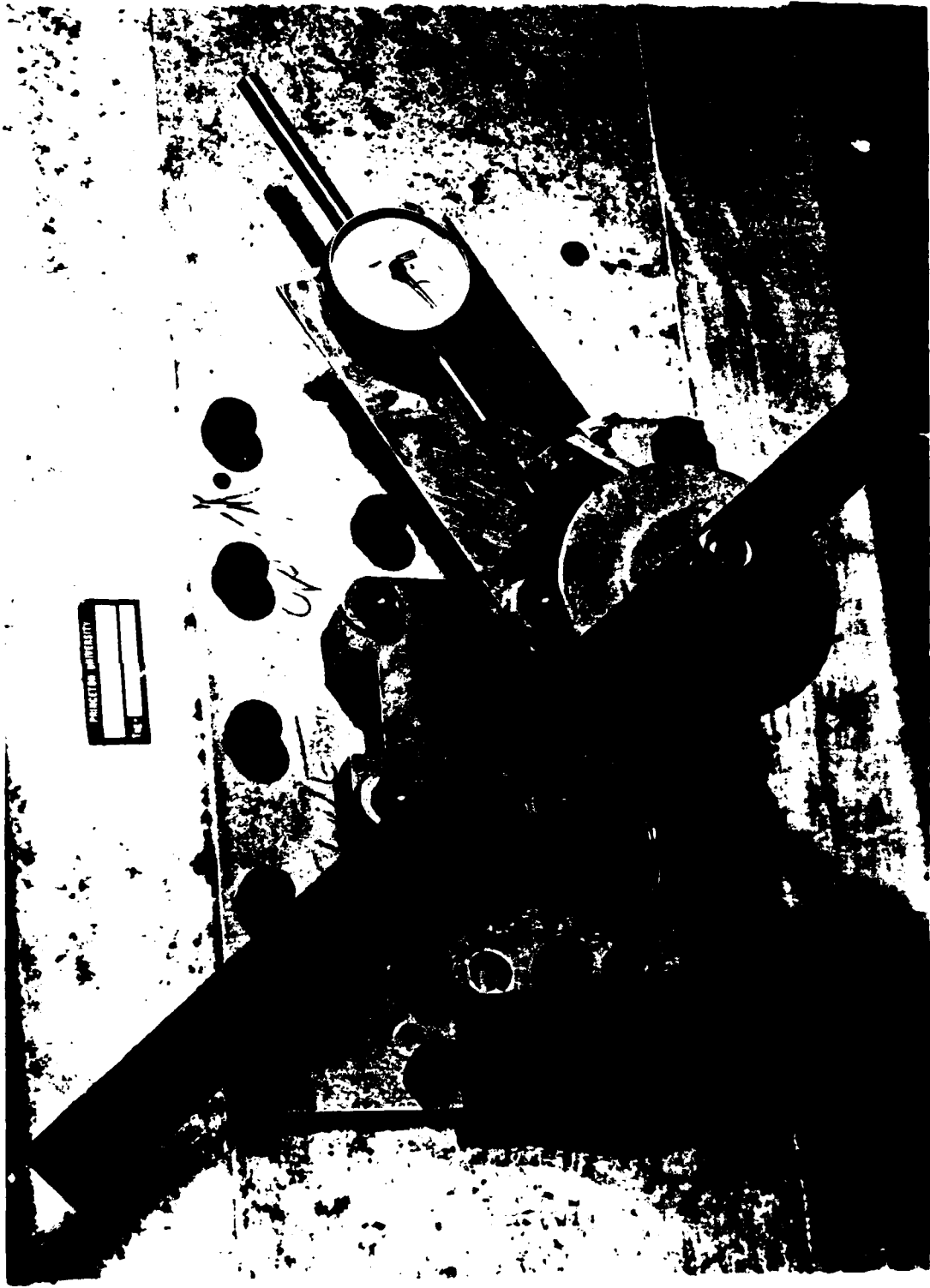
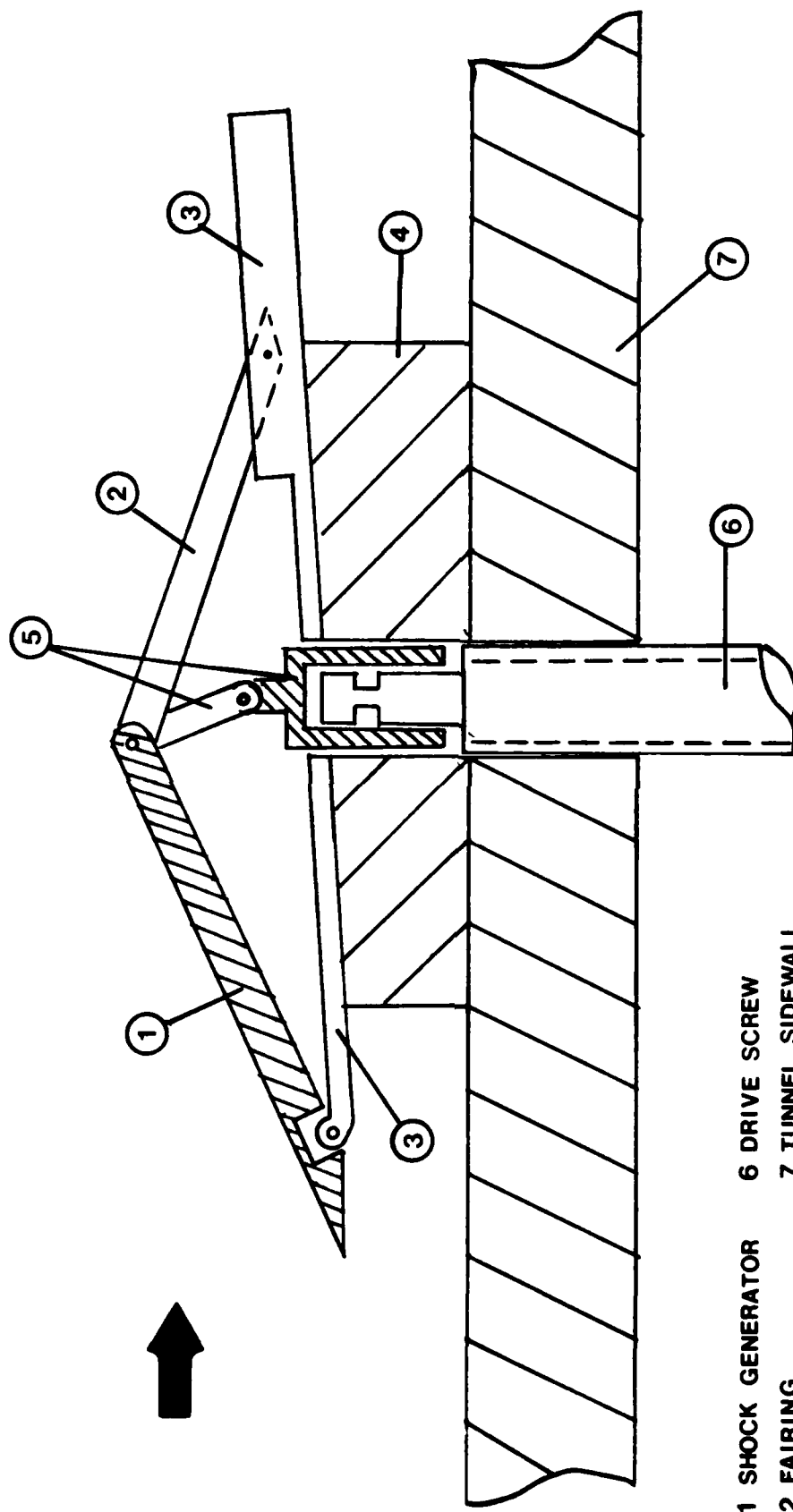


Figure 11. Photograph of External Drive Mechanism.



- 1 SHOCK GENERATOR
- 2 FAIRING
- 3 MOUNTING PLATE
- 4 AERODYNAMIC SPACER
- 5 LINK PINS
- 6 DRIVE SCREW
- 7 TUNNEL SIDEWALL

Figure 12. Plan View of Shock Generator Assembly.

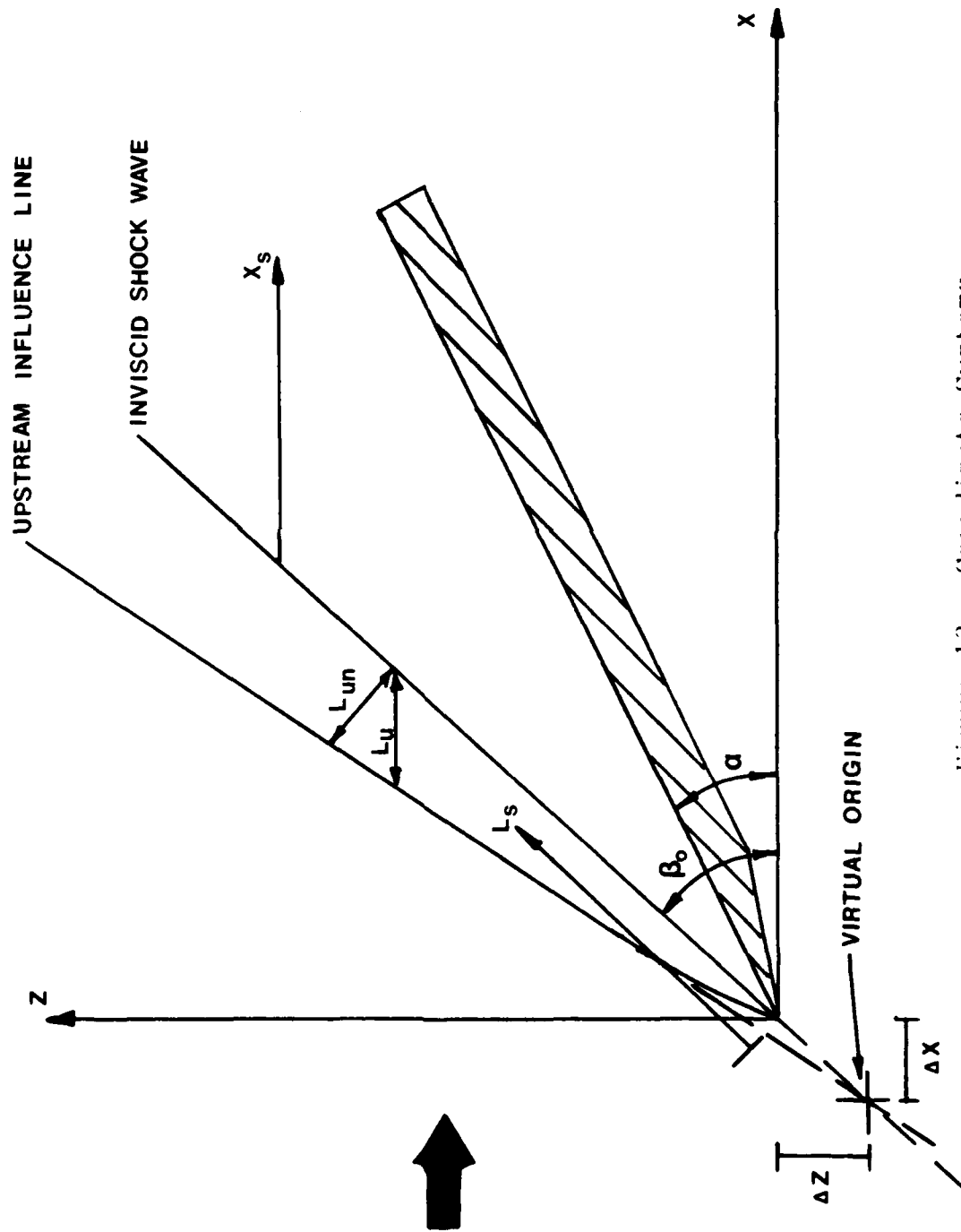


Figure 13. Coordinate Systems.



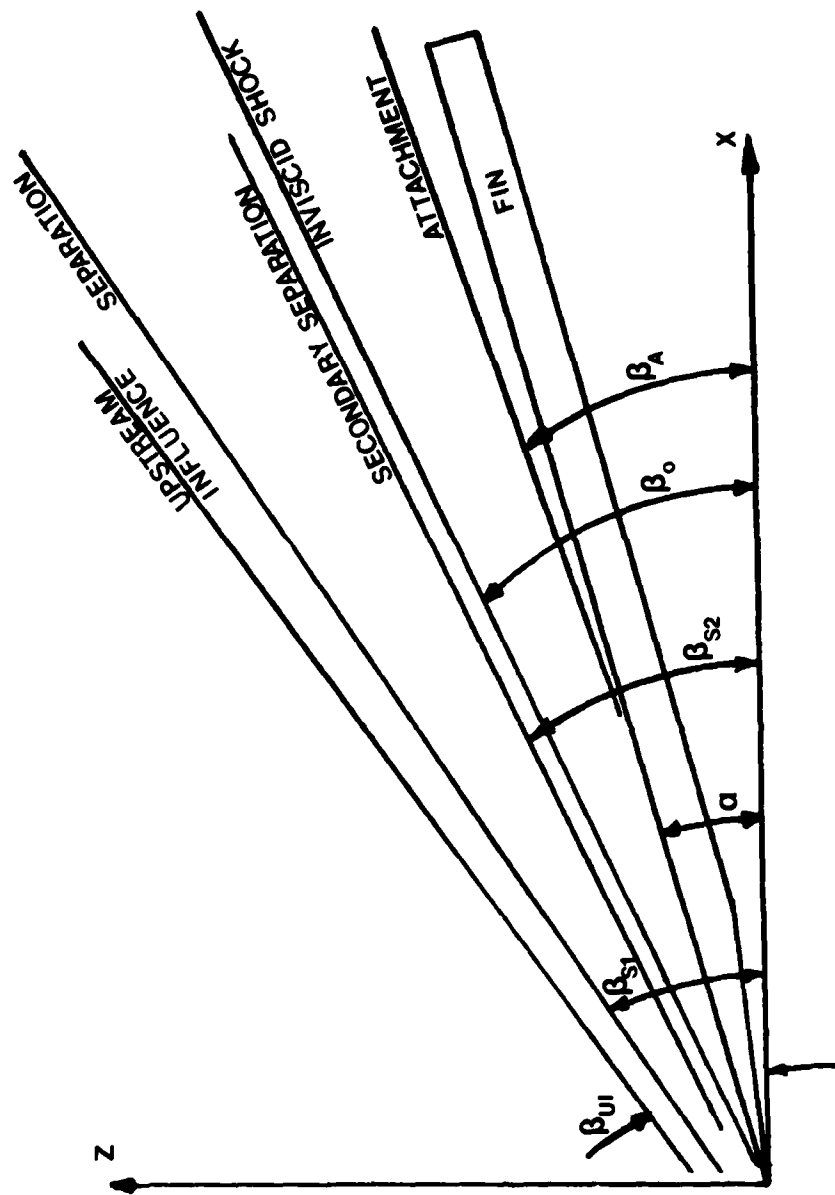


Figure 14. Definition of Surface Feature Angles.

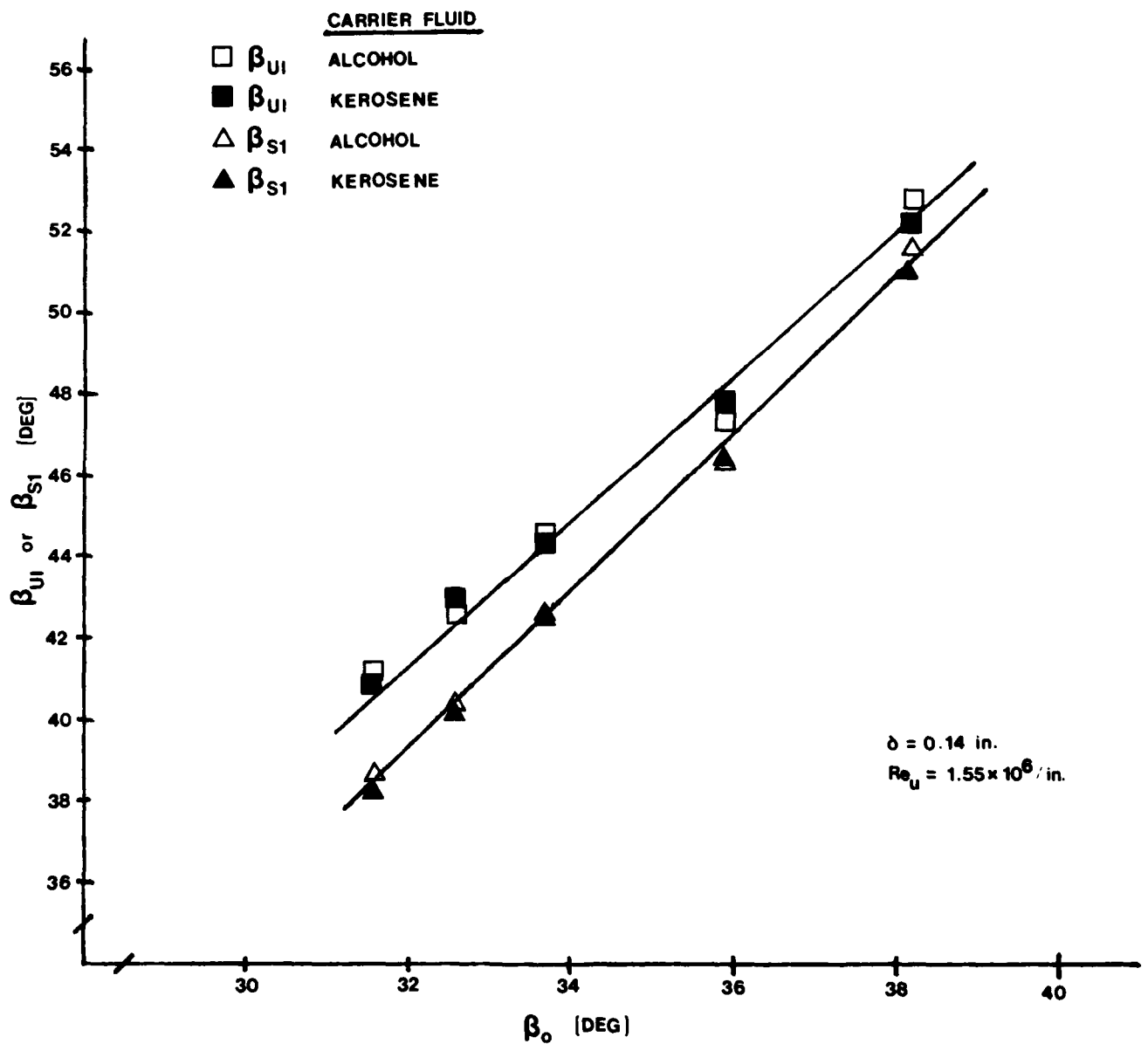


Figure 15. Alcohol Washdown/Kerosene-Lampblack Comparison.

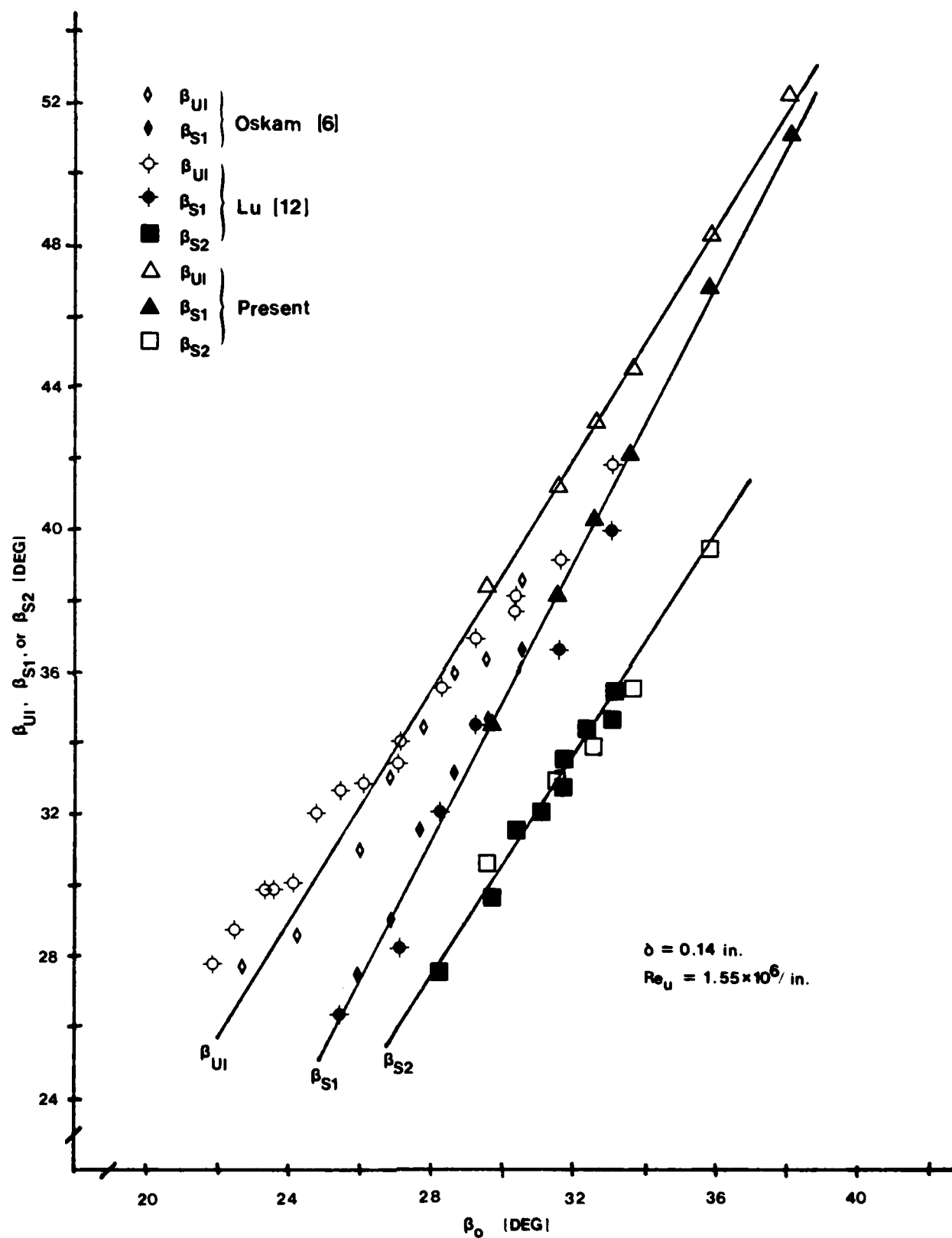


Figure 16. Comparison of Surface Feature Angles with Previous Data.

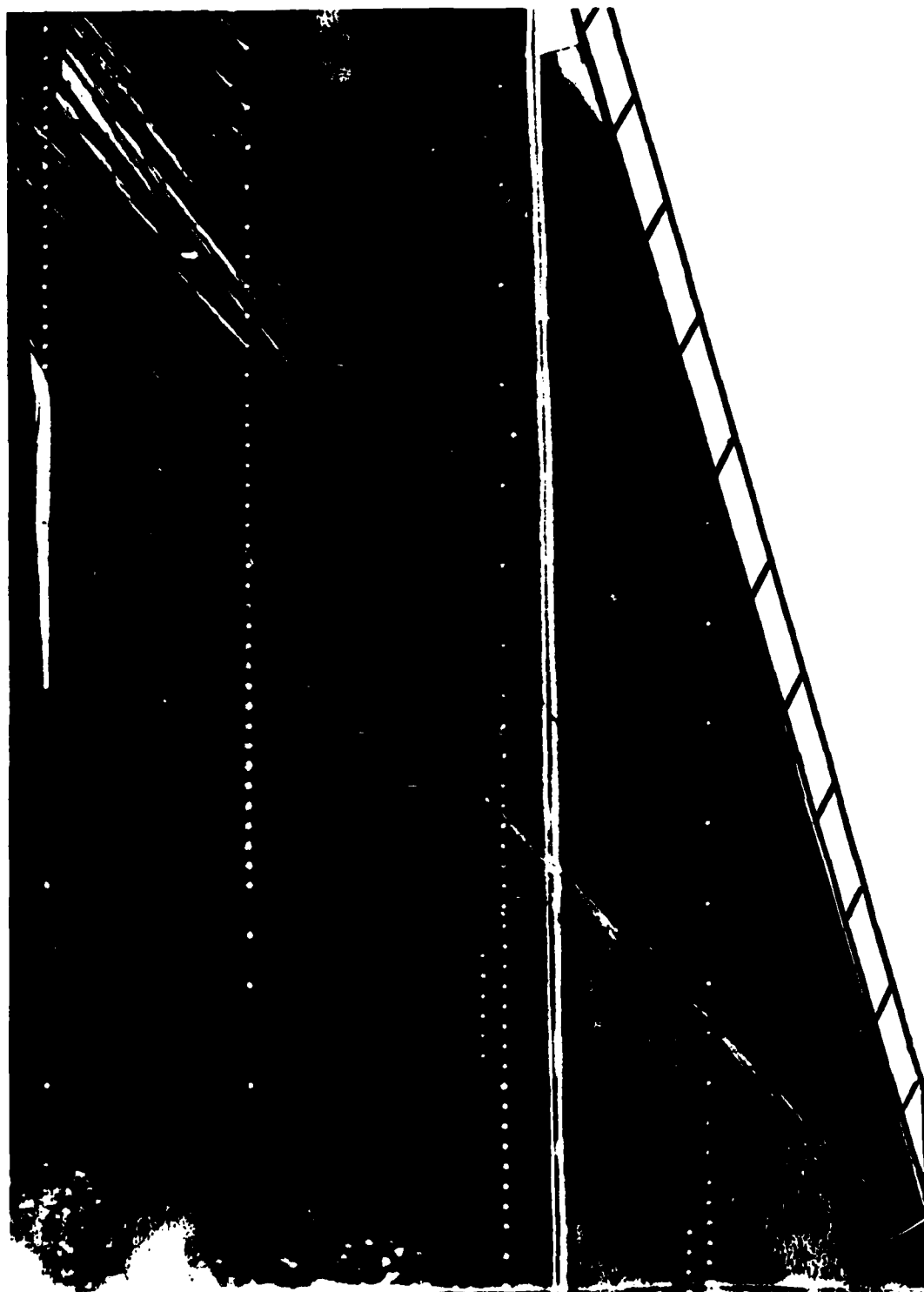


Figure 17. Photograph of Typical Kerosene-Lampblack Trace,  
 $\alpha = 16$  deg., Thin Boundary Layer.

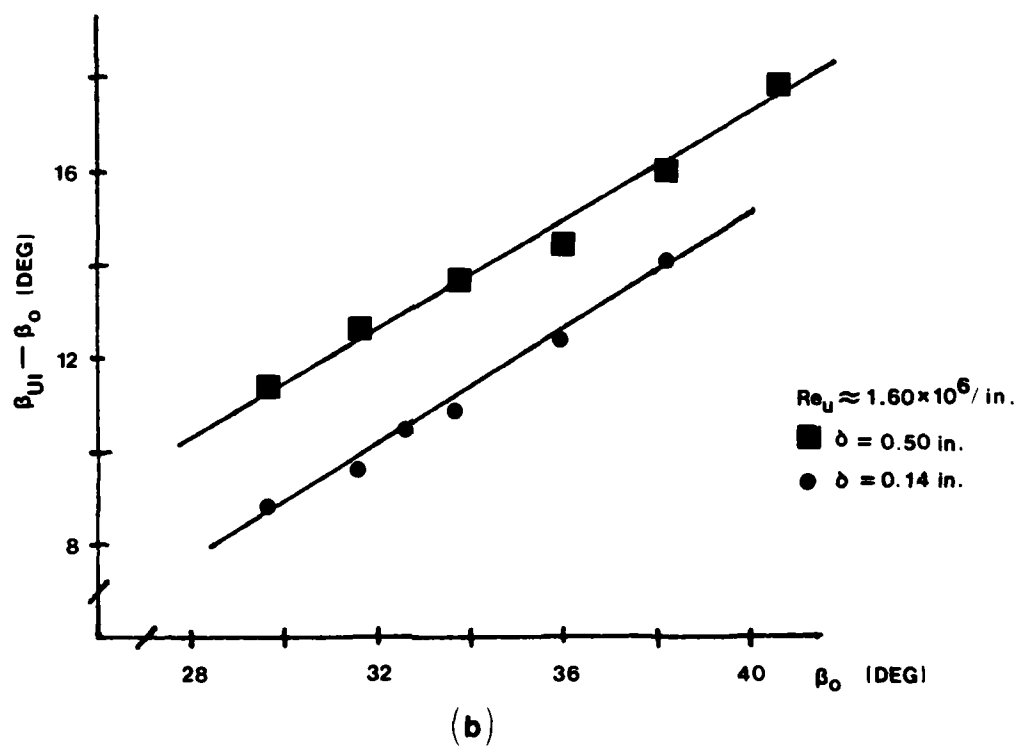
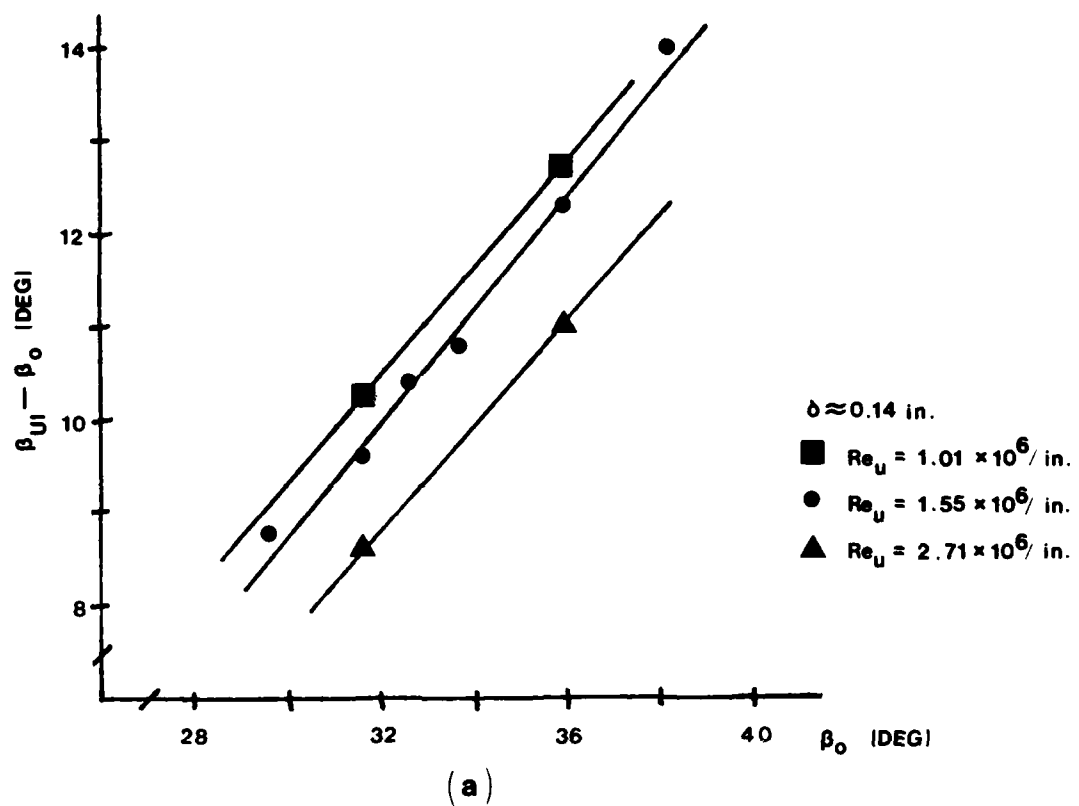


Figure 18. Effect of Test Variables on Upstream Influence Line Angle; (a) Unit Reynolds Number Effect, (b) Boundary Layer Thickness Effect.

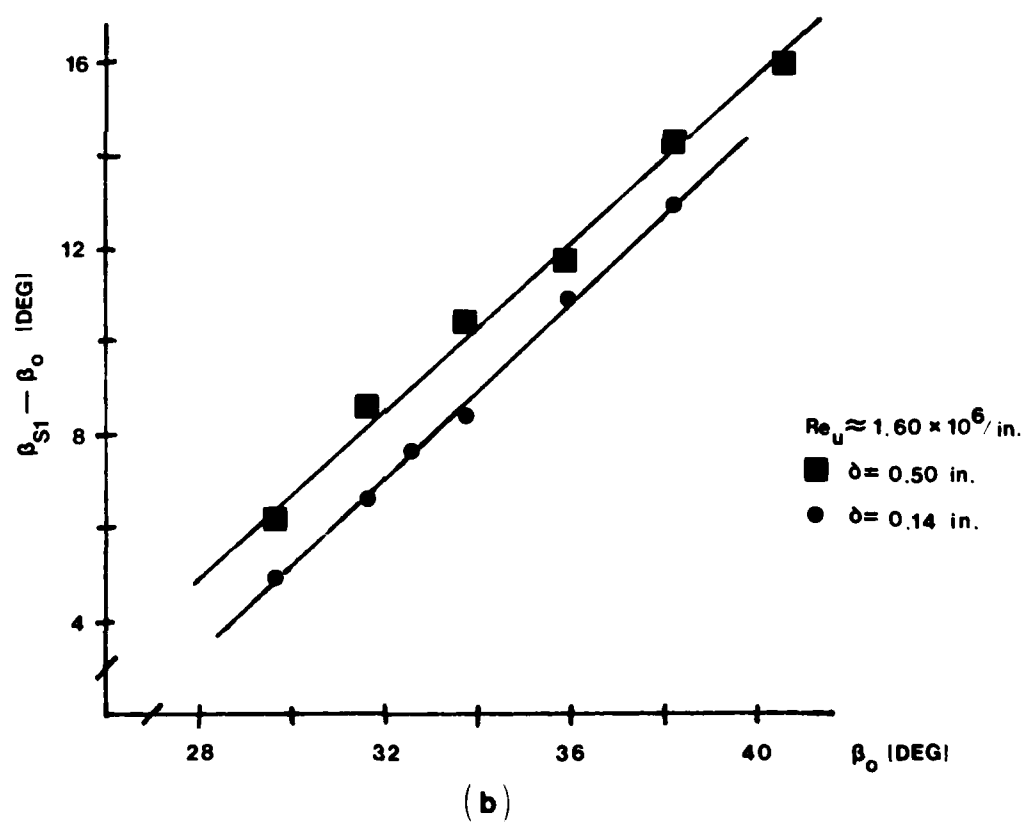
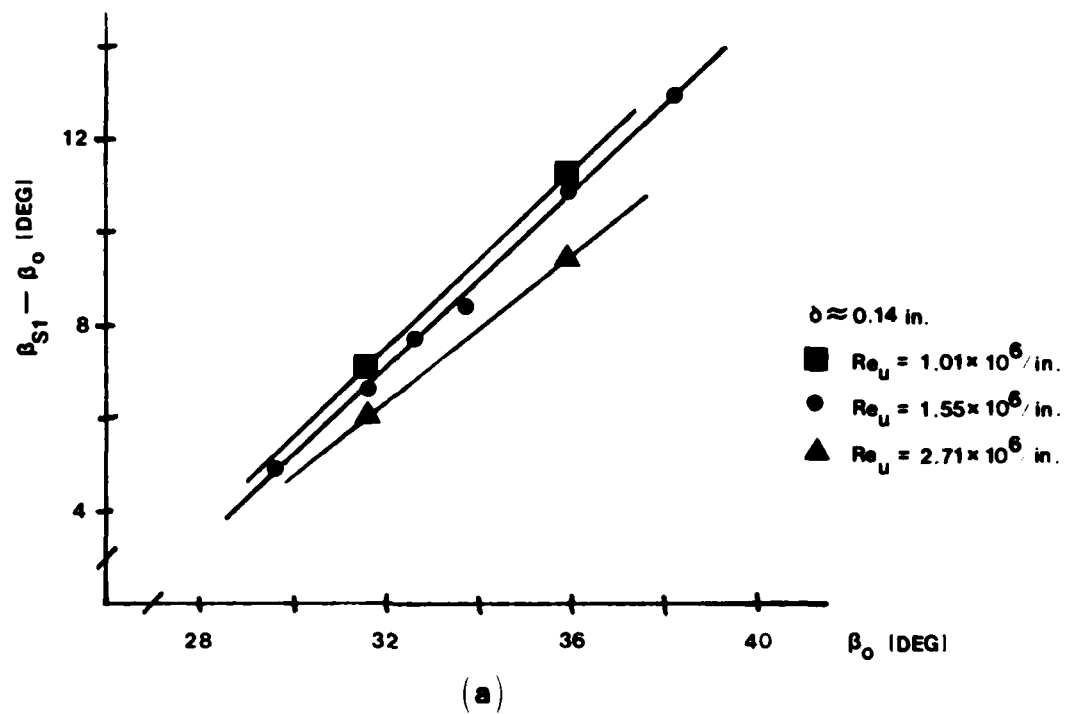


Figure 19. Effect of Test Variables on Separation Line Angle; (a) Unit Reynolds Number Effect, (b) Boundary Layer Thickness Effect.

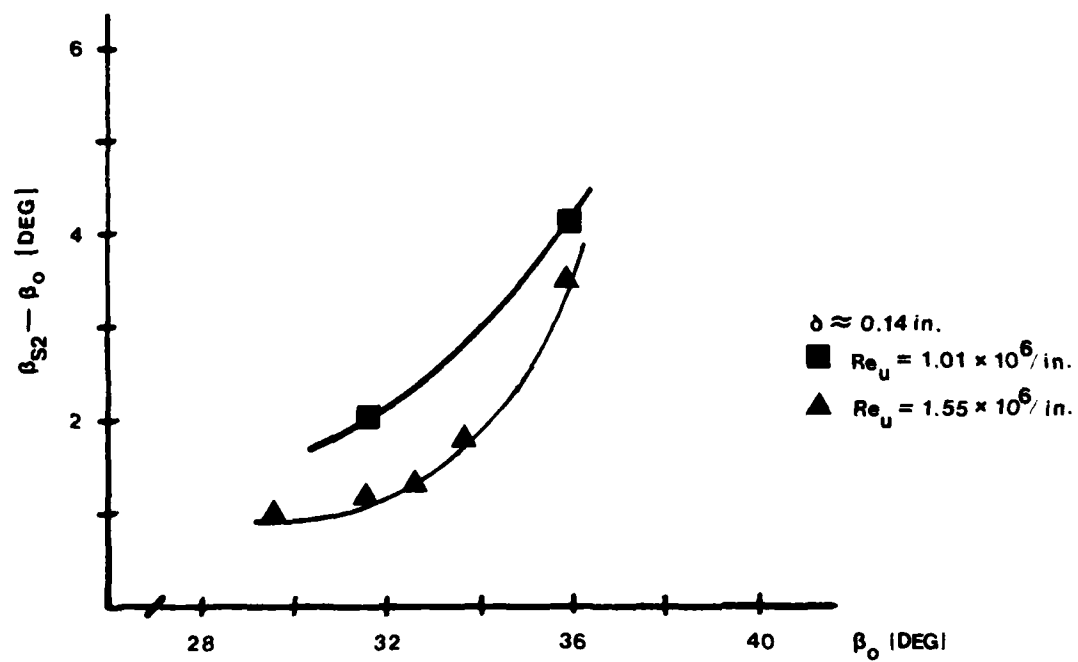


Figure 20. Effect of Unit Reynolds Number on Secondary Separation Line Angle.

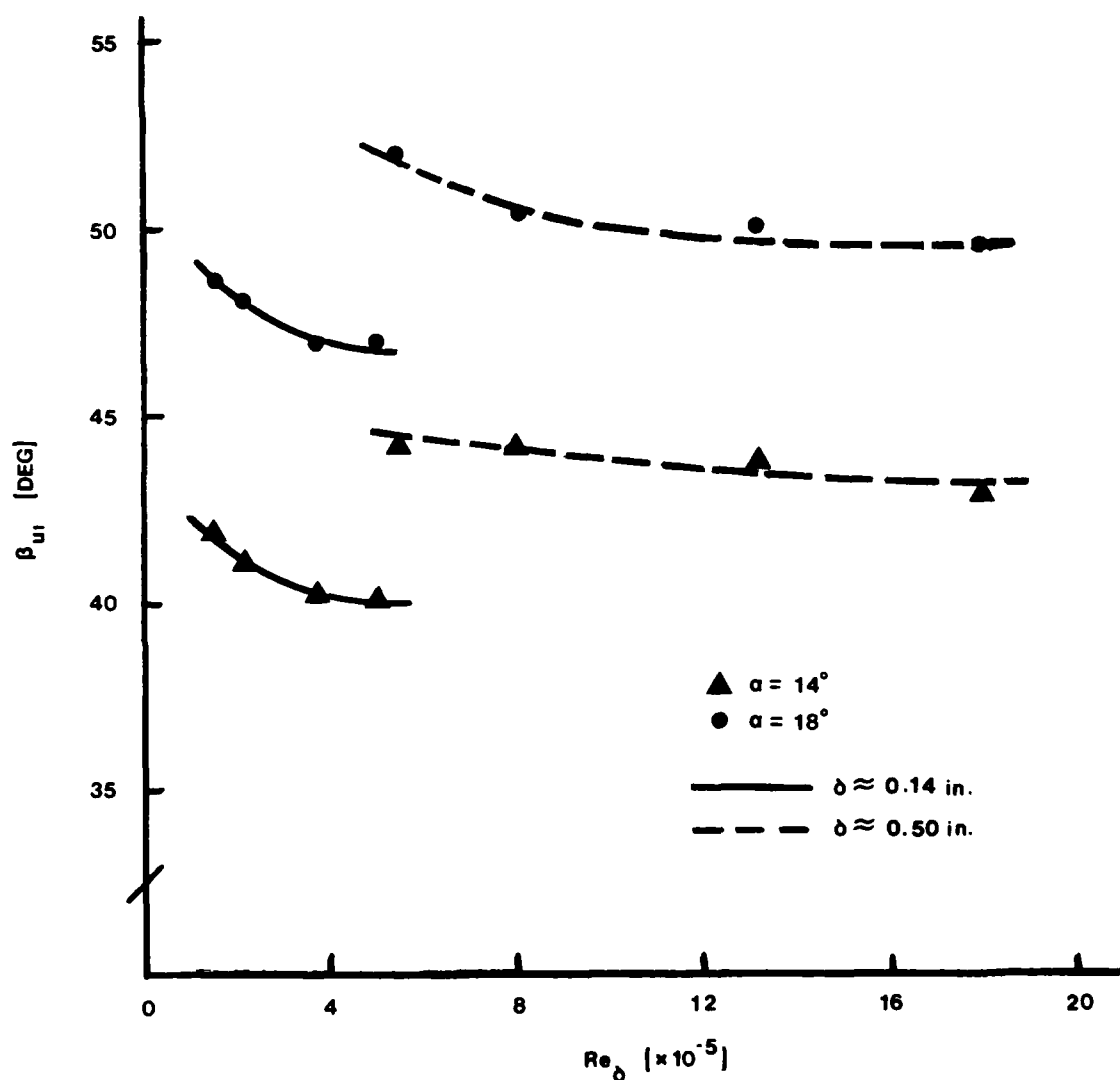


Figure 21. Effect of Reynolds Number on Upstream Influence Angle for Curves of Constant Boundary Layer Thickness.



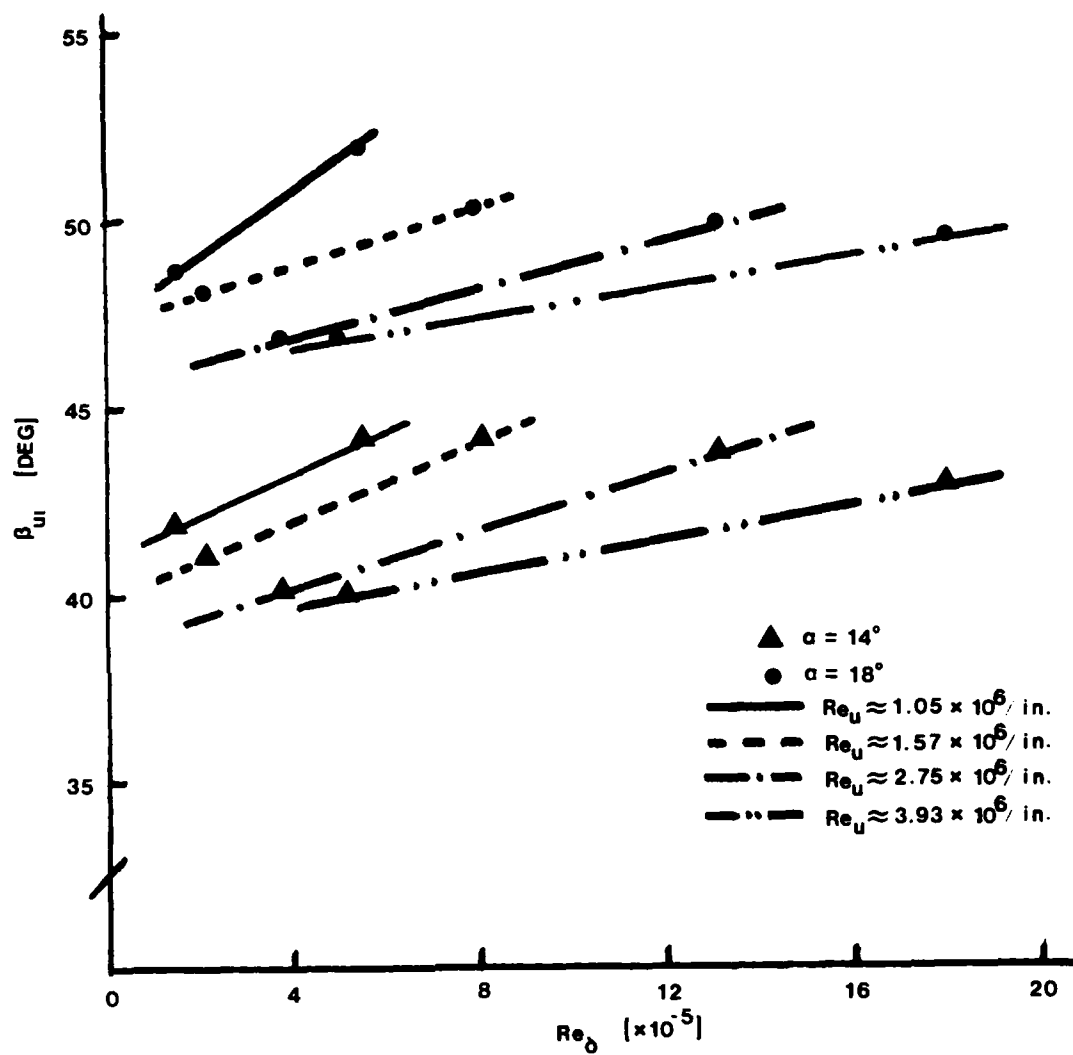


Figure 22. Effect of Reynolds Number on Upstream Influence Angle for Curves of Constant Unit Reynolds Number.

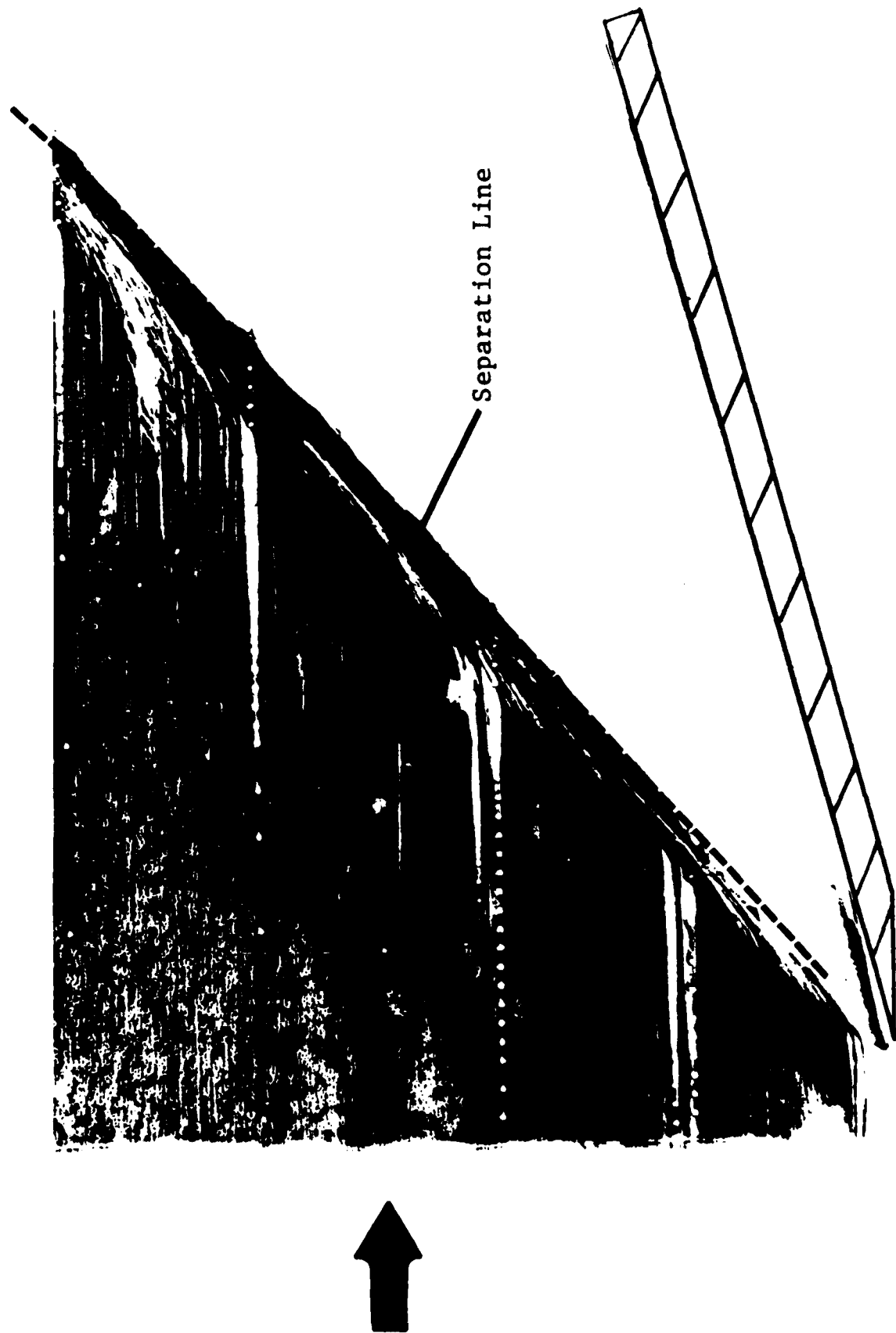


Figure 23. Photograph of local Kerosene-Lampblack Trace, Upstream Application,  $\alpha = 15^\circ$ , Thin Boundary Layer.

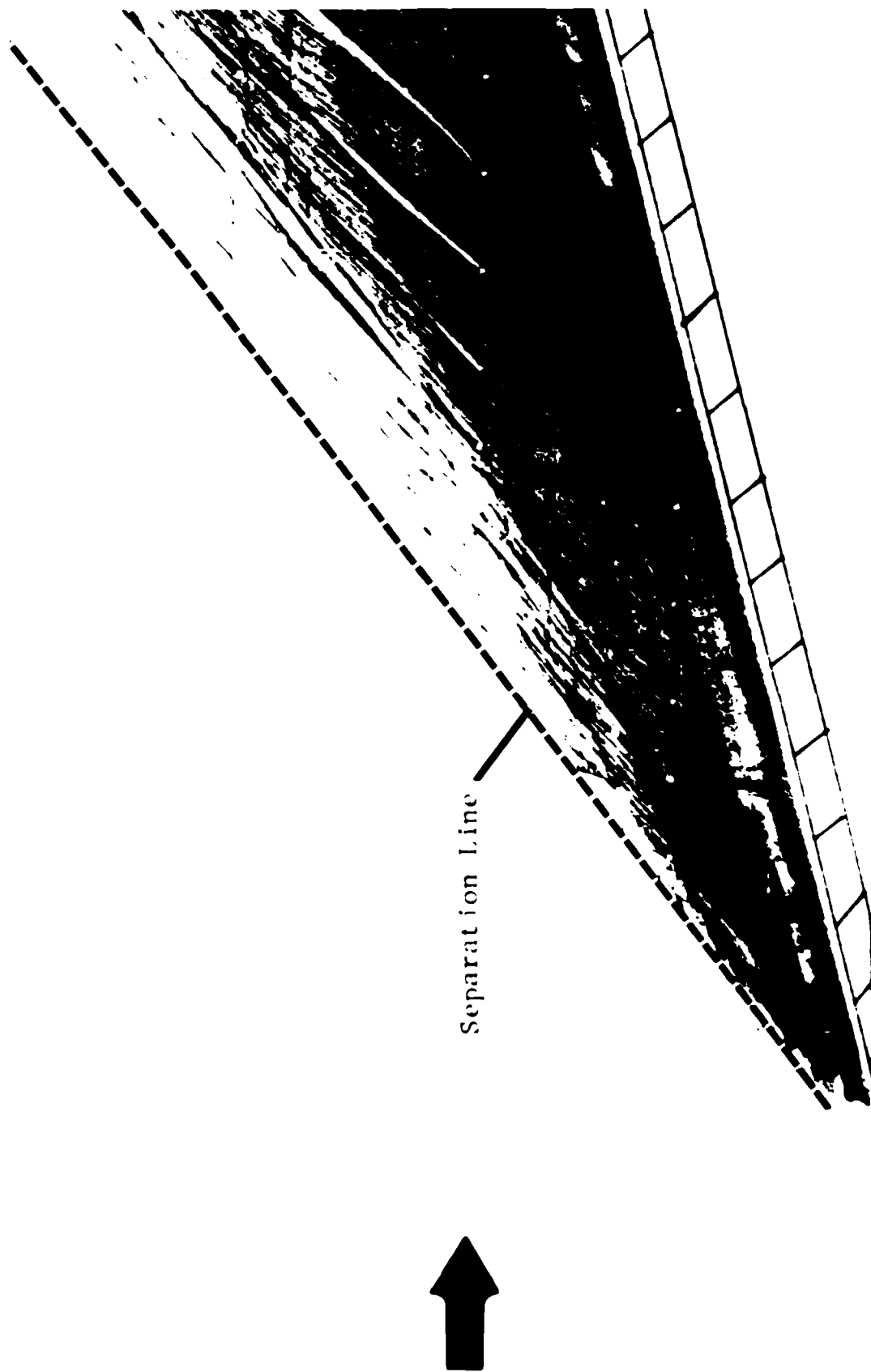


Figure 24. Photograph of Local Kerosene-Lampblack Trace, Downstream Application,  $\alpha = 15^\circ$ , Thin Boundary layer.

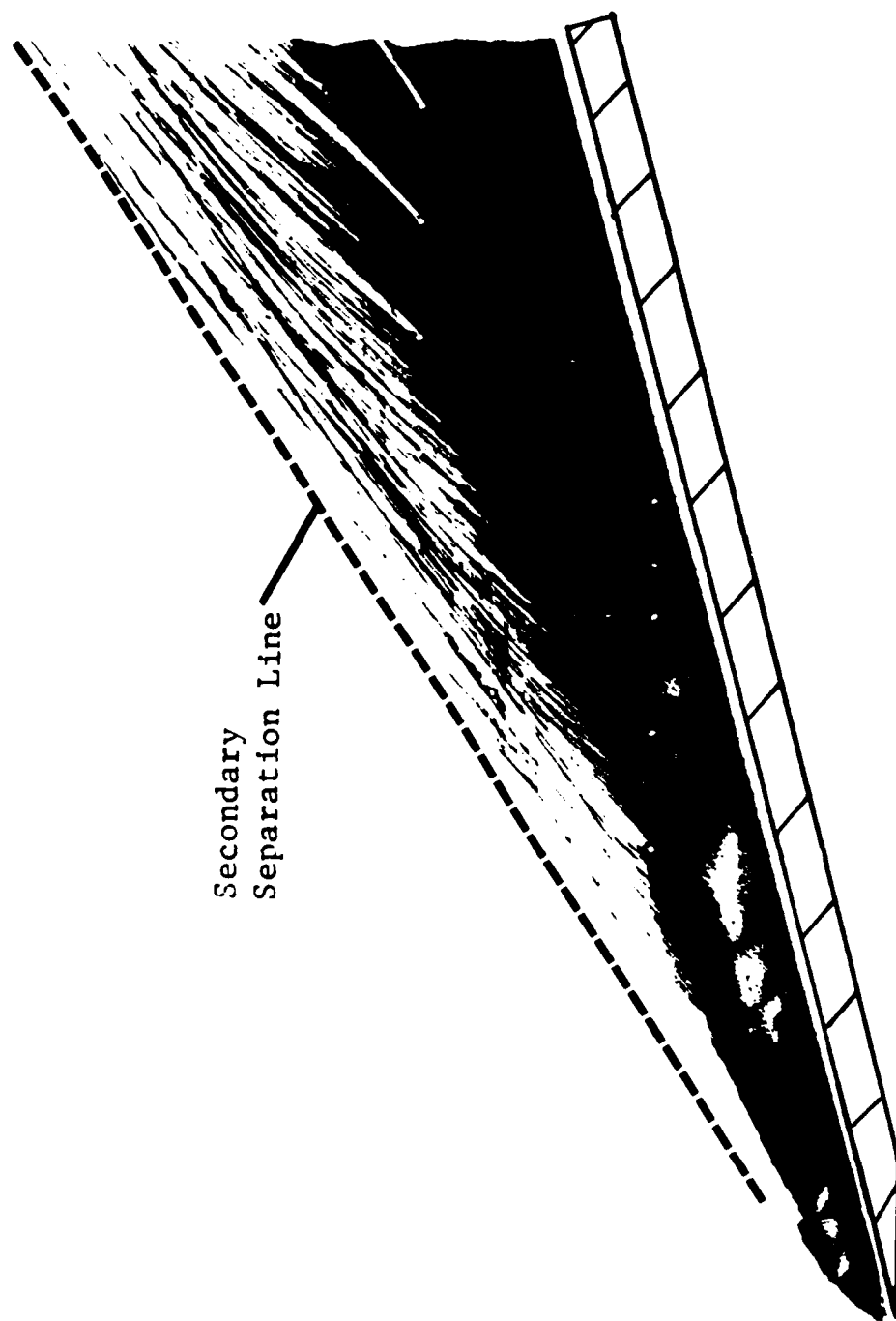


Figure 25. Photograph of Local Kerosene-Lampblack Trace,  
 $\alpha = 15^\circ$ , Thin Boundary Layer.



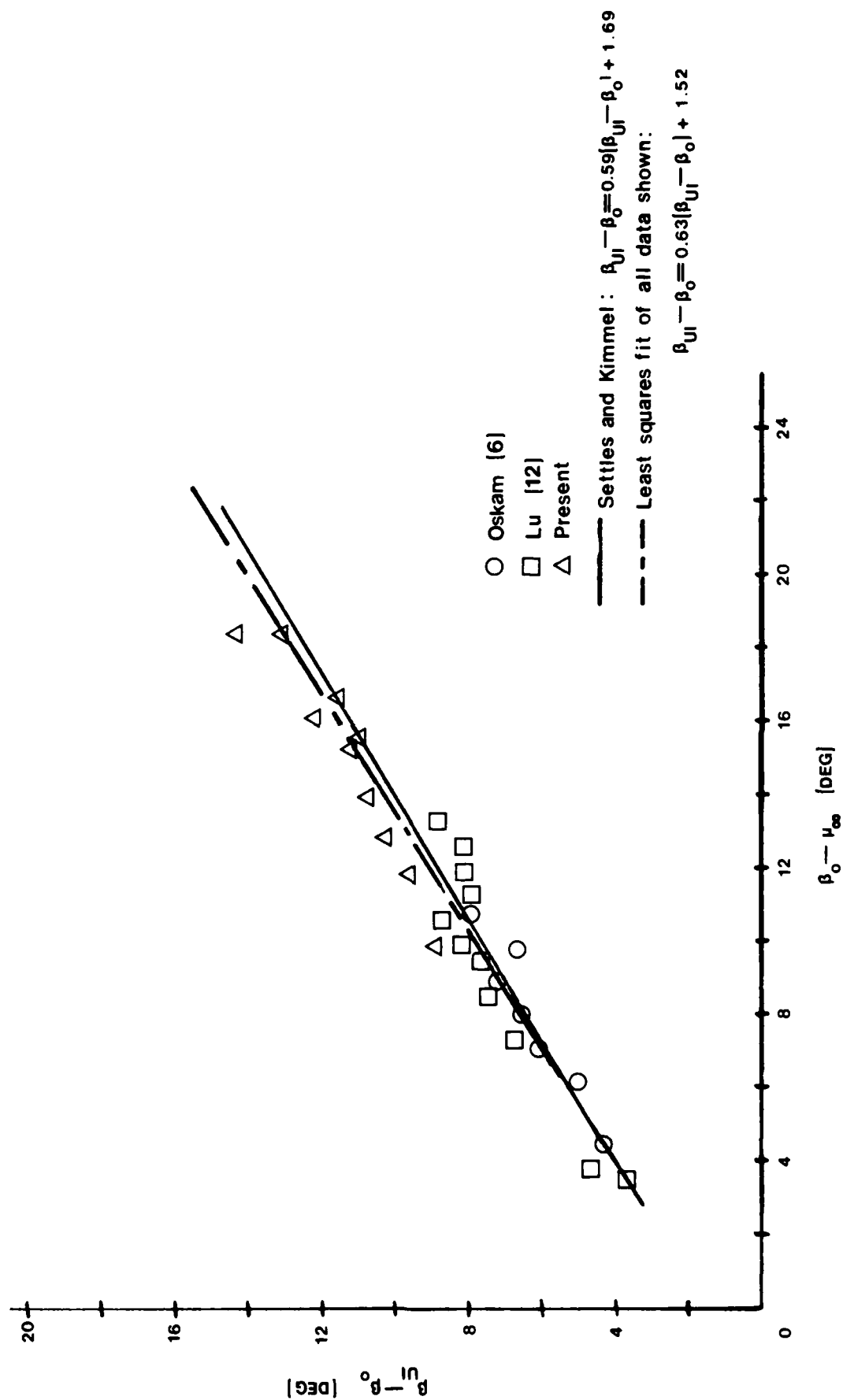


Figure 26. Plot of Conical Similarity Interaction Response Functions.

# UPSTREAM INFLUENCE

MACH NO. = 2.95

RUN NO. TEST NO.  $\alpha$ , DEG.  $\beta_0$ , DEG.  $\delta_{1N}$ , IN  $RE_U \times 10^{-6}$  /IN

□	611	5	12.0	29.62	0.14	1.55
△	611	9	14.0	31.59	0.14	1.55
+	611	11	15.0	32.62	0.14	1.55
×	612	3	16.0	33.67	0.14	1.55
◇	618	6	18.0	35.86	0.14	1.55
⬆	613	1	20.0	38.16	0.14	1.55

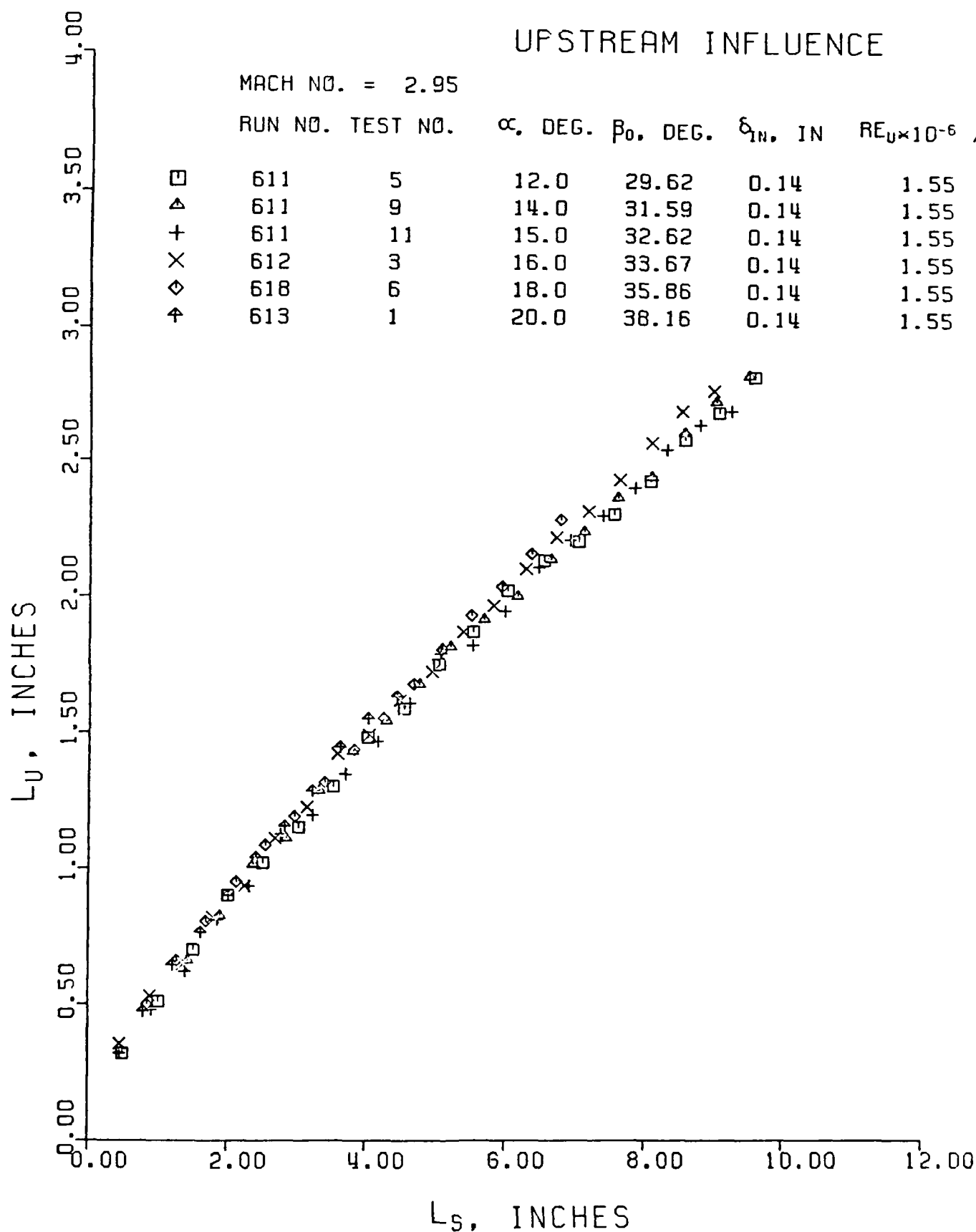


Figure 27. Effect of Shock Strength on Upstream Influence in  $L_u$  vs.  $L_s$  Coordinates.

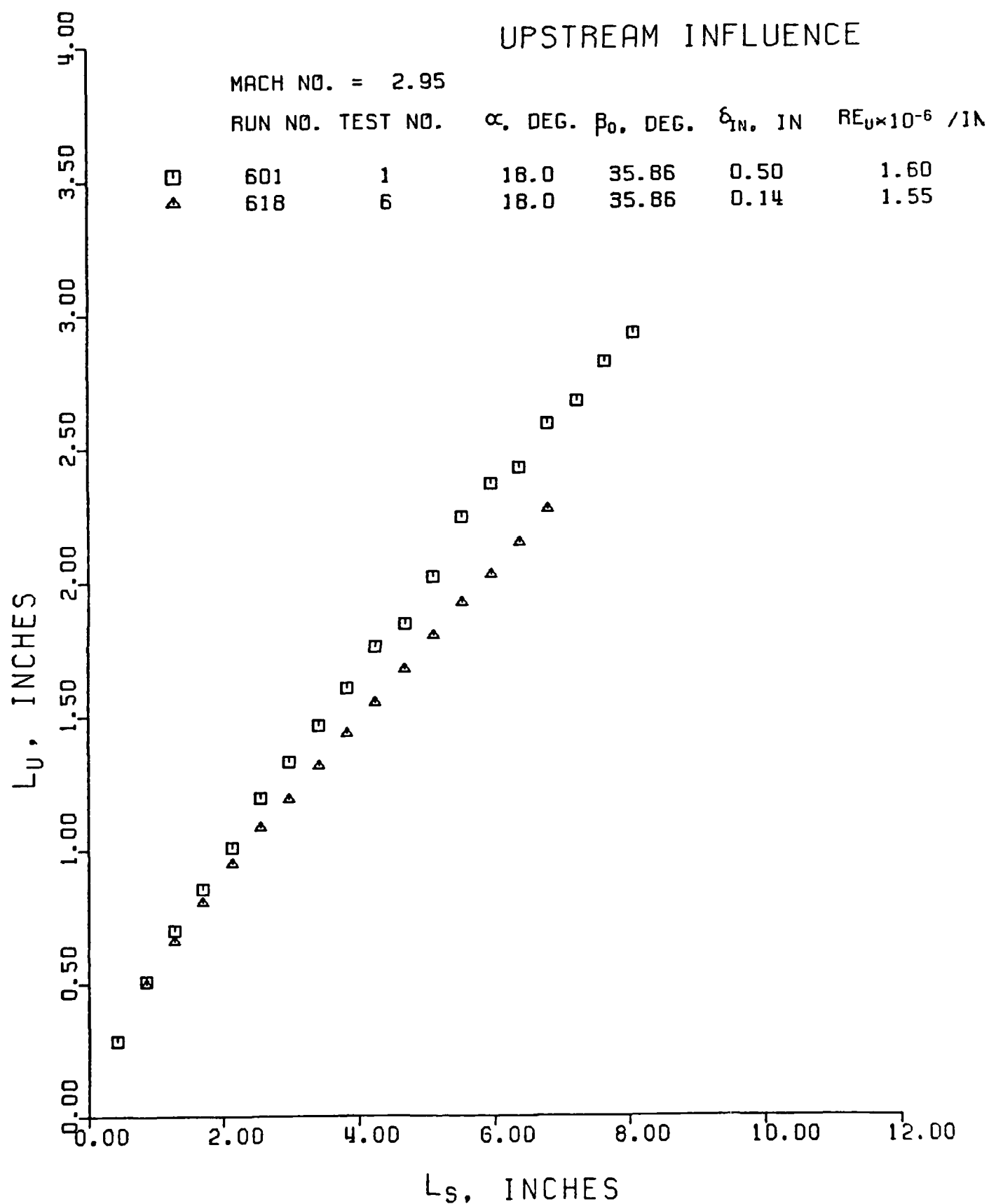


Figure 28. Effect of Boundary Layer Thickness on Upstream Influence in  $L_u$  vs.  $L_s$  Coordinates.

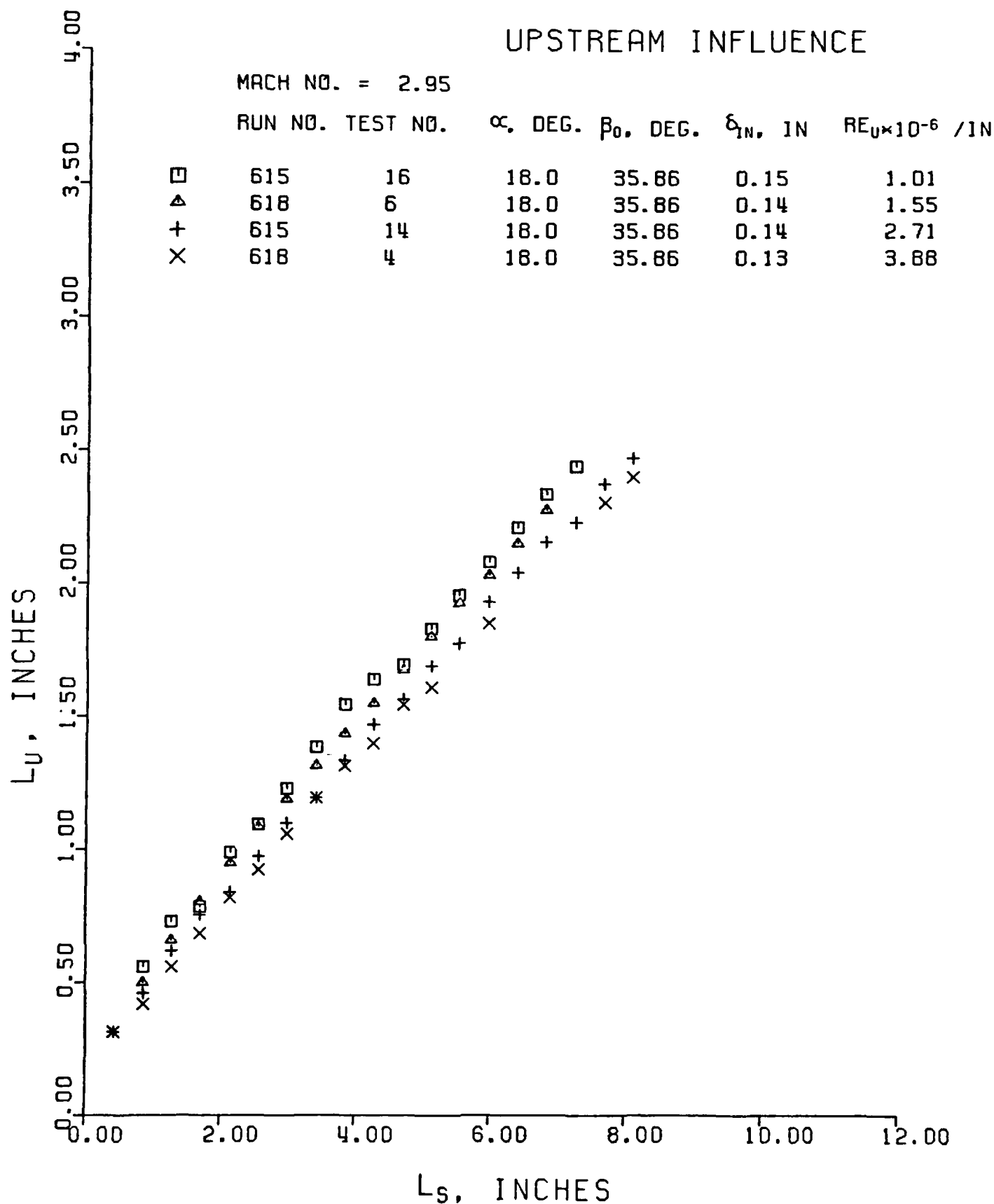


Figure 29. Effect of Unit Reynolds Number on Upstream Influence in  $L_u$  vs.  $L_s$  Coordinates.



# UPSTREAM INFLUENCE

MACH NO. = 2.95

	RUN NO.	TEST NO.	$\alpha$ , DEG.	$\beta_0$ , DEG.	$\delta_{IN}$ , IN	$RE_{0.5} \times 10^{-6}$ /IN
□	531	8	12.0	29.62	0.50	1.60
△	530	2	16.0	33.67	0.50	1.60
+	601	3	20.0	38.16	0.50	1.60

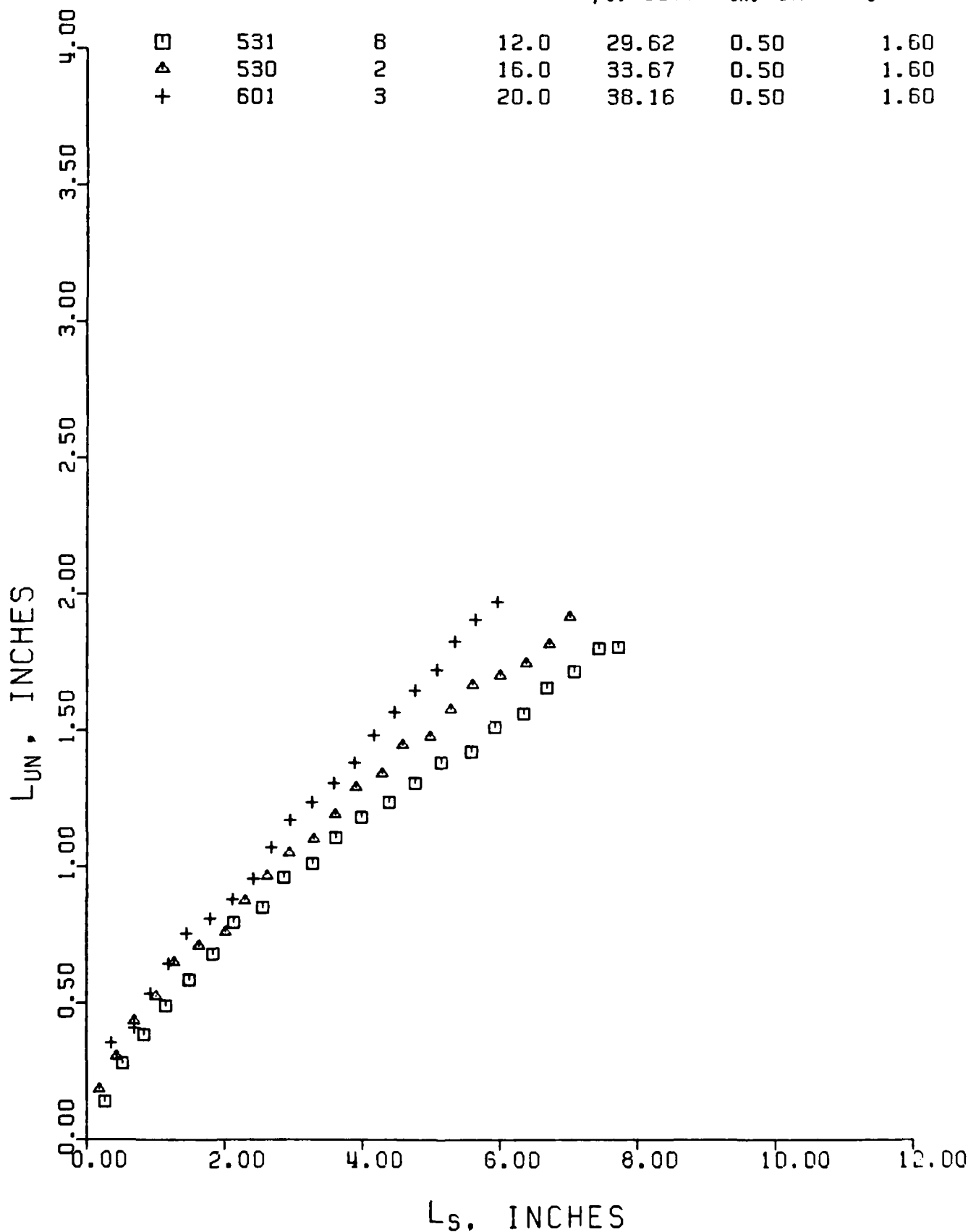


Figure 30. Effect of Shock Strength on Upstream Influence in L<sub>un</sub> vs. L<sub>s</sub> Coordinates.

# UPSTREAM INFLUENCE

MACH NO. = 2.95

RUN NO.	TEST NO.	$\alpha$ , DEG.	$\beta_0$ , DEG.	$\delta_{IN}$ , IN	$RE_U \times 10^{-6}$ /IN
601	1	18.0	35.86	0.50	1.60
618	6	18.0	35.86	0.14	1.55

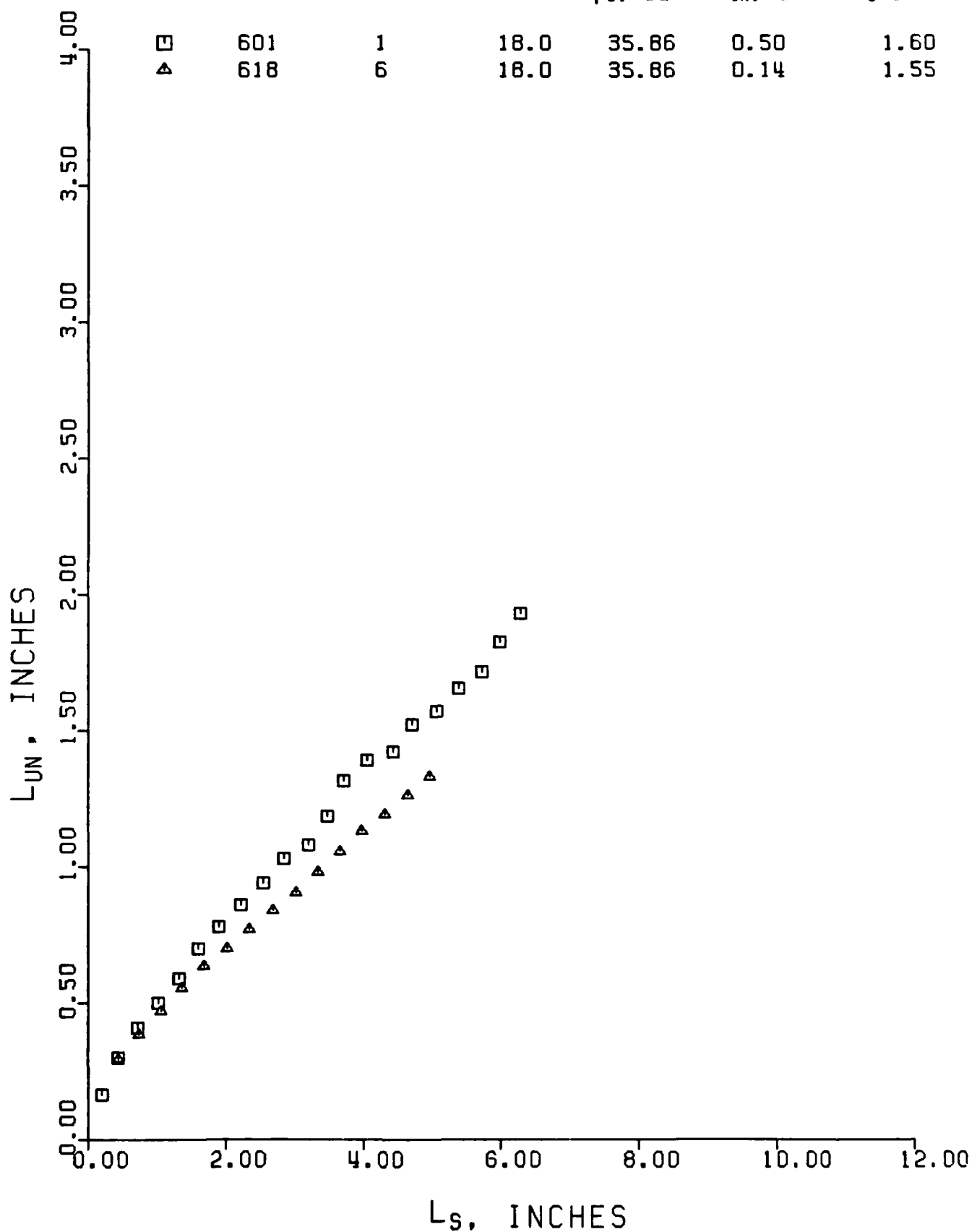


Figure 31. Effect of Boundary Layer Thickness on Upstream Influence in  $L_{un}$  vs.  $L_s$  Coordinates.

# UPSTREAM INFLUENCE

MACH NO. = 2.95

RUN NO.	TEST NO.	$\alpha$ , DEG.	$\beta_0$ , DEG.	$\delta_{1N}$ , IN	$RE_U \times 10^{-6}$ /IN
621	14	22.0	40.61	0.51	1.08
604	5	22.0	40.61	0.50	1.60
621	9	22.0	40.61	0.47	2.80
621	6	22.0	40.61	0.45	3.98

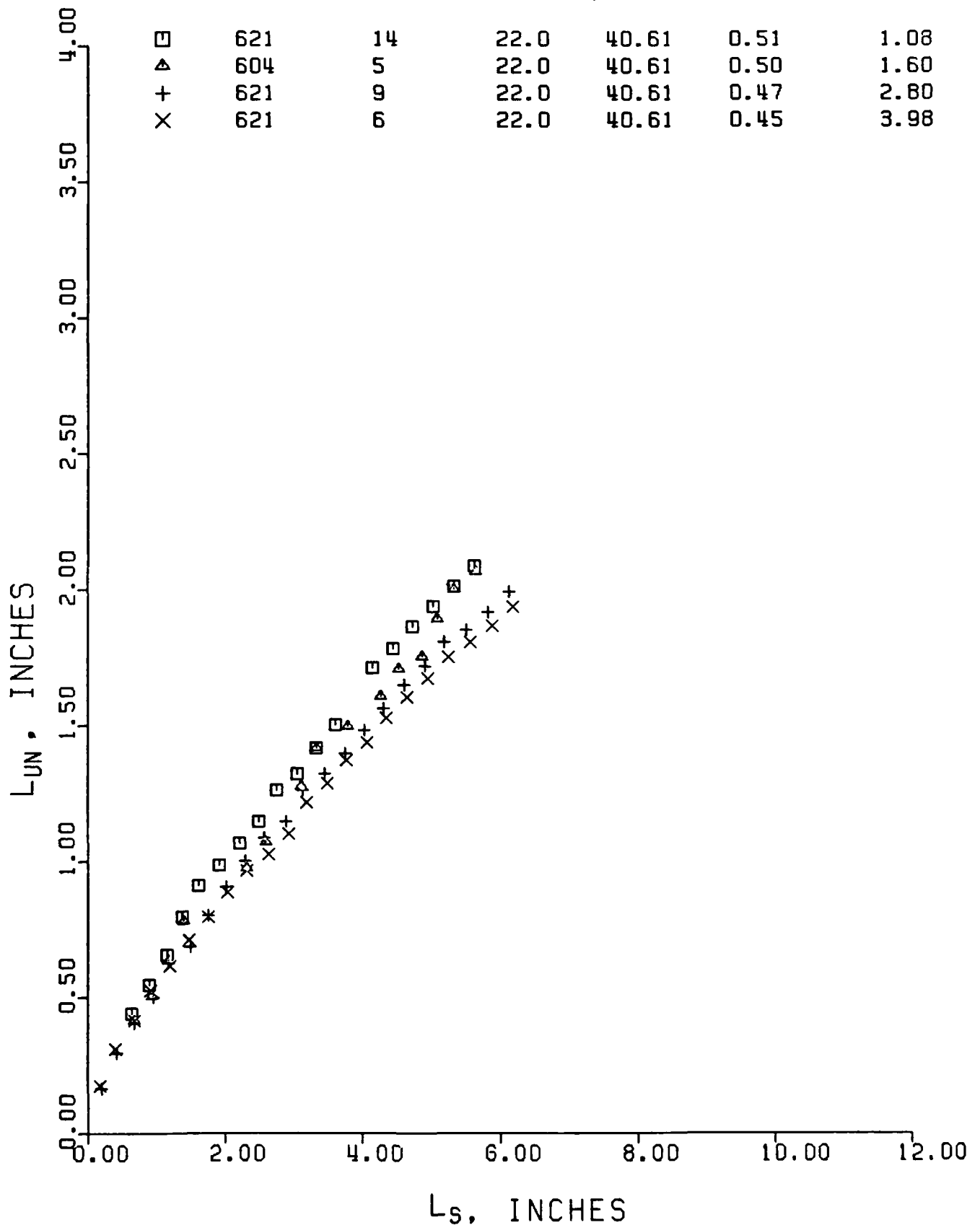


Figure 32. Effect of Unit Reynolds Number on Upstream Influence in L<sub>un</sub> vs. L<sub>s</sub> Coordinates.

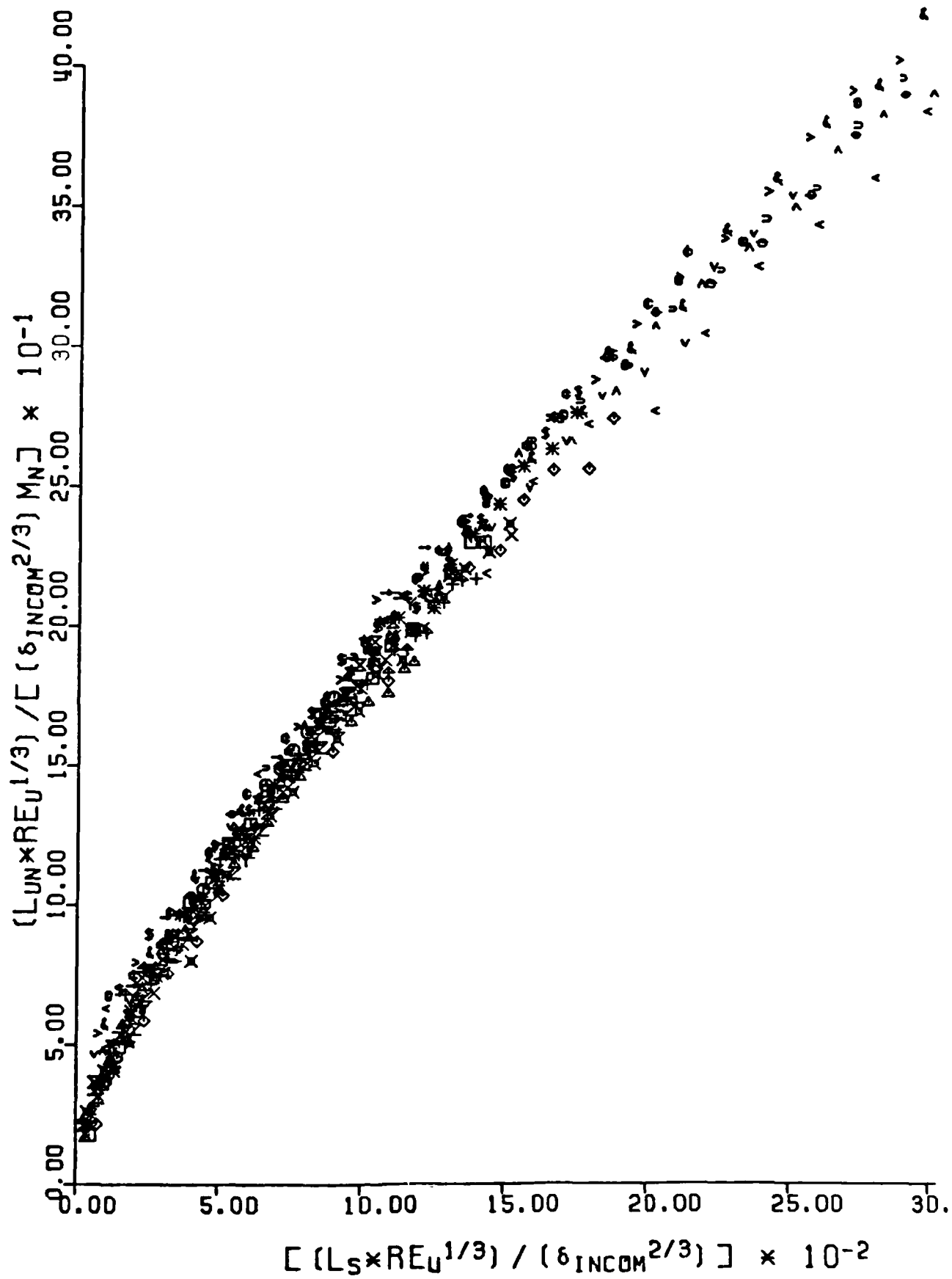
# UPSTREAM INFLUENCE

MACH NO. = 2.95

	RUN NO.	TEST NO.	$\alpha$ , DEG.	$\beta_0$ , DEG.	$\delta_{IN}$ , IN	$RE_U \times 10^{-6}$ /IN
□	531	8	12.0	29.62	0.50	1.60
△	621	10	14.0	31.59	0.51	1.08
+	531	11	14.0	31.59	0.50	1.60
X	621	7	14.0	31.59	0.47	2.80
◇	621	4	14.0	31.59	0.45	3.98
↑	531	12	15.0	32.62	0.50	1.60
×	530	2	16.0	33.67	0.50	1.60
Z	621	12	18.0	35.86	0.51	1.08
Y	601	1	18.0	35.86	0.50	1.60
⌘	621	8	18.0	35.86	0.47	2.80
*	621	5	18.0	35.86	0.45	3.98
Σ	601	3	20.0	38.16	0.50	1.60
⊙	621	14	22.0	40.61	0.51	1.08
★	604	5	22.0	40.61	0.50	1.60
#	621	9	22.0	40.61	0.47	2.80
⊕	621	6	22.0	40.61	0.45	3.98
⊖	611	5	12.0	29.62	0.14	1.55
∇	615	15	14.0	31.59	0.15	1.01
⊃	611	9	14.0	31.59	0.14	1.55
<	615	13	14.0	31.59	0.14	2.71
^	611	11	15.0	32.62	0.14	1.55
>	612	3	16.0	33.67	0.14	1.55
\$	615	16	18.0	35.86	0.15	1.01
⊙	618	6	18.0	35.86	0.14	1.55
&	615	14	18.0	35.86	0.14	2.71
⊙	618	4	18.0	35.86	0.13	3.88
→	613	1	20.0	38.16	0.14	1.55

(a)

Figure 33. Collapse of Upstream Influence Data Using Scheme of Dolling and Bogdonoff (23); (a) Key, (b) Data.



(b)

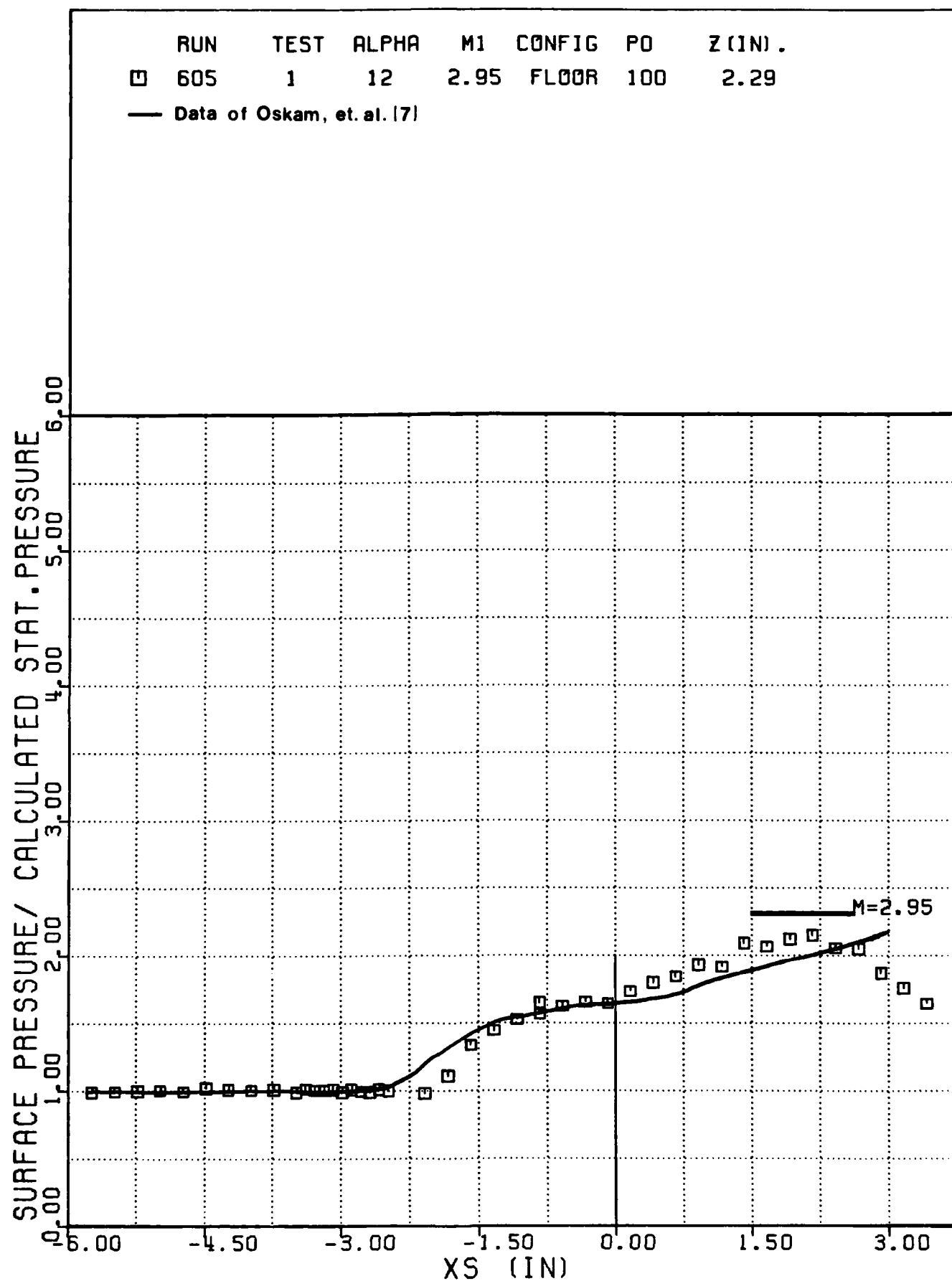


Figure 34. Comparison of Surface Pressure Data with Oskam, et. al. (7).

	RUN	TEST	ALPHA	M1	CONFIG	PO	Z (IN)	Z+DZ (IN)
□	906	1	15	2.95	PLATE	100	1.10	1.69
△	906	1	15	2.95	PLATE	100	2.10	2.69
+	906	1	15	2.95	PLATE	100	3.35	3.94
X	906	1	15	2.95	PLATE	100	4.35	4.94
◇	911	2	15	2.95	PLATE	100	0.50	1.09
Y	911	2	15	2.95	PLATE	100	1.00	1.59
↑	911	2	15	2.95	PLATE	100	1.75	2.34
X	911	2	15	2.95	PLATE	100	2.50	3.09

Run 906 : present configuration

Run 911 : duplicated test of Lu (12)

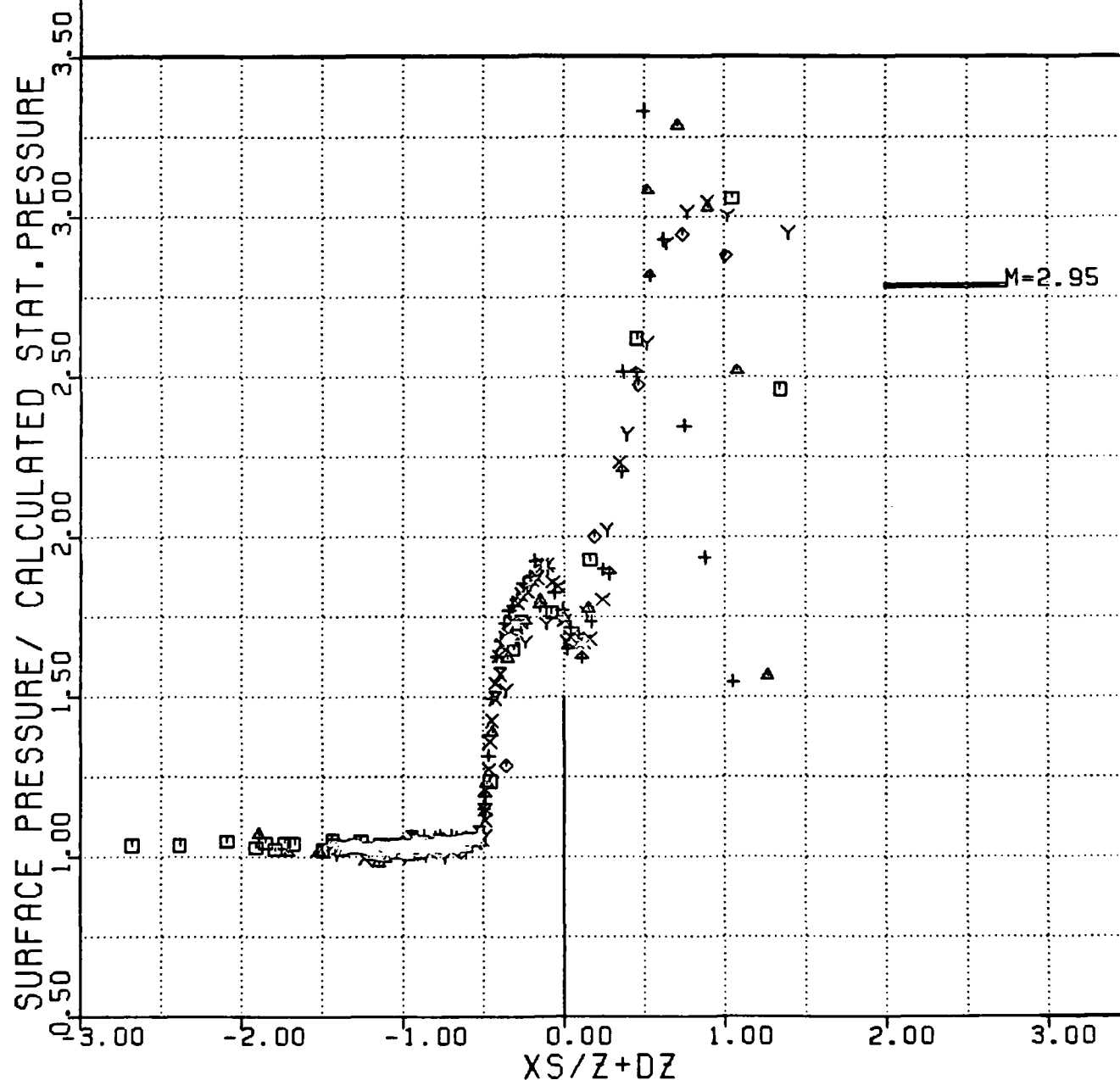


Figure 35. Comparison of Surface Pressure Data with Duplicated Data of Lu (12).

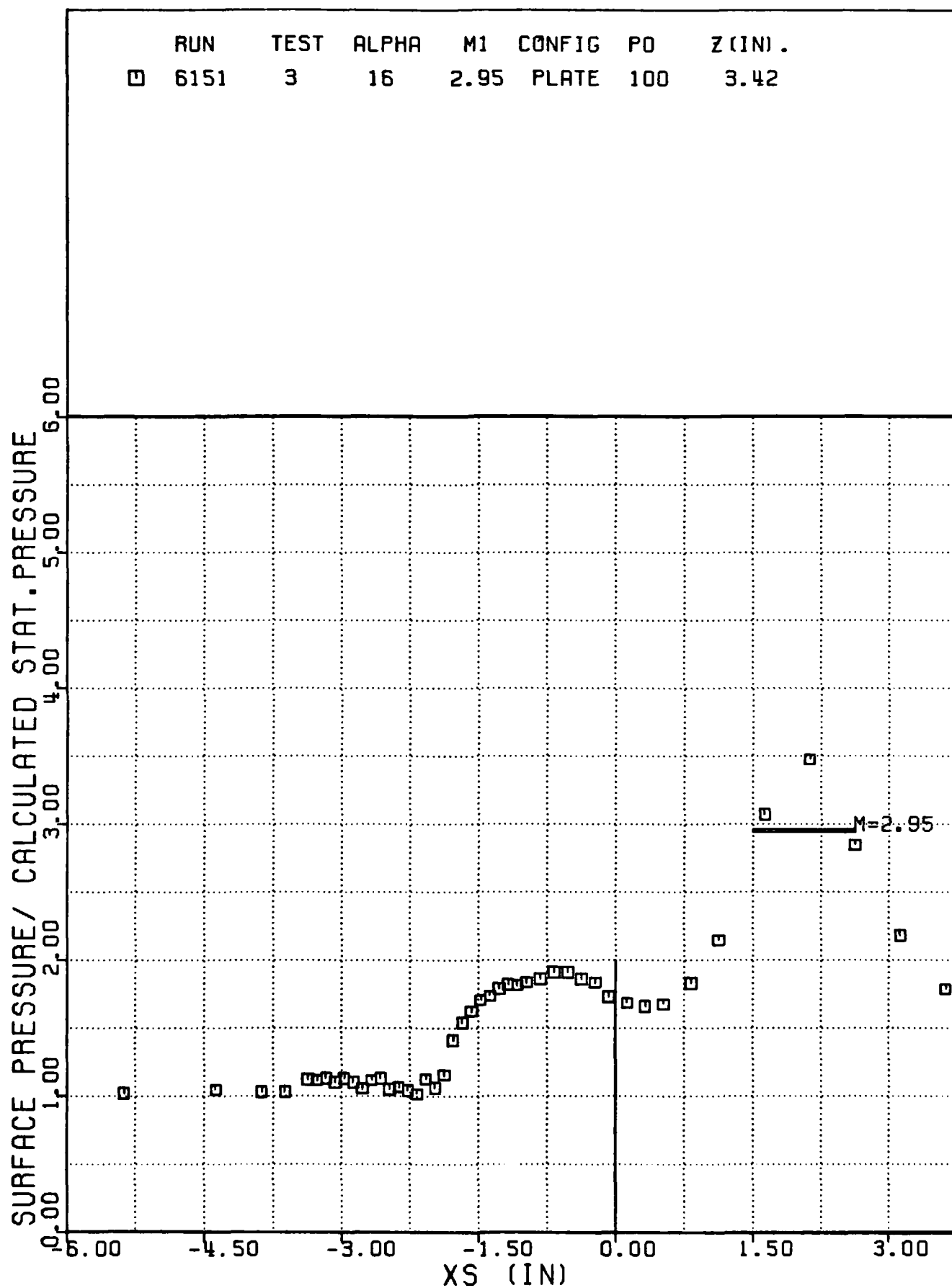


Figure 36. Typical Surface Pressure Distribution.



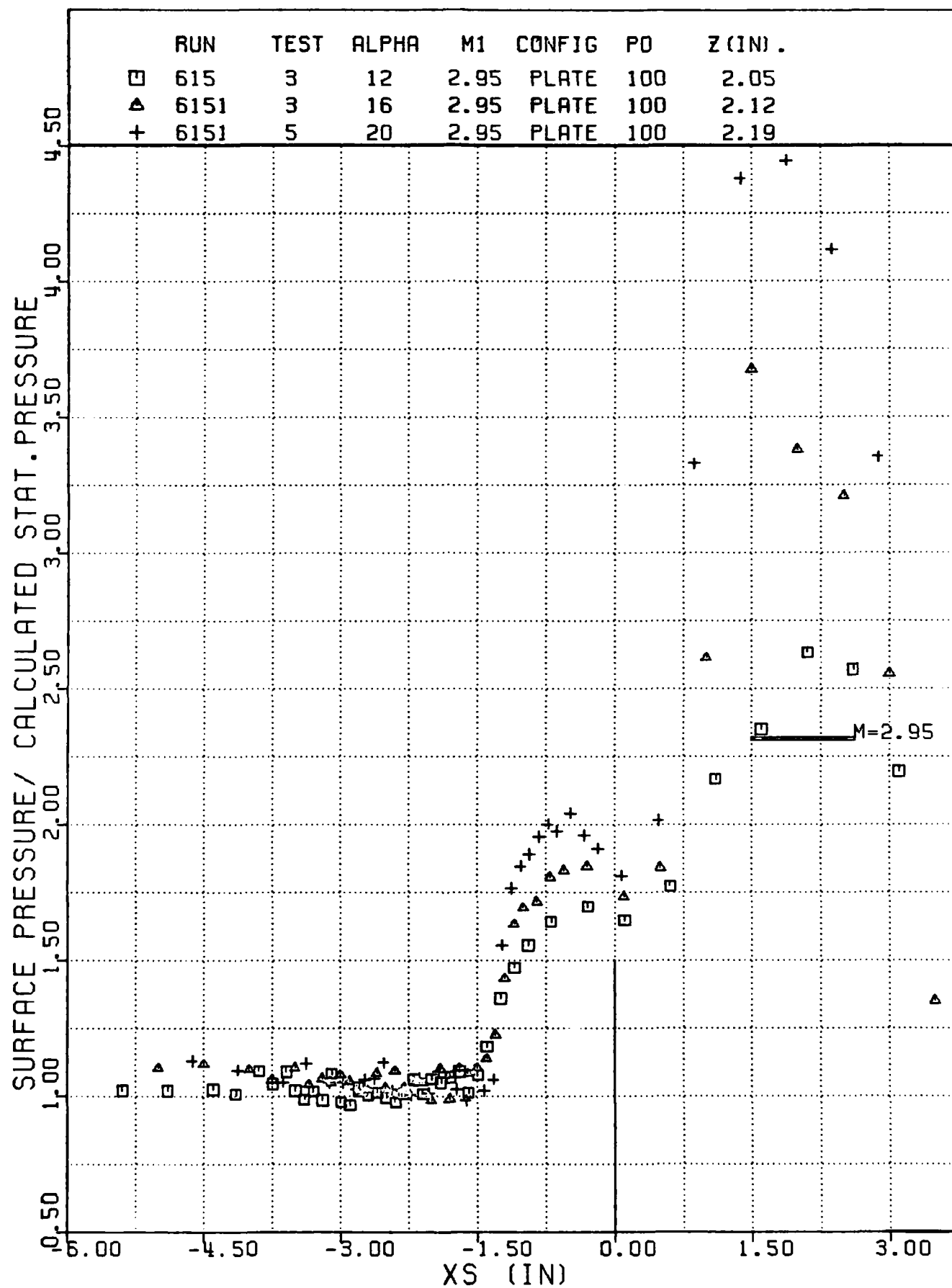


Figure 37. Effect of Shock Strength on the Surface Pressure Distribution.

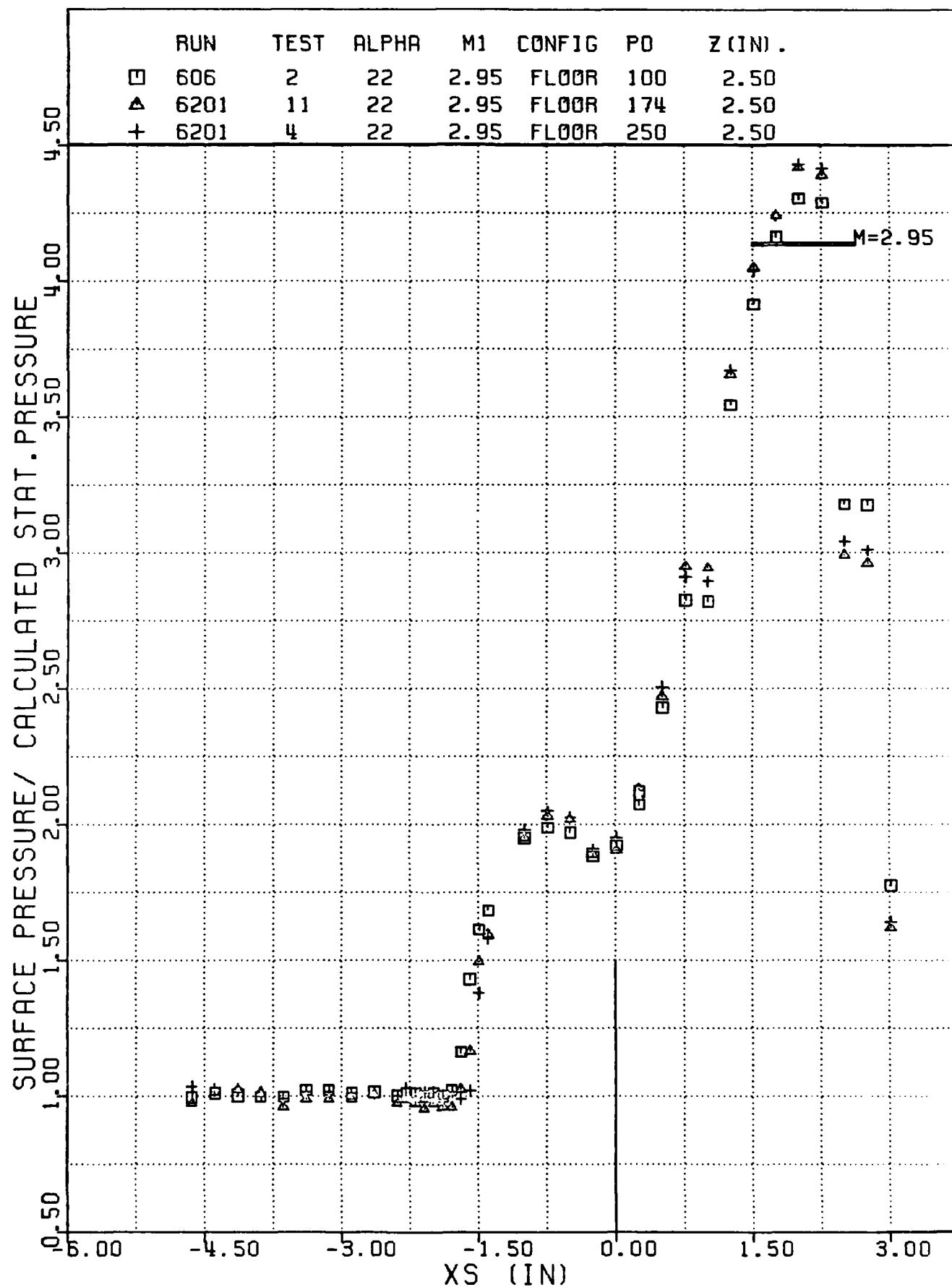


Figure 38. Effect of Unit Reynolds Number on the Surface Pressure Distribution.

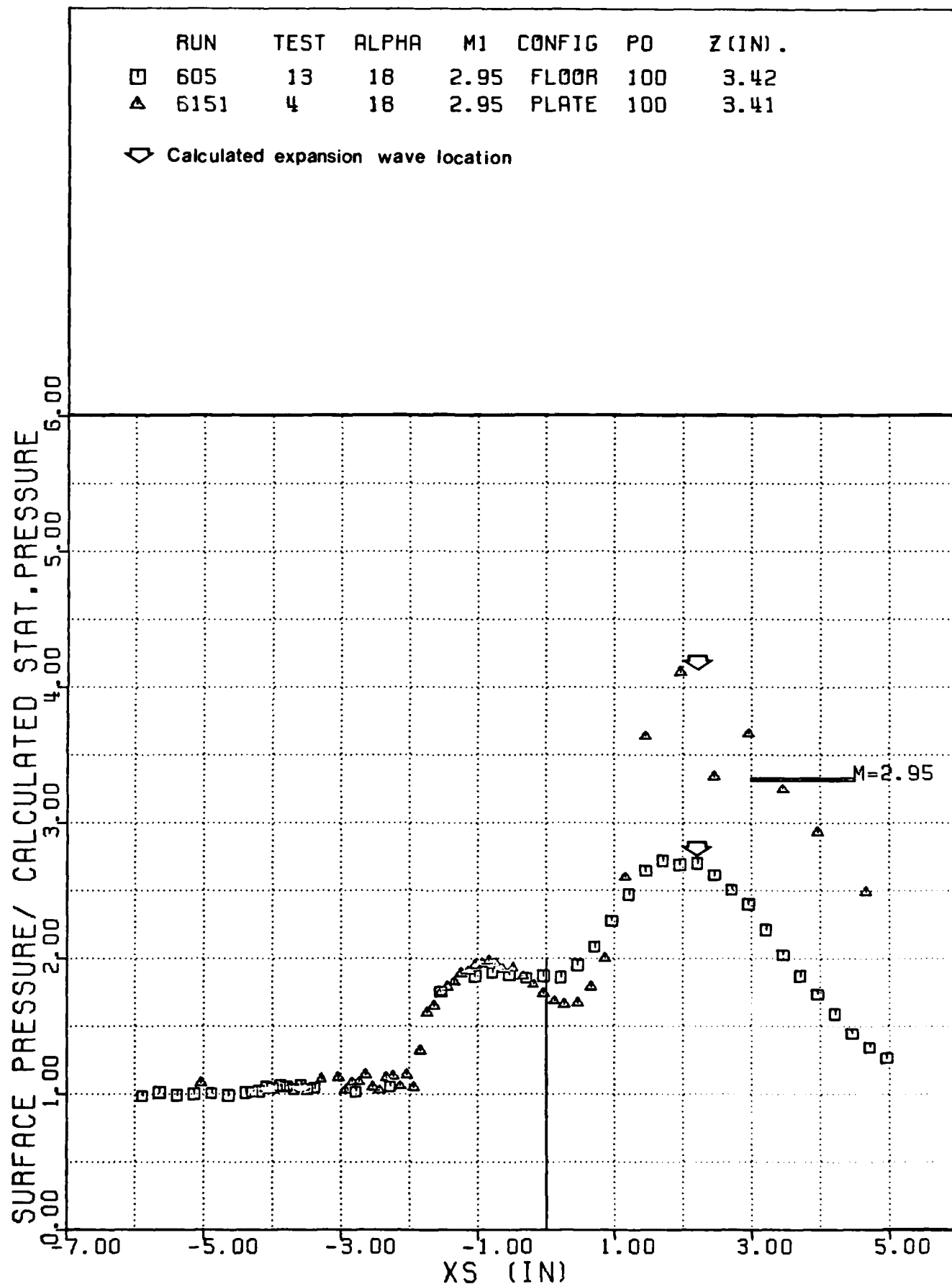


Figure 39. Effect of Boundary Layer Thickness on the Surface Pressure Distribution.

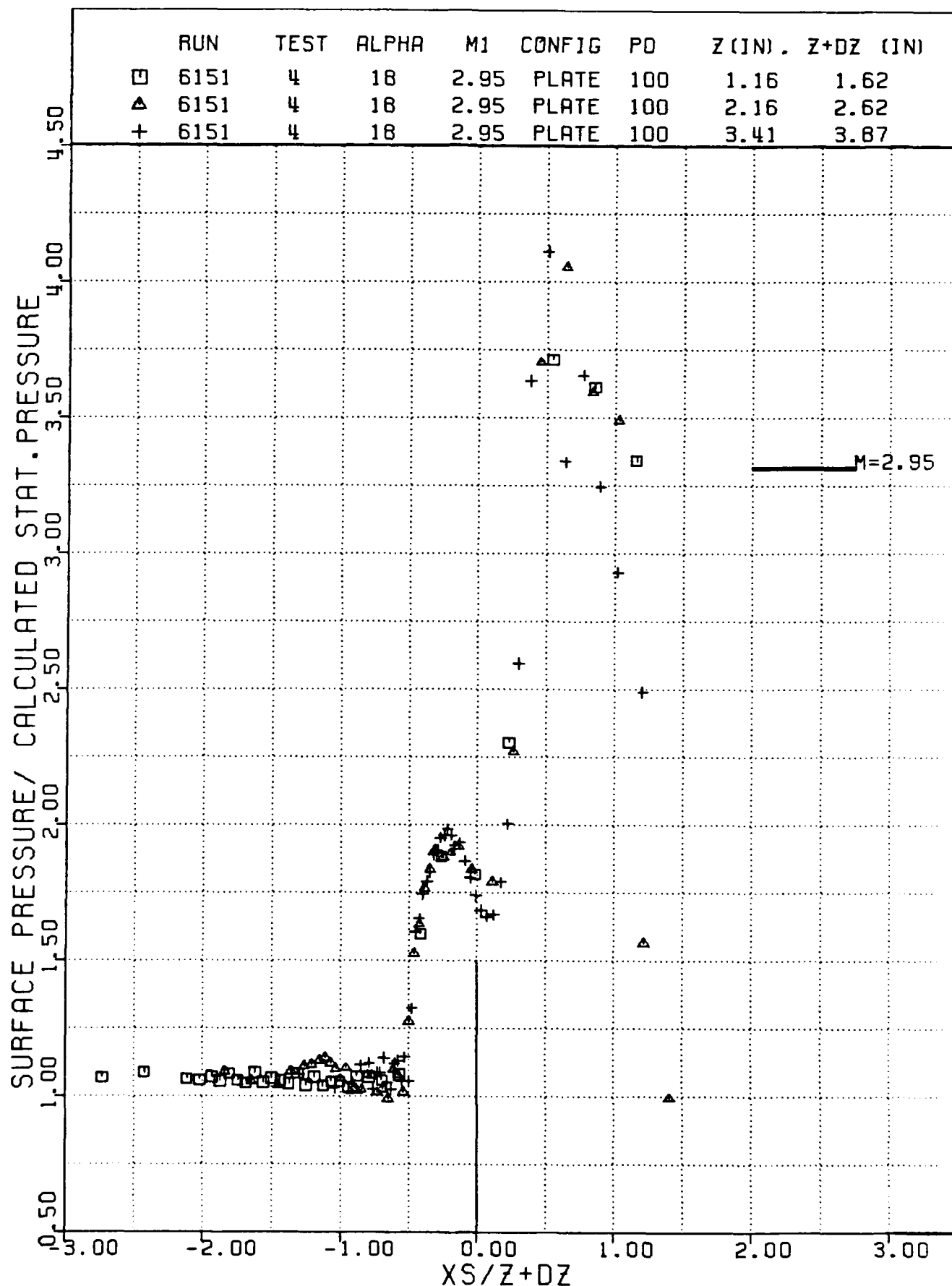


Figure 40. Typical Collapse of the Surface Pressure Data.

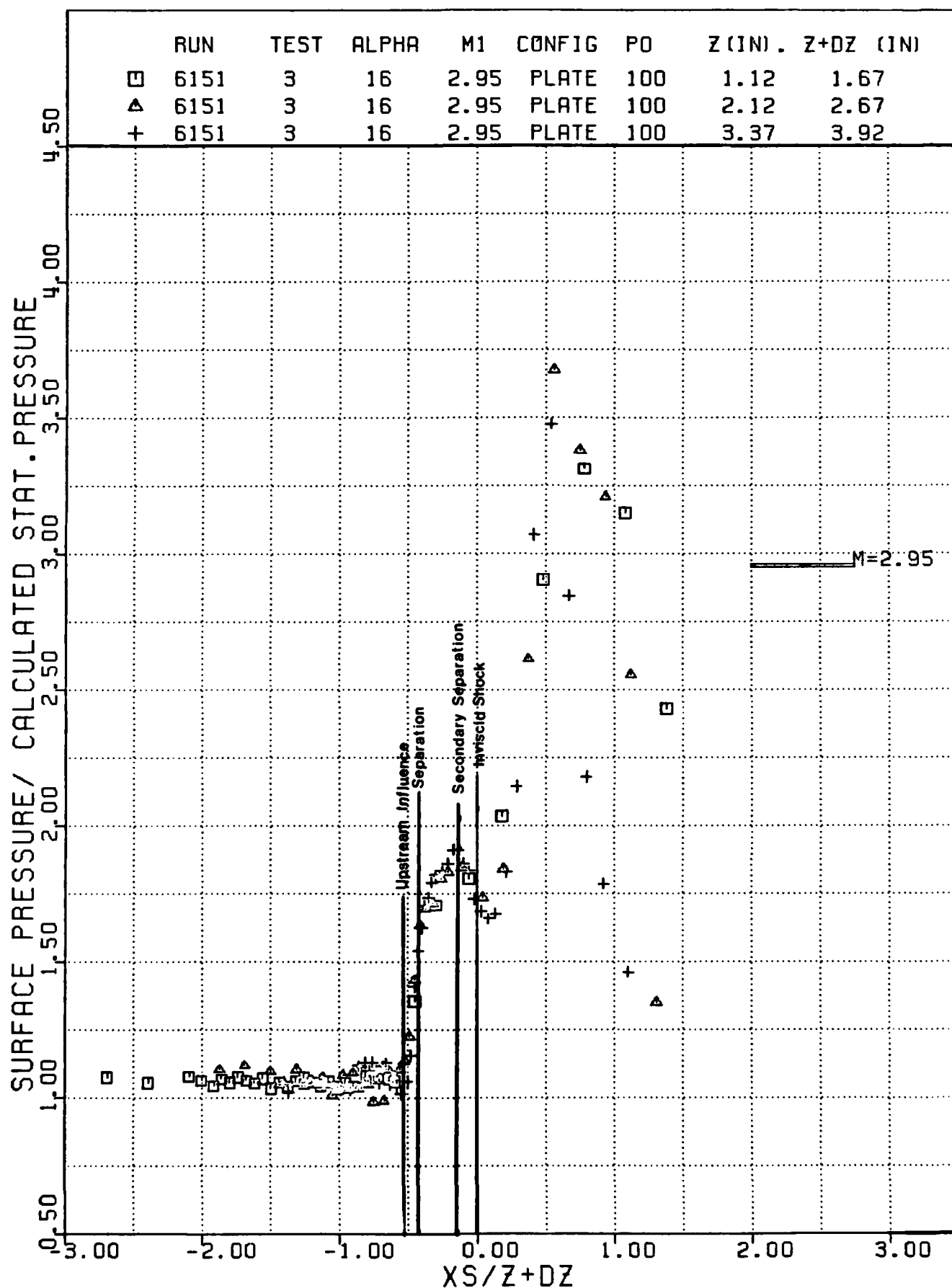


Figure 41. Typical Pressure Distribution/Kerosene-Lampblack Comparison Plot.

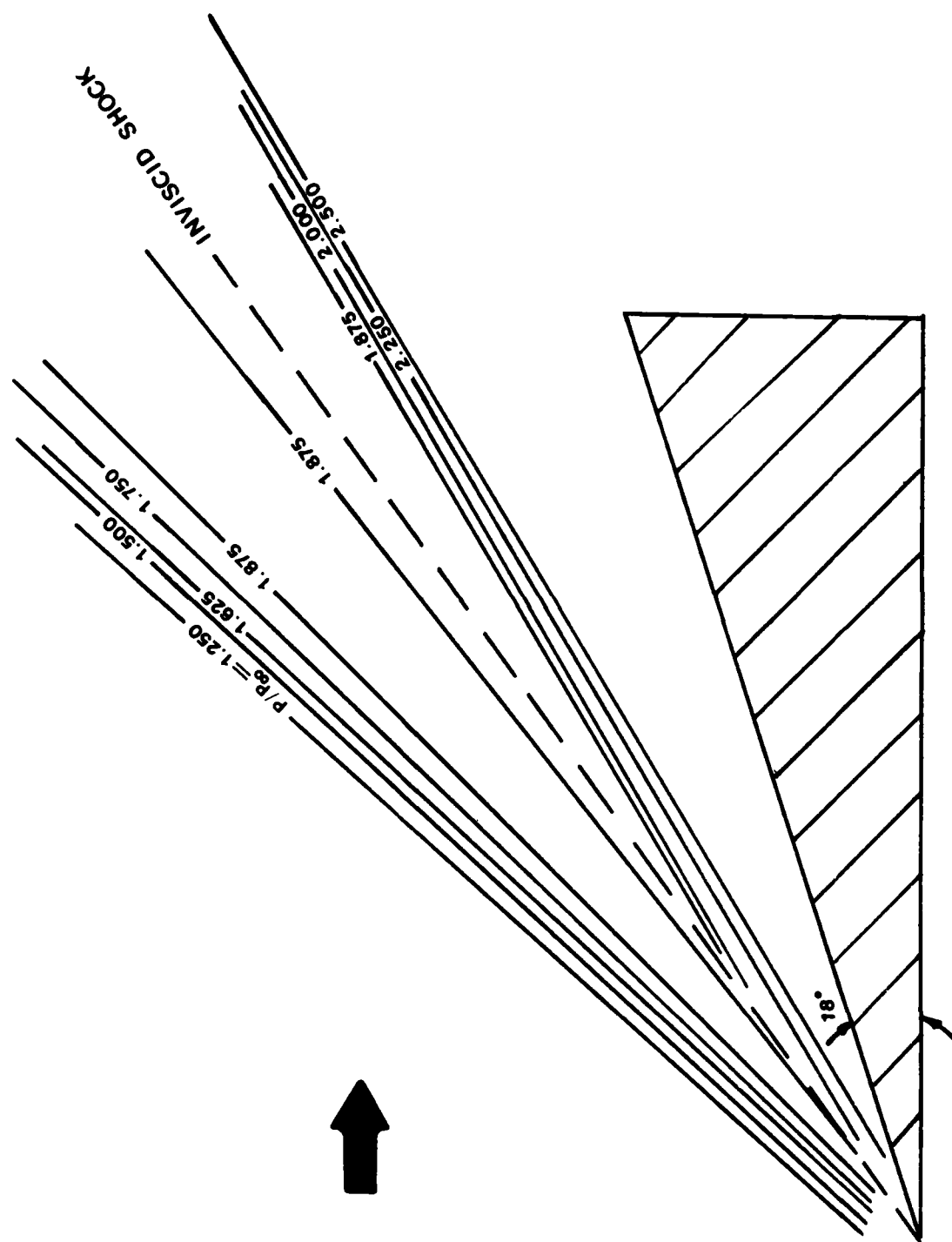


Figure 42. Topographic Pressure Plot.

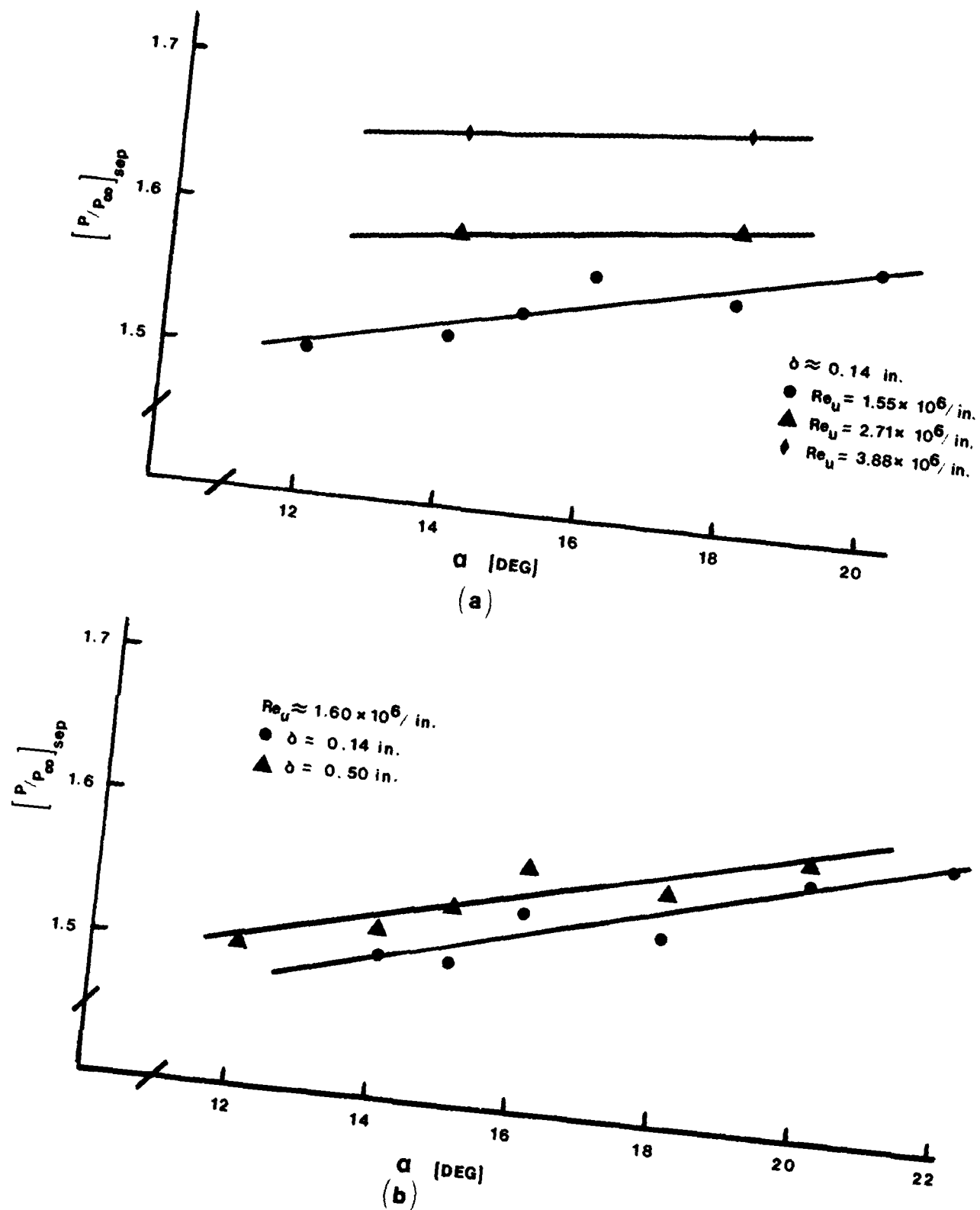


Figure 43. Effect of Test Variables on Separation Pressure Ratio; (a) Unit Reynolds Number Effect, (b) Boundary Layer Thickness Effect.

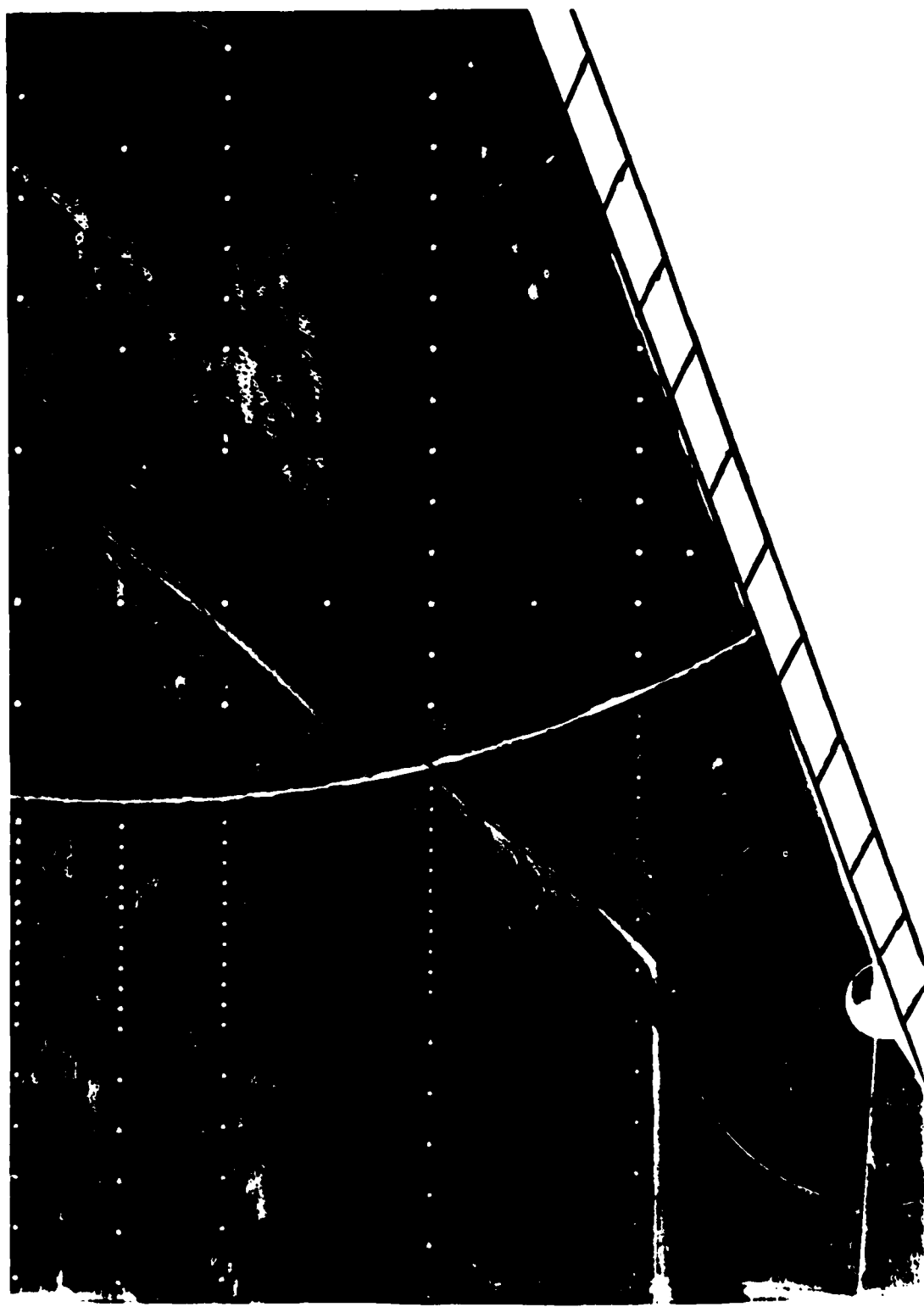


Figure 44. Photograph of  $\alpha = 20$  deg., Thick Boundary Layer  
Kerosene-Lampblack Trace.



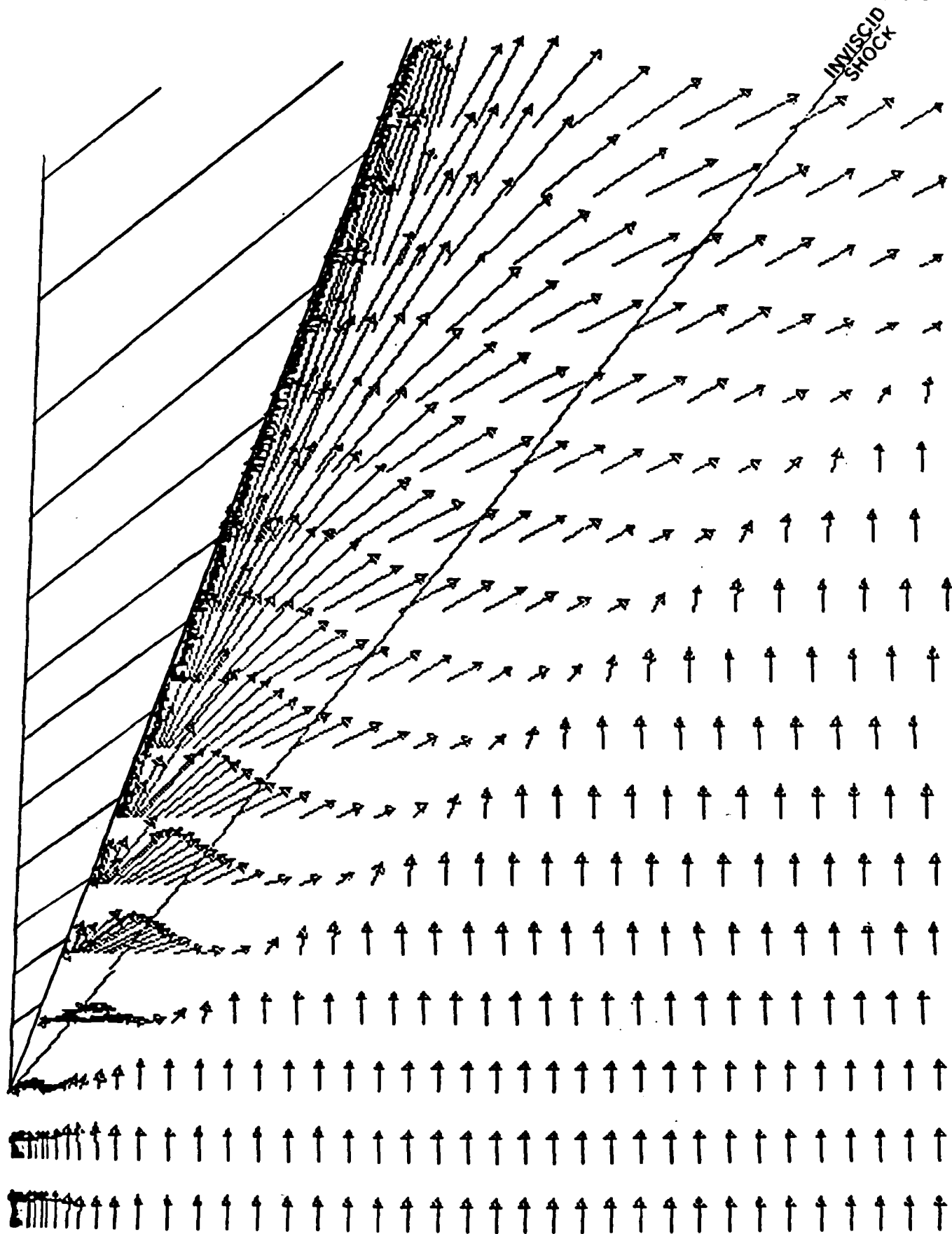


Figure 45. Computed Surface Shear Vectors of Knight (44).

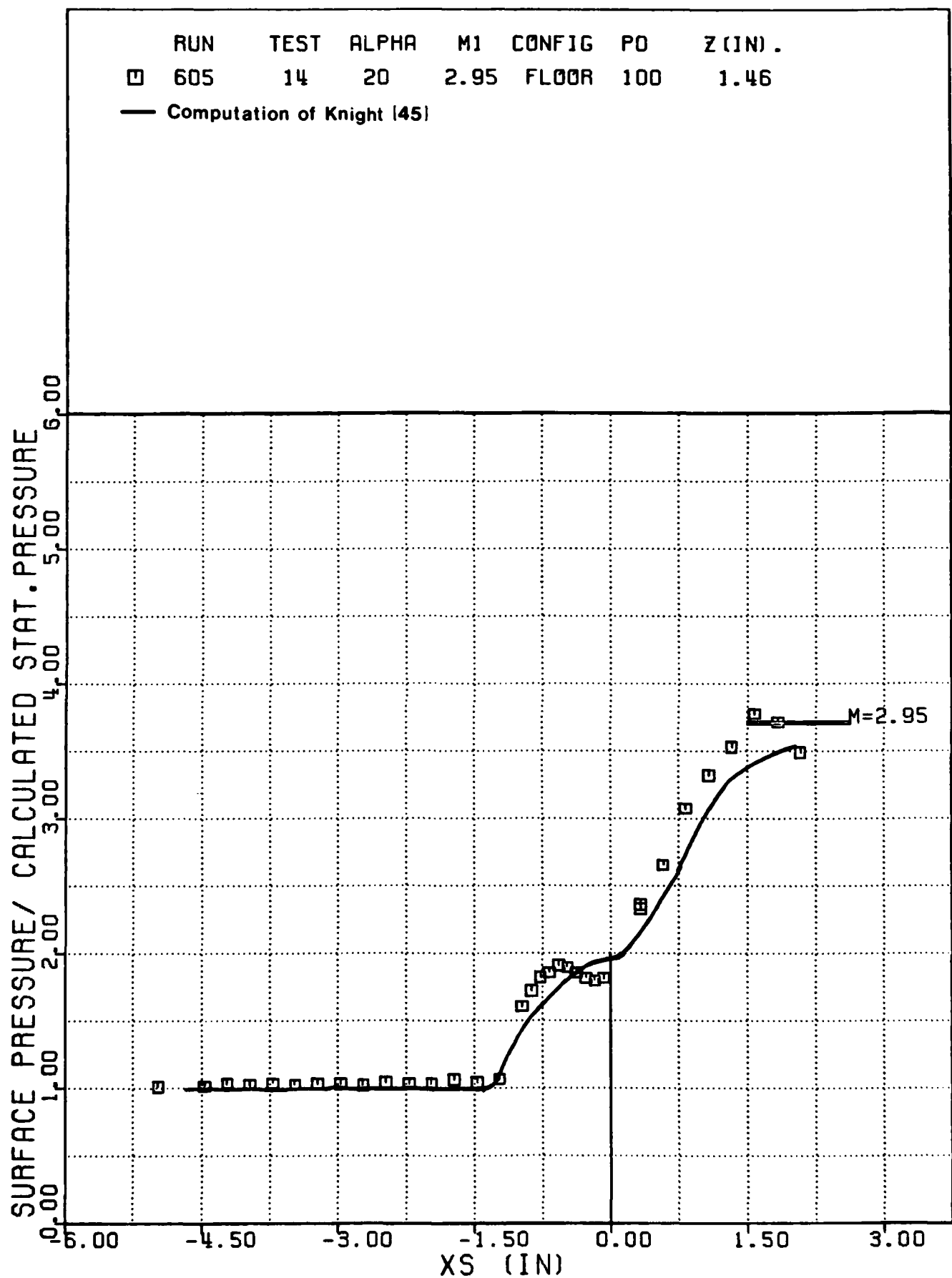


Figure 46. Comparison of a Surface Pressure Distribution with Computed Data of Knight (44).

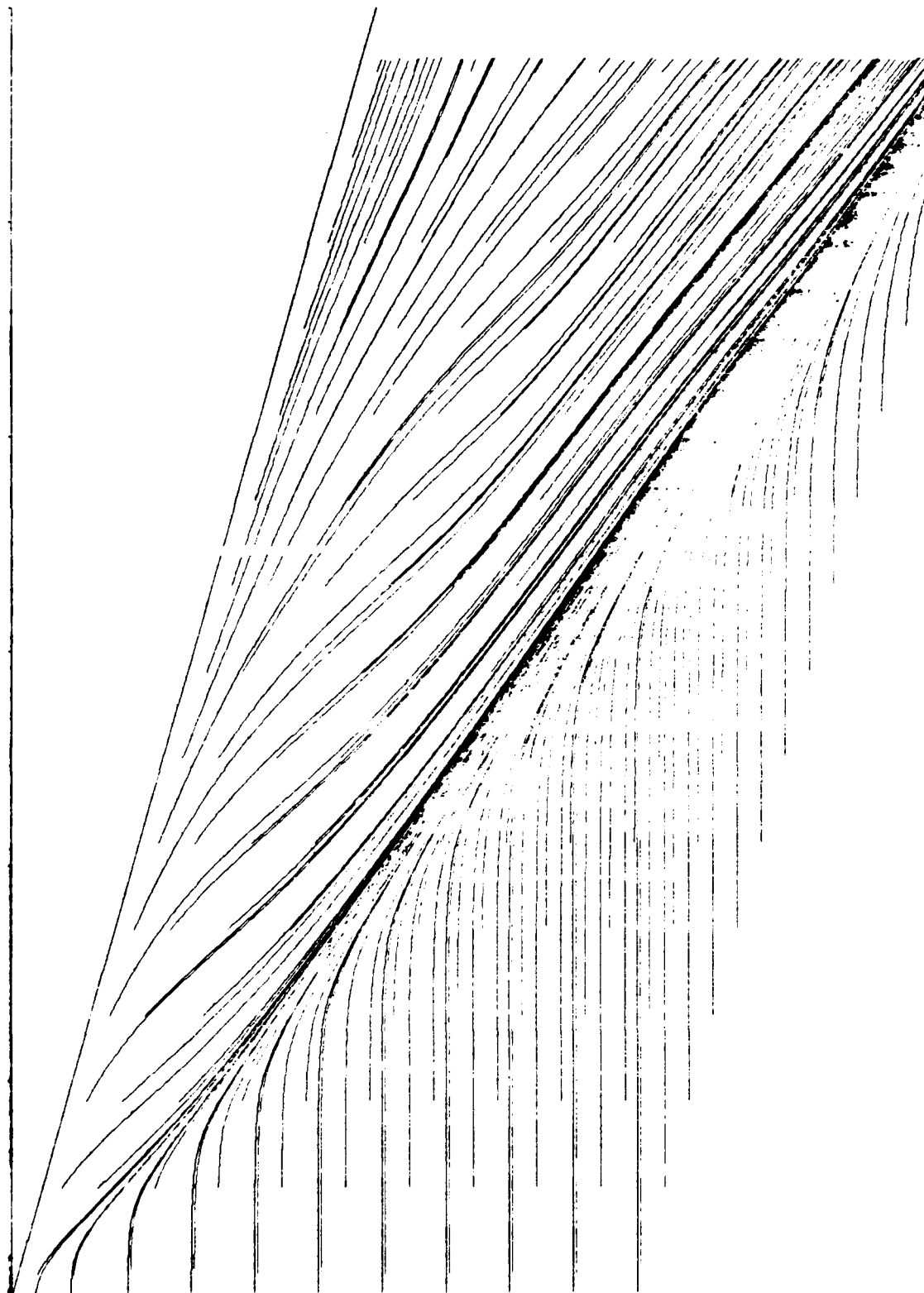


Figure 47. Computed Surface Streamlines of Horstman (45).

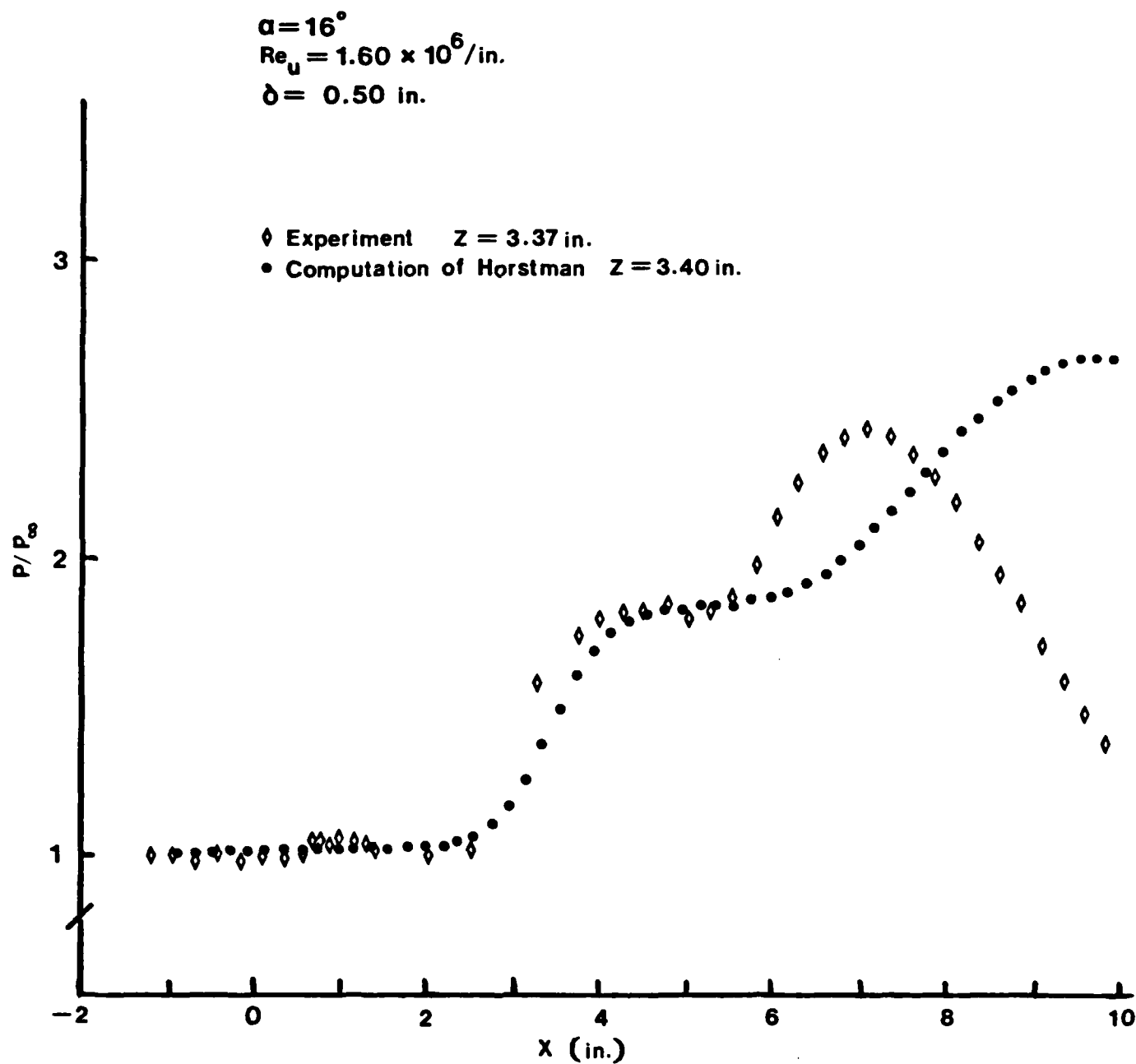


Figure 48. Comparison of a Surface Pressure Distribution with Computed Data of Horstman (45).

**END**

**FILMED**

**4-85**

**DTIC**